Role of GluA2-containing AMPARs in Oligodendrocyte Lineage Cells

Dissertation

zur Erlangung des Doktorgrades (PhD)

der Medizinischen Fakultät

der Rheinischen Friedrich-Wilhelms-Universität

Bonn

Vicky Faure geb. Nicolas

aus Avignon, France

2024

Angefertigt mit der Genehmigung

der Medizinischen Fakultät der Universität Bonn

1. Gutachter: Prof. Dr. med. Dirk Dietrich
2. Gutachter: Prof. Dr. med. Leda Dimou

Tag der Mündlichen Prüfung: 01.12.2023

Aus der Klinik und Poliklinik für Neurochirurgie

Direktor: Prof. Dr. Hartmut Vatter

Table of content

1 Introduction 8

1.1 Properties of Oligodendrocyte lineage cells 9
1.1.1 Identification of oligodendrocyte lineage cells 9
1.1.2 Origin of NG2 cells 11
1.1.3 NG2 cell fate 13
1.1.4 Myelination by oligodendrocytes 15
1.1.5 Neuronal activity modulates NG2 cell fate 17
1.2 Electrical properties of NG2 cells 18
1.2.1 NG2 cells receive direct neuronal synaptic input 18
1.2.2 Synaptic input integration into NG2 cells 19
1.2.2.1 AMPA receptors in NG2 cells 20
1.2.2.2 Modulatory effect of AMPARs on NG2 cell fate 22
1.3 Calcium signaling in NG2 cells 23
1.3.1 Glutamatergic synaptic input induces calcium signal in NG2 cells 23
1.3.2 Calcium transient properties in oligodendrocyte lineage cells 24
1.3.3 The role of calcium signaling in NG2 cell fate 25
1.4 Aim of the study 26

2 Materials and methods 28

2.1 Animals 28
2.2 Solutions 30
2.2.1 Slicing solution 30
2.2.2 Fixative solution 30
2.2.3 Staining solution 31
2.2.4 Tamoxifen solution 31
2.2.5 BrdU solution 31
2.2.6 EdU solution 31
2.3 Antibodies 31
2.3.1 Primary antibodies 31
2.3.2 Secondary antibodies 32
2.3.3 Dye / cell marker 32
2.4 Images acquirement with Confocal Microscopy 33

2.4.1 Confocal imaging principle. 33
2.4.2 Image acquisition....34
2.4.2.1 Nikon system....35
2.4.2.2 Leica system....35
2.4.2.3 Zeiss system....35
2.5 Behavioral methods....35
2.5.1 Rotarod....35
2.5.2 Running wheel....35
2.6 Experimental procedure to follow the fate of GluA2 deleted NG2 cells. 37
2.6.1 Tamoxifen administration 37
2.6.2 BrdU administration....37
2.6.3 Tissue preparation....38
2.6.3.1 Slice fixation 38
2.6.3.2 Slice resection 38
2.6.4 Immunohistochemistry....38
2.6.4.1 Quadruple BrdU labeling 39
2.6.4.2 Quadruple PCNA labeling 39
2.6.4.3 Quadruple CC1 labeling 40
2.6.5 Images acquirement....41
2.6.6 Cell Counting....41
2.6.6.1 Identification of NG2 cells....41
2.6.6.2 Mitotic figures identification 42
2.6.7 Analysis 43
2.6.7.1 NG2 cell fate mapping with BrdU labeling....43
2.6.7.2 NG2 cell fate mapping using PCNA as marker 44
2.6.7.3 NG2 cell density 44
2.6.7.4 NG2 cell differentiation 44
2.7 Experimental procedure to determine the role of GluA2 on internode length. 45
2.7.1 Tamoxifen administration 46
2.7.2 Tissue preparation....46
2.7.3 Immunohistochemistry....46
2.7.4 Image acquirement....46
2.7.5 Internode length measurement....47
2.7.6 Analysis 47
2.8 Experimental procedure to determine the role of GluA2 on NG2 cell fate and oligodendrocyte properties after a motor task. 48
2.8.1 Tamoxifen administration 49
2.8.2 Assessment of motor coordination with the rotarod 49
2.8.3 Motor learning task with the running wheel 49
2.8.4 EdU administration 50

2.8.5 Tissue preparation 50
2.8.6 Immunohistochemistry 50
2.8.7 Image acquirement 51
2.8.8 Analysis 51
2.8.8.1 Motor coordination with rotarod 51
2.8.8.2 Running wheel experiment 51
2.8.8.3 Myelination analysis 51
2.8.8.4 Proliferative fraction 52

3 Results 53

3.1 Increased proliferation in GluA2 deficient NG2 cells 53
3.1.1 Increased DNA replication in GluA2 deficient NG2 cells. 53
3.1.2 Unchanged cell cycle growth fraction after GluA2 deletion in NG2 cells. 57
3.1.3 NG2 cell mitotic fraction is unaffected by GluA2 deletion in NG2 cells. 58
3.1.4 Differential regulation of proliferation by the GluA2 subunit during development 60
3.2 Role of GluA2 deletion on density of oligodendrocyte lineage cells. 61
3.2.1 GluA2 deletion in NG2 cells affects the NG2 cell density in a region dependent manner. 61
3.2.2 Cell death remains stable in the NG2 cell population after GluA2 ablation. 64
3.3 Differentiation is unaltered in GluA2 deleted NG2 cells. 65
3.4 Dysregulation of the oligodendrocyte internode length by GluA2 deletion. 69
3.4.1 Early postnatal internode length is shortened by GluA2 deletion in NG2 cells 69
3.4.2 Late postnatal internode length is unchanged by GluA2 deletion in NG2 cells. 72
3.4.3 GluA2 subunit deletion affects the internode length differently regarding their position in the cortex layer 73
3.5 GluA2 deletion in NG2 cells in the context of motor learning activity. 74
3.5.1 Motor skills are not affected by GluA2 deletion. 74
3.5.2 Motor learning is impaired by GluA2 deletion in NG2 cells. 75
3.5.3 GluA2 subunit deletion in NG2 cells did not alter the internode length in the motor cortex during a motor learning paradigm. 78
3.5.4 GluA2 subunit deletion in NG2 cells does not affect NG2 cell proliferation after a wheel motor learning task. 80

4 Discussion 84

5 Abstract 93

6 List of figures 95

7 References 97

8 Acknowledgement 105

List of abbreviations

CNS	Central nervous system
OPCs	Oligodendrocyte precursor cells
O2A	Oligodendrocyte-type2-astrocyte
PDGFRα	Platelet-derived growth factor alpha receptor
NG2	nerve glial antigen 2
PLP	proteolipid protein
CNP	2',3'-cyclic-nucleotide 3'-phosphodiesterase
MAG	myelin-associated glycoprotein
MBP	myelin basic protein
MOG	myelin oligodendrocyte glycoprotein
Enpp6	ectonucleotide pyrophosphatase phosphodiesterase family member 6
BAC	Bacterial artificial chromosome
MGE	medial ganglionic eminence
AEP	anterior entopeduncular region
LGE	lateral ganglionic eminence
VZ	ventricular zone
SVZ	subventricular zone
DNA	deoxyribonucleic acid
PCNA	proliferating cell nuclear antigen
AMPA	α-amino-3-hydroxy-5-methyl-4-isoxazolepropionic acid
AMPAR	AMPA receptor
NMDA	N-methyl-D-aspartate
NMDAR	NMDA receptor
GABA	Gamma-aminobutyric acid
VGCC	Voltage-Gated Ca^{2+} channel
EdU	5-ethynyl-2-deoxyuridine

BrdU	bromodeoxyuridine
Caspr	Contactin associated protein
AP	Action potential
TTX	tetrodotoxin
PND	postnatal day
E	Embryonic day
AGC	axo-glial current
VGKC	voltage-gated potassium channel
VGNaC	voltage-gated sodium channels
PSP	postsynaptic potential
TBS	theta burst stimulation
ER	endoplasmic reticulum
NCX	Na^{+}-Ca^{2+} exchanger
SOCC	store-operated calcium channel
TRP	transient receptor potential
CDK	cyclin-dependent kinase
CAK	CDK activating kinase
CKI	CDK inhibitor
mEPSCs	Miniature excitatory postsynaptic currents
LVA	Low-voltage-activated Ca^{2+} channels
HVA	High-voltage-activated Ca^{2+} channels
IP	Intraperitoneal
TMX	tamoxifen
YFP	Yellow Fluorescent Protein
GFP	Green Fluorescent Protein
CC1	anti-adenomatous polyposis coli clone CC1
PNW	Postnatal week
RW	Regular wheel
CW	Complex Wheel
CDF	Cumulative Distribution Frequency
ACSF	Artificial cerebrospinal fluid
RPM	Rotation per minute

C1	First day in complex wheel
C6	Last day in complex wheel
R2	Last day in regular wheel

1 Introduction

It goes without saying that individuals belonging to the same species remain unique among their peers. Reactions to their environment are unique for each individual and the explanation for this individuality remains under investigation in the psychology field of research. Behavioral experiments attempt to answer this question. However, to fully decipher the unique individual behavior, we have to understand its biological substrate. Neuroscience opened the Black Box of the Brain by not just analyzing its inputs and outputs but delving into its inner working. Since the brain was identified as the biological substrate for behavior, biologists started to investigate the main questions emerging from the psychology field. Neuroscience explains the human behavior through their brain function. Advancement of today's technology allows us to investigate the brain in a nanoscopic scale. Each component and function of brain structures, networks and cells can be unraveled. Therefore, one can aim to finally understand how the brain physiology determines individual behaviors.

The brain is composed of two main classes of cells: neurons and glia cells. Neurons are electrically excitable cells communicating with each other via synapses. They are known as the main component of the nervous system. Glia were discovered in the 19th century when it became possible to describe their morphology using the resolution provided by microscopes. They were called glial cells because they were thought to have no other role than to glue neurons together and maintain the neuronal network architecture. Currently, glia cells are classified in 4 main types: microglia, astrocytes, oligodendrocytes and oligodendrocyte precursor cells. Further investigations have shown an essential role for glia to maintain neuronal function. At different stages of life, glia may have different roles in establishing and maintaining the structure and function of the neuronal network (Allen & Lyons, 2018). A constant bidirectional interaction between glial cells and neurons determines their fate. For example, during the myelination process, neuronal activity increases the production of oligodendrocytes. In return, oligodendrocytes myelinate the axons and increase the neuronal conduction velocity (Allen & Lyons, 2018).

1.1 Properties of Oligodendrocyte lineage cells

Oligodendrocytes are key cells in the evolution of the brain. They extend their processes and wrap axons with a myelin sheath. Gaps between two myelin sheaths are called node of Ranvier and are the place where the neuronal signal is transmitted in a saltatory manner along the axon from one node to the next until it reaches the presynaptic site (Bercury & Macklin, 2015). This form of electrical transmission increases the conduction velocity. Hence, it speeds up neuronal transmission. An alteration of the myelin as in multiple sclerosis, induces motor and sensory disorders. This demyelinating disorder shows clearly the importance of myelination. Myelinating oligodendrocytes arise from the differentiation of oligodendrocyte precursor cells (OPCs) also called nerve glial antigen 2 (NG2) expressing cells or NG2 cells. To build a fast transmitting and thus functional central nervous system (CNS), the differentiation of NG2 cells into myelinating oligodendrocytes is critical (Bercury & Macklin, 2015).

1.1.1 Identification of oligodendrocyte lineage cells

First, OPCs were described as oligodendrocyte-type2-astrocyte (O2A) progenitor cells. In vitro studies described the O2A progenitor cells as bipotential progenitors for oligodendrocytes and type-2 astrocytes (Ffrech-Constant & Raff, 1986). Later, in vivo studies failed to identify the bipotentiality of these progenitors, but the O2A cell population was found to express the platelet-derived growth factor alpha receptor (PDGFRα). PDGFRα positive cells were then described as oligodendrocyte progenitors (Espinosa de los Monteros, Zhang, & De Vellis, 1993). In 1996, Nishiyama et al. showed the colocalization of PDGFRα positive cells and non-vascular NG2 positive cells (A. Nishiyama, Lin, Giese, Heldin, & Stallcup, 1996). Currently, the NG2 protein is commonly used as a marker to identify OPCs. The NG2 protein is an integral membrane chondroitin sulphate proteoglycan of 300 kDa expressed by the *cspg4* gene. Since A2B5 ganglioside is present on 95 % of NG2 cells, it can be considered as a marker of the OPCs as well (Akiko Nishiyama, Komitova, Suzuki, & Zhu, 2009b) (Figure1.1).

In addition to NG2 cells markers, their typical morphology helps for their identification. NG2 cell morphological identification is based on their typical highly branched appearance with fine processes equally arranged around a small body size ranging from 5 to 10 µm in

diameter (Sun & Dietrich, 2013). These processes represent 90 % of the cell surface and are very thin, around 200 nm in diameter (Haberlandt et al., 2011; Sun & Dietrich, 2013). NG2 cells downregulate NG2 and PGDFRα along with their differentiation into oligodendrocytes. Oligodendrocytes are then identified by their expression of proteolipid protein (PLP) and the 2',3'-cyclic-nucleotide 3'-phosphodiesterase (CNP) as well as by myelin markers as the myelin basic protein (MBP), the myelin-associated glycoprotein (MAG), or the myelin oligodendrocyte glycoprotein (MOG) (Figure1.1).

Deciphering the role of NG2-expressing cells as OPCs was facilitated by the use of transgenic mice. NG2-Cre or PDGFRα-Cre mouse lines were used for this approach. The production of transgenic mice relies on different methods as the knock-in technique or the Bacterial Artificial Chromosome (BAC) transgenic approach. The knock-in model is a targeted gene insertion into a specific locus in the genome. The BAC transgene is the insertion of a plasmid containing the promoter sequence and the gene to express into a non-specific locus in the genome. In the case of the NG2-Cre BAC transgenic mouse line, Cre was expressed under the NG2 promotor (Zhu, Bergles, & Nishiyama, 2007). As well as in the PDGFRα-Cre BAC transgenic mouse line, Cre was expressed under the PDGFRα promotor. Crossing these transgenic mouse lines with a Cre reporter mouse line was an important step in the field of oligodendroglia research. Cre reporter mouse lines permanently express a marker as a reporter of the cre recombination, a fluorescent protein in general. Cre recombination occurs under the presence of tamoxifen. Crossing the NG2-Cre BAC transgenic mouse line or the PDGFRα-Cre BAC transgenic mouse line with a Cre reporter mouse line contributed to the fate mapping of oligodendroglia lineage cells. The colocalization of the reporter and of mature oligodendrocyte markers proved the origin of oligodendrocytes to be PDGFRα or NG2 expressing cells. Moreover, PDGFRα or NG2 were not expressed anymore in the reporter positive oligodendrocyte cells showing that NG2 cells differentiate into oligodendrocytes and no longer express the progenitor markers (Akiko Nishiyama, Komitova, Suzuki, & Zhu, 2009). Recently, a new marker was found to label the transitory state between the precursor cells and the mature oligodendrocyte. Ectonucleotide pyrophosphatase phosphodiesterase (ENPP6) was found to be present only in pre-oligodendrocytes (Xiao et al., 2016). Henceforth, we will refer to the OPCs or non-vascular expressing NG2 cells, as NG2 cells.

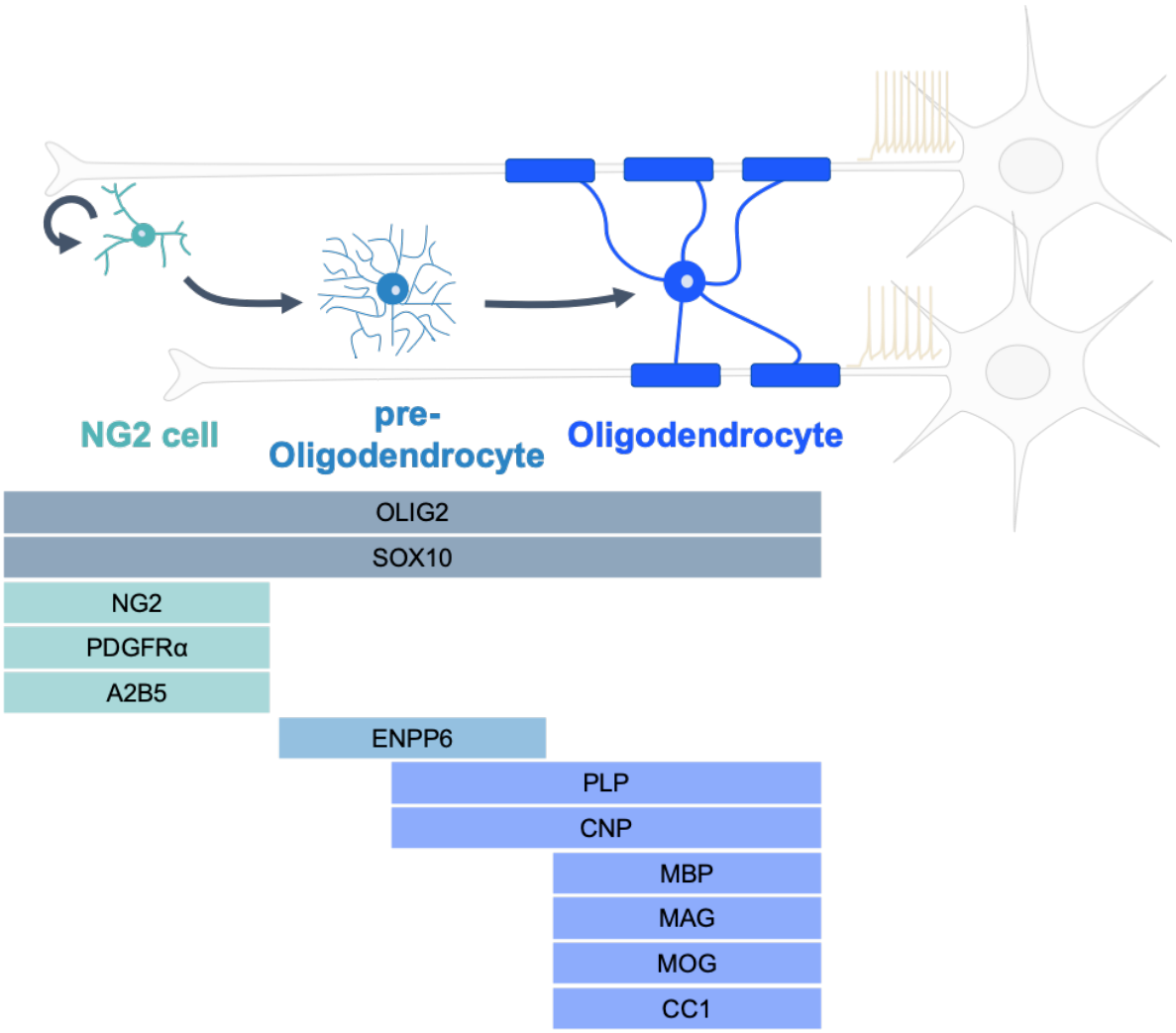

Figure 1.1 Oligodendrocyte lineage cell markers. Schematic representation of NG2 cell, pre-oligodendrocyte, and oligodendrocyte morphology. Identification markers corresponding to each stage of the differentiation in the oligodendroglia lineage are presented below each cell type. OLIG2 and SOX10 are oligodendroglia lineage markers. NG2, PDGFRα, and A2B5 are specific markers for NG2 cells. Enpp6 is only expressed in pre-oligodendrocytes. PLP and CNP are expressed in oligodendrocytes independently of their maturation. MBP, MAG, and MOG are specific markers for myelinating oligodendrocytes. (Adapted from Nishiyama, Komitova, Suzuki, & Zhu, 2009).

1.1.2 Origin of NG2 cells

NG2 cells represent 5 % of brain cells (Dawson, Polito, Levine, & Reynolds, 2003; Pringle & Richardson, 1993). Their maximum number is reached at postnatal day (PND) 3 in the cerebrum (A. Nishiyama et al., 1996). NG2 cells are present ubiquitously through

the CNS, but do not all originate from the same region. Neither are they generated at the same time during development but emerge in different waves. First, on embryonic day (E) 12, Nkx2.1 lineage cells give rise to NG2 cells in the medial ganglionic eminence (MGE) and the anterior entopeduncular region (AEP). In the embryo, a second wave takes place at E 16.5 in the lateral ganglionic eminence (LGE), when NG2 cells originate from Gsh2-expressing precursor cells. Embryonic NG2 cells populate the ventral and dorsal forebrain. However, Nkx2.1-derived-NG2 cells do not persist after birth in the dorsal forebrain. At birth, a third generation wave of NG2 cells emerges from the dorsal neural precursor cells, expressing Emx1 in the cortical ventricular zone (VZ), and populates the dorsal forebrain (Hill, Patel, Goncalves, Grutzendler, & Nishiyama, 2014; Kessaris et al., 2006; Naruse, Ishizaki, Ikenaka, & Tanaka, 2017). In the adult period, a small portion of OPCs derived from the type B cells are created in the subventricular zone (SVZ) (Menn et al., 2006).

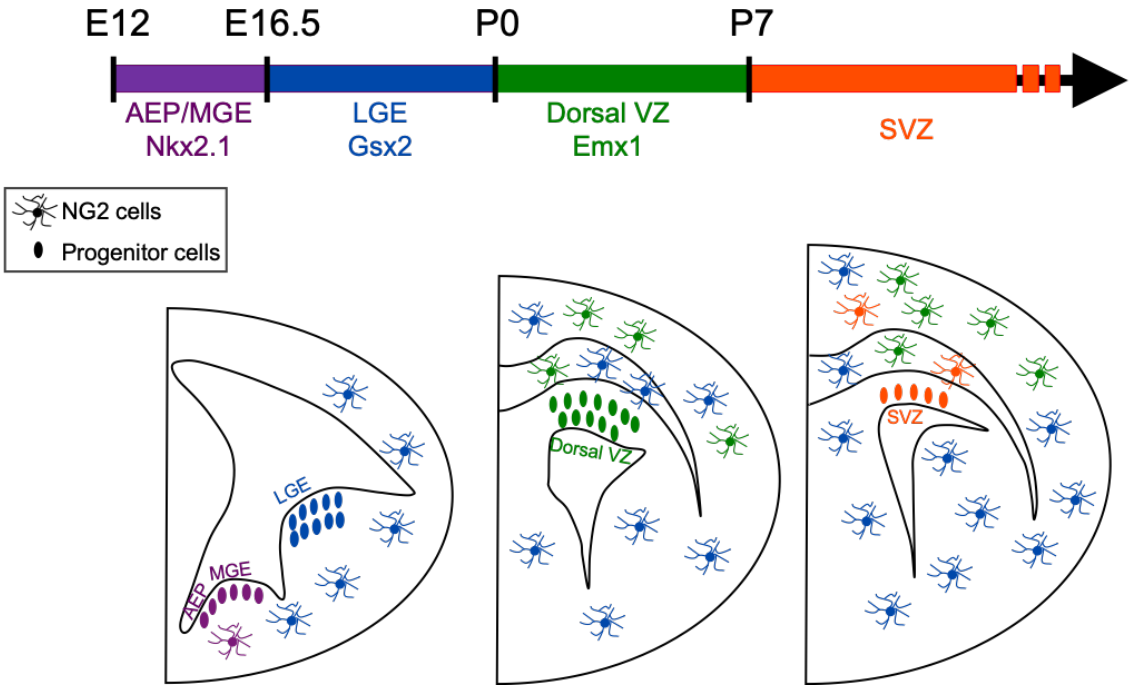

Figure 1.2. NG2 cells origins. Timeline indicating the different waves of NG2 cell generation in the embryonic (E) and the postnatal (P) period. The corresponding brain region and precursor cells are associated with the wave generation date. On the brain hemispheres the distribution of NG2 cells in relation to their region of origin are represented following the timeline of wave generation (modified from Hill et al., 2014).

1.1.3 NG2 cell fate

The main function of NG2 cells is to differentiate into oligodendrocytes. Highly proliferative, they are able to proliferate and migrate in a short time window in order to maintain their coverage throughout the CNS. NG2 cells are able to sense their environment using fine filopodia and can fill the gaps of differentiated or dead NG2 cells either by proliferation or by migration. This exceptional ability to proliferate, results in a replenishment of the NG2 cell population, in 2 to 6 weeks after a massive ablation (Hughes, Kang, Fukaya, & Bergles, 2013; Jäkel & Dimou, 2017).

NG2 cell fate is a choice between proliferation to increase the NG2 cell population or differentiation to produce more oligodendrocytes. Despite an increasing interest in understanding which factors determine NG2 cell fate, the parameters leading NG2 cells to decide for proliferation or differentiation are still unknown.

Currently, we know that NG2 cells first proliferate to produce two NG2 daughter cells. Later, NG2 cells will either remain as they are or differentiate into oligodendrocytes in 2 to 3 days. Their proliferation and differentiation rate depends on the developmental stage and the brain area (Dimou & Gallo, 2015). Early during development, pre-oligodendrocytes are detected at PND 8. Myelinating oligodendrocytes are detected around PND 13 with only some myelinating processes. Finally, fully myelinating oligodendrocytes are present in the brain starting from PND 18 (Kukley, Nishiyama, & Dietrich, 2010). The peak of proliferation occurs during the first week of life and the differentiation of NG2 cells peaks during the second postnatal week (Akiko Nishiyama et al., 1999).

The proliferation speed of a cell population relies on two parameters. First, the growth fraction is the percentage of actively dividing cells. Second, the cell cycle length is the time for an NG2 cell to divide into two daughter cells. To enter the cell cycle, the cells must leave the resting phase (G0) to enter the G1 phase. According to the timeline of the cell cycle, the NG2 cell will enter subsequently the S phase, the G2 phase, and finally the M phase. During the S phase, the DNA is replicated to create the DNA material for the two future daughter cells. During the M phase, also called the mitotic phase, the two separated daughter cells are generated. They undergo metaphase, where the DNA material lines up in the cell center. Then comes the anaphase, when the DNA replicates are equally

separated to each side of the cell. Finally, during the telophase, the membranes of the two daughter cells are created around each DNA replicate (Figure 1.3).

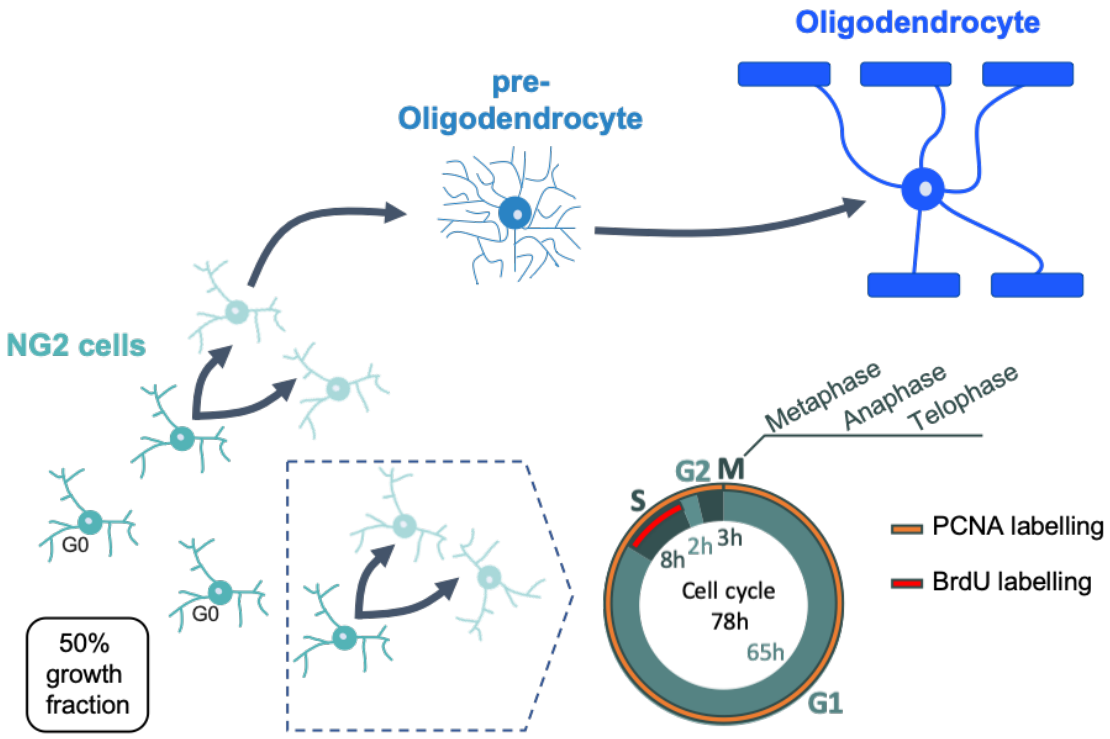

Figure 1.3. NG2 cell fate and cell cycle. The fraction of dividing NG2 cells represents 50 % of the population. About half of all NG2 cells are in the resting phase (G0) and the other half are cycling to produce daughter cells. The daughter cells will remain as NG2 cells or differentiate into oligodendrocytes. The NG2 cell cycle lasts for 78 hours including 65 hours in G1 phase, 8 hours in S phase, 2 hours in G2 phase and 3 hours in M phase. NG2 cell cycling are labeled by PCNA through the whole cell cycle and by BrdU in S phase only.

To study proliferation, the endo-markers, proliferating cell nuclear antigen (PCNA) and Ki67, and the external marker, bromodeoxyuridine (BrdU), are commonly used. BrdU is an analog of thymidine that integrates into replicating DNA during the S-phase. Afterwards, BrdU can be revealed via immunohistochemistry. Using a cumulative BrdU labeling in order to constantly expose NG2 cells to BrdU and a co-labeling with PCNA, Kukley et al. in 2008 determined the cell cycling speed of postnatal NG2 cells to last for 78 hours. The S phase was estimated to last for 8 hours in NG2 cells. After 6 hours of BrdU exposition, NG2 cells already displayed a mitotic-like DNA figure (Kukley et al., 2008). This finding indicates that the NG2 cell G2 phase is short (Figure 1.3). Overall, the

fraction of proliferating NG2 cells, also called growth fraction, was estimated at 50 %. Only half of the NG2 cell population takes part in the proliferation process. This finding was supported by additional studies looking at the NG2 cell fate using other transgenic mouse lines (Dimou, Simon, Kirchhoff, Takebayashi, & Götz, 2008; Psachoulia, Jamen, Young, & Richardson, 2010; Rivers, Young, Rizzi, & Jamen, 2008).

Using the PDGFRα-Cre or O lig2-Cre mouse lines, NG2 cell fate was studied for several developmental stages. NG2 cell proliferation was assessed with a cumulative BrdU protocol where NG2 cells are exposed to BrdU for several consecutive days. The proportion of BrdU positive cells in the cell population of interest, NG2 cells or oligodendrocytes, gives an idea of the proliferation and differentiation rate during this time. Comparative experiments between different brain structures and animal ages provided a better understanding of the NG2 cell fate heterogeneity in the brain. Early in life, NG2 cells need to populate the CNS as well as to produce oligodendrocytes for myelination to occur. Hence, perinatal NG2 cells show a higher proliferation and differentiation rate than late postnatal and adult NG2 cells. As the white matter is mainly composed of axons, it has a higher need for axonal myelination compared to grey matter that contains the neuronal cell bodies. NG2 cell proliferation and differentiation rates in the white matter are indeed increased in comparison to the grey matter (Dimou et al., 2008; Psachoulia et al., 2010; Rivers et al., 2008; Zhu et al., 2011). Even if oligodendrocytes are still produced in the adult grey matter, it seems that a great fraction are unmyelinating oligodendrocytes compared to the white matter (Rivers et al., 2008).

1.1.4 Myelination by oligodendrocytes

Oligodendrocytes myelinate axons to increase the conduction velocity of the neuronal signal. They are crucial for the CNS function. The perturbation of myelin formation or maintenance leads to motor or cognitive impairment (Czopka & Auer, 2017).

During the myelination process, several myelin segments are placed next to each other. They are called internodes because they are bounded by unmyelinated axonal segments called nodes of Ranvier (Figure 1.4). An enrichment of voltage-gated sodium channels (VGNaC) at the node of Ranvier allows for a fast saltatory electrical conduction of the action potential (AP) from node to node. Therefore, the electrical signal is carried

through the axon up to the pre-synaptic site regardless of its length (Czopka & Auer, 2017).

Axonal insulation takes place with the myelin sheath enwrapping of multiple layers around the axon. The myelin layer in contact with the axon is the inner tongue and the myelin layer the closest to the oligodendrocyte cell body describes the outer tongue (Figure 1.4). At the node of Ranvier, the different membrane layers of the myelin are anchored to the axon from the outer to the inner layer, in the direction of the node to the myelinated segment. This part is called the paranode (Figure 1.4). The proteins involved in the anchoring of the myelin to the axon are the Contactin associated protein (Caspr), contactins, and neurofascin (Snaidero & Simons, 2014).

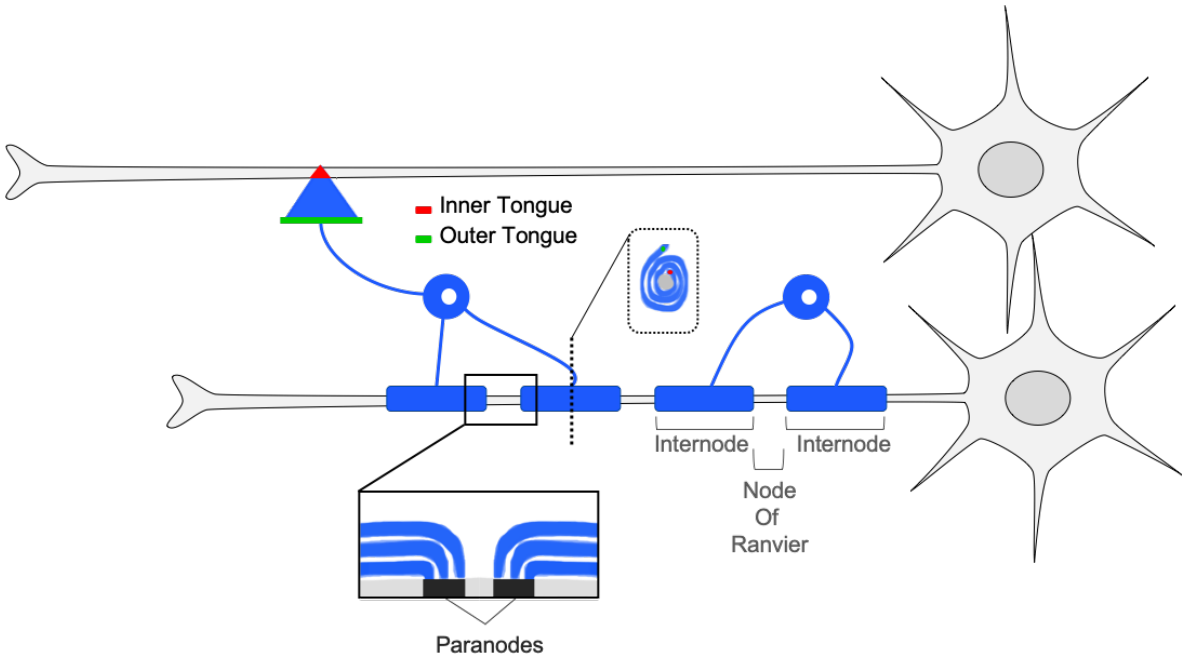

Figure 1.4. Axonal Myelination. Oligodendrocyte processes contact the axon and start the axonal enwrapping from the inner tongue (red) to the outer tongue (green). The myelin sheath is the superposition of several layers of myelin, with the inner tongue being the closest to the axon and the outer tongue the closest to the oligodendrocyte. Along the axon, the myelin sheath segments are called internodes and the gaps in-between are called nodes of Ranvier. The myelin sheath is anchored to the axon at the paranode site.

Myelination starts at birth and the first axons to be myelinated are the thickest ones. The smallest axons begin to be myelinated at PND 20 and the myelination process ends around PND 60. In the cortex or corpus callosum (CC), oligodendrocytes produce 30 to

80 internodes ranging from 20 to 200 µm length with up to 60 layers. Myelinated and unmyelinated axons are found in the range of 0.2 to 0.8 µm axon diameter (Snaidero & Simons, 2014). Therefore, axonal size cannot be the only factor to govern the properties of myelin. Recently, myelination has been implicated in the process of neuronal plasticity. Indeed, the internode length can affect the AP conduction speed. Ford et al. in 2015 demonstrated how myelination controls spatial hearing by modulating the timing of the action potential arrival at the auditory brainstem (Ford et al., 2015). An efficient neuronal signal depends on the fine tuning of the timing of the signal transmission. It allows for the coincidence detection of neuronal signals, which relies on the synchrony of several neuronal networks. In the cortex, the axons are not fully myelinated (Tomassy et al., 2014). These unmyelinated gaps leave the opportunity to influence the conduction speed. In the same way, complex motor skill acquirement has been shown to depend on the generation of newly created oligodendrocytes (McKenzie et al., 2014). Furthermore, the myelination process is not as slow as we thought. In zebrafish, stable myelin processes originating from newly created oligodendrocytes can be produced in 5 hours, which places myelination as a fast plasticity mechanism (Czopka, ffrench-Constant, & Lyons, 2013).

1.1.5 Neuronal activity modulates NG2 cell fate

It is well accepted that neuronal activity is necessary for the myelination process. Blocking neuronal activity in the optic nerve by application of tetrodotoxin (TTX) decreases myelination (Demerens et al., 1996). Since NG2 cell rate of differentiation defines the speed of myelination, NG2 cell fate should be under tight regulation of the myelination requirement for the neural network establishment. Indeed, NG2 cell fate has been shown to be modulated by neuronal network activity. Axonal electrical activity is correlated to an increase in NG2 cell proliferation (Barres & Raff, 1993). Similarly, electrical stimulation increases their proliferation rate (Keiner et al., 2017; Mitew et al., 2018). Therefore, NG2 cells have the ability to integrate the surrounding neuronal activity.

1.2 Electrical properties of NG2 cells

1.2.1 NG2 cells receive direct neuronal synaptic input

Amongst glial cells, NG2 cells have the unique feature to receive direct synaptic input from neurons. This feature was first described by Bergles et al. in 2000 in the rat hippocampus (Bergles, Roberts, Somogyi, & Jahr, 2000). Later, axo-glial currents (AGCs) were recorded in NG2 cells of the corpus callosum (Kukley et al., 2010). Several experiments have provided proof of direct synaptic input onto NG2 cells in the grey matter and white matter. Firstly, NG2 cells display a fast rising AMPARs mediated post-synaptic current dependent on calcium releasing machinery at the pre-synaptic site. Secondly, these AMPARs currents, evoked by stimulation of the presynaptic component, are sensitive to TTX. Thirdly, miniature excitatory postsynaptic currents (mEPSCs) were recorded from NG2 cells arguing for vesicular release. Finally, electron micrographs show NG2 cells processes filled with biocytin affixed to neuronal sites containing synaptic vesicles (Bergles et al., 2000; Haberlandt et al., 2011; Kukley, Capetillo-Zarate, & Dietrich, 2007).

Throughout life, NG2 cell – neuron synapses are present in the grey and white matter (De Biase, Nishiyama, & Bergles, 2010; Ziskin, Nishiyama, Rubio, Fukaya, & Bergles, 2007). Despite their high proliferation dynamics, all NG2 cells have synaptic contacts. Although, we would expect some NG2 cells to be immature and lack synapses immediately after division, Kukley et al. in 2008 explained how NG2 cells by inheriting their synapses during their division are able to constantly assess the neural network activity (Kukley et al., 2008). Constant synaptic contact with neurons may increase their speed of colonization and myelination. In addition, synaptic plasticity dependent on calcium signaling through AMPARs takes place in NG2 cells. This finding enlightens the physiological importance for NG2 cells to receive direct synaptic input form neurons (Woo-Pin Ge et al., 2006). Synaptic currents in NG2 cells were detected from PND 5 on with small amplitudes (Kukley et al., 2010). The synaptic current amplitude increases during development until PND 20 – PND 30, in a more mature state of the CNS (Ziskin et al., 2007). In the white matter, the quantal response is estimated at 6 pA. By evoking a maximal response through axonal stimulation in the corpus callosum, one OPC was estimated to be contacted by 141 axons. Therefore, the density of synaptic input into NG2

cells is supposed to represent one synaptic input every 14 μm^2 on the NG2 cell membrane (Kukley et al., 2007). Two types of NG2-neuronal synapse morphology exist in the grey matter: either as a direct contact between NG2 cell process and neuronal pre-synapse or as a third party where the NG2 process shows an inclusion in the synaptic cleft of a neuron-neuron synaptic contact (Bergles et al., 2000).

Amongst the oligodendroglia lineage cells, only NG2 cells receive direct synaptic input from neurons. During the maturation of NG2 cells into oligodendrocytes, there is a decrease in spontaneous synaptic currents, the synaptic connections get lost (De Biase et al., 2010; Kukley et al., 2010). AMPAR expression is downregulated and glutamate transporters are upregulated during the differentiation process. Mature oligodendrocytes have the ability to detect the overall network activity but not as precisely as their precursors, NG2 cells (Kukley et al., 2010).

1.2.2 Synaptic input integration into NG2 cells

NG2 cells have a resting membrane potential of approximately -85 mV. Three main channels are implicated in the response of NG2 cell to voltage step induction. In the order of activation, first, the fast voltage-activated sodium channels, with a short time constant activation below 0.5 ms and a short deactivation, lead to NG2 cell depolarization. Second and third, the A-type potassium channels and delayed-rectifier potassium channels lead to NG2 cell repolarization (Sun & Dietrich, 2013). Because the resting membrane potential is close to the potassium equilibrium (-80 mV), it seems logic to think that the potassium channels are responsible for maintaining the resting membrane of NG2 cells. (Larson, Zhang, & Bergles, 2016).

NG2 cells integrate direct glutamatergic and GABAergic synaptic input through AMPARs and $GABA_A$ receptors, respectively recognized as the main glutamatergic and GABAergic receptors expressed in NG2 cells. The NMDA receptor is present on NG2 cells, but it is not crucial for synaptic input integration (Kukley & Dietrich, 2009). Both Glutamatergic and GABAergic synaptic input results into NG2 cell depolarization. Due to the high chloride concentration in NG2 cells compared to the external chloride concentration, the reversal potential of $GABA_A$ receptors are increased to -40 mV in NG2 cells. Hence, $GABA_A$ receptor activation induces a depolarization of NG2 cells (Lin and Bergles, 2004).

Although NG2 cells do not fire AP, they express voltage-gated calcium channels (VGCCs) to integrate synaptic input through calcium signaling (Lin & Bergles, 2004). VGCCs are composed of low voltage-activated calcium channels (LVA) and high voltage-activated calcium channels (HVA). The LVAs are activated at -70 mV and present a small and transient current. In contrast, HVAs are activated at -20 mV and present a large and long-lasting current (Catterall, Perez-reyes, Snutch, & Striessnig, 2005). Using RT-PCR, all VGCCs types were detected in NG2 cells. The L-type and R-type VGCCs are the predominant ones, whereas the P/Q type and N-type channels are expressed only in a small amount (Haberlandt et al., 2011). The deletion of the Cav1.2 subunit, present in the L-type VGCCs, was shown to decrease the calcium response after NG2 cell depolarization by 75 % (Cheli, Santiago González, Spreuer, & Paez, 2015). This result implies that L-type calcium channels would be mostly responsible for the depolarization-induced calcium transient. Later, Sun et al. in 2016 determined which VGCCs are involved in the calcium signal induced by synaptic input. A train of mock post-synaptic potentials (PSP), mimicking the glutamatergic input, induces calcium transients in the soma and processes of NG2 cells which were sensitive to cadmium and nifedipine. Therefore, R-type and T-type calcium channels are the VGCCs mainly responsible for the calcium transients induced by mock PSPs recording in NG2 cells (Sun, Matthews, Nicolas, Schoch, & Dietrich, 2016).

1.2.2.1 AMPA receptors in NG2 cells

NG2 cells glutamatergic synaptic currents are mediated by AMPARs (Kukley et al., 2007). The heterotetrameric receptor is composed of the GluA1, GluA2, GluA3, and GluA4 subunits association. The GluA2 subunit is also called GluR-B or GluR2. It is known that AMPARs have the ability to be permeable or impermeable to calcium ions depending on their composition. On one hand, the presence of the GluA2 subunit in the AMPAR determines the calcium permeability of the receptor due to the presence of an arginine at the Q/R site in the pore. This positively charged amino acid prevents calcium to pass through the pore of the GluA2-containing AMPAR. On the other hand, the GluA2-lacking AMPAR is permeable to calcium with a glutamine edition at the Q/R site (Figure 1.5). GluA2-containing AMPARs are the most commonly expressed form of AMPARs. However, the GluA2 insertion in AMPARs is highly dynamic and depends on neuronal

activity. A decrease in AMPARs stimulation leads to an increase of GluA2-lacking AMPARs in neurons (Cull-candy, Kelly, & Farrant, 2006). The GluA2-lacking AMPARs are polyamine sensitive. Extracellular philanthotoxin application or intracellular spermine application blocks the GluA2-lacking AMPARs. Resulting in an inward rectification of the I/V curve in presence of polyamine when GluA2-lacking AMPARs are expressed (Figure 1.5).

The expression of GluA2-lacking AMPARs in NG2 cells depends on the animal age and the brain region. In the white matter, NG2 cells of adult rodents express GluA2-lacking AMPARs, although postnatal NG2 cells only express GluA2-containing AMPARs (Ziskin et al., 2007). Moreover, in young animals, GluA2-lacking AMPARs are expressed in grey matter NG2 cells but not in the white matter (Kukley et al., 2007; Woo-Pin Ge et al., 2006).

The presence of synaptic currents in NG2 cells does not seem to predict NG2 cell differentiation into myelinating oligodendrocytes. Indeed, NG2 cells are ubiquitously localized in the brain and receive synaptic input in the white matter as well as in the grey matter although the number of myelinating oligodendrocytes is more abundant in the white matter. However, the calcium permeability of AMPARs seems to change according to the myelination demand. The high demand for myelination in the white matter of young animals correlates with the expression of GluA2-containing AMPARs, impermeable to calcium. GluA2-containing AMPARs synaptic currents seem to be a crucial point in NG2 cell behavior.

The regulation of GluA2-lacking AMPARs and GluA2-containing AMPARs balance is tightly controlled and highly dynamic in NG2 cells. Metabotropic glutamatergic receptors activation in NG2 cells induces an increase of GluA2-lacking AMPARs currents. Contrarily, ATP increases the GluA2-containing AMPARs currents in NG2 cells (Zonouzi, Renzi, Farrant, & Cull-Candy, 2011). The GluA2-lacking AMPARs are recruited in NG2 cells after a tetanic burst stimulation of the Schaffer collateral synapses. Indeed, a long-term potentiation dependent on the GluA2-lacking AMPARs currents and the calcium signaling takes place in NG2 cells (Woo-Pin Ge et al., 2006). The GluA2 subunit insertion in AMPARs is dependent on neuronal activity. This plasticity in the AMPARs subunit composition supposes an important role for the AMPARs in synaptic integration of NG2

cells. In consequence, it also supposes a role for AMPARs in the process of NG2 cells to adapt their fate to the surrounding neuronal activity.

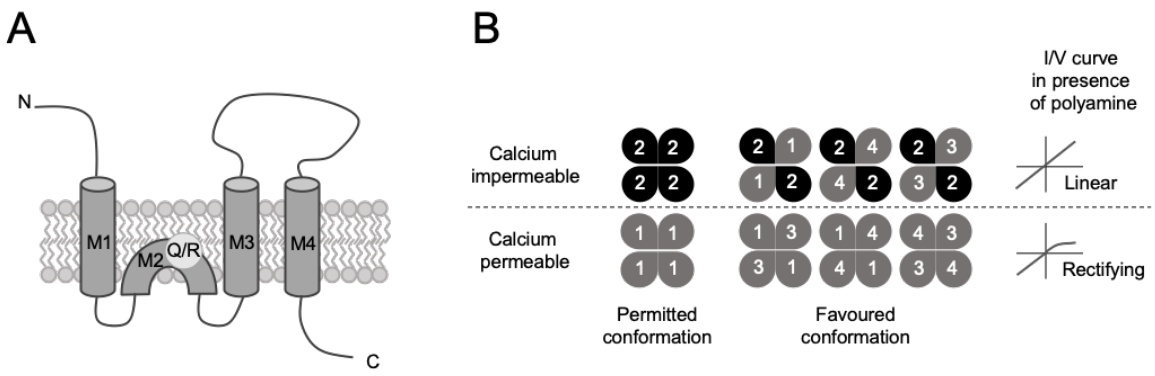

Figure 1.5. GluA2 subunit insertion in AMPAR composition. A. AMPAR subunits are composed of four membrane domains, M1 to M4. M2 contains the Q/R site, where an arginine is edited for the GluA2 subunit and a glutamine is edited for the other subunits. B. The AMPAR is a dimer of dimers, a schematic representation of the permitted and favored conformations is depicted in the top row for GluA2-containing AMPARs and the bottom row for the GluA2-lacking AMPARs. The corresponding calcium permeability and I/V curve shape are respectively depicted for each AMPARs subtype.

1.2.2.2 Modulatory effect of AMPARs on NG2 cell fate

The observation that NG2 cell fate is regulated by neuronal activity and that NG2 cells sense the release of neurotransmitter via receptors like AMPA and GABA, suggests that these receptors play a role in the NG2 cell fate.

AMPAR activation has been correlated to a decrease in NG2 cell proliferation and differentiation. Blocking the AMPAR activation in organotypic slices increases BrdU incorporation in NG2 cells and the number of oligodendrocytes among the oligodendroglia lineage cells (Fannon, Tarmier, & Fulton, 2015). Also in culture, the application of the AMPAR antagonist, DNQX (6,7-dinitroquinoxaline-2,3-dione), increases the number of O2A cells (Gallo et al., 1996). The application of an AMPAR agonist on organotypic slices decreases BrdU incorporation in NG2 cells and the levels of CNP mRNA, which suggests a decrease in differentiation (Yuan, Eisen, McBain, & Gallo, 1998). In contrast, the application of AMPARs agonist increases the BrdU incorporation in the oligodendrocyte lineage cells in cell culture, labeled with the immature oligodendrocyte antigen, O4 marker. Moreover, it increases the number of mature oligodendrocytes, labeled with the O1 marker (Redondo et al., 2007). In summary, the previous findings support the hypothesis that the activity of AMPARs in NG2 cells decrease NG2 cell

proliferation and differentiation (Fannon, Tarmier, & Fulton, 2015 Yuan, Eisen, McBain, & Gallo, 1998; Gallo et al., 1996). However, controversial results claim the opposite (Redondo et al., 2007), and neuronal activity seems to favor NG2 cell proliferation and differentiation to establish axonal myelination (Barres & Raff, 1993; Li, Brus-Ramer, Martin, & McDonald, 2010). Furthermore, the above investigations of the AMPARs activity on the NG2 cell fate are based on cell cultures or organotypic slice cultures that fail to represent the physiological environment of NG2 cells. Additional in vivo experiments are needed to finally determine the role of AMPARs in NG2 cells fate.

1.3 Calcium signaling in NG2 cells

Although NG2 cells do not fire AP, calcium acts as a second messenger in NG2 cells to integrate their synaptic input. Therefore, studying calcium signaling in NG2 cells contributes to decipher the role of synaptic input in NG2 cells.

Calcium signaling describes a transient increase of the intracellular calcium concentration which is dependent on calcium entry and calcium extrusion. Extracellular calcium can enter the cell through different types of channels: ligand-gated ion channels, and VGCCs. Moreover, calcium can be released from internal stores as the endoplasmic reticulum (ER) or the mitochondria. To decrease the intracellular calcium concentration, calcium extrusion is processed through the Na^{+}-Ca^{2+} exchanger (NCX), ATP-dependent pumps, or captured by internal stores (Butt, 2006).

1.3.1 Glutamatergic synaptic input induces calcium signal in NG2 cells

Synaptic input elicits calcium response in dendrites of NG2 cells. As seen above, NG2 cells receive glutamatergic synaptic input and they express glutamatergic ligand channels as NMDARs and AMPARs. Localized glutamatergic release on dendrites of NG2 cells elicits calcium response in NG2 cells (Sun et al., 2016). Because the NMDARs are not associated with the synaptic input-induced calcium transient in NG2 cells (Kukley et al., 2007), we focus on AMPARs. As a direct effect of glutamatergic synaptic input, only the activation of GluA2-lacking AMPARs which are permeable to calcium, can lead to an intracellular calcium transient. Calcium signals induced by glutamate bath application were reduced by 40 % in NG2 cell somas when the GluA2-lacking AMPARs were blocked

by spermine in NG2 cells (Woo-Pin Ge et al., 2006). This result suggest that calcium signal induced by glutamatergic application depends on GluA2-lacking AMPARs. Unpublished data from our laboratory, demonstrated the role of GluA2 subunit in calcium signal in response to glutamatergic input. GluA2 subunit deletion in NG2 cell resulted in an increased calcium signal in response to glutamatergic uncaging stimulation on NG2 cell dendrites. This result suggests that the GluA2-containing AMPARs expression decrease the calcium entry in response to glutamatergic input in NG2 cells. Further investigations are needed to determine the role of GluA2 subunit expression in the regulation of calcium signaling in NG2 cells.

1.3.2 Calcium transient properties in oligodendrocyte lineage cells

Up to now, the calcium transients in NG2 cells have been studied in most detail in zebrafish. This animal model allows cell development tracking through in vivo recording, fast gene manipulation, and imaging through its transparent membrane. With all these features, it is possible to characterize in the zebrafish changes in the intracellular calcium concentration during the maturation of NG2 cells. As described before, neuronal activity triggers calcium transients in NG2 cells. Their properties differ between the soma and the processes. After neuronal activity, most of the calcium transients occur in the processes rather than in the soma of NG2 cells. They present a higher frequency and duration in the processes. However, during the differentiation, calcium transients decrease in the processes (Krasnow, Ford, Valdivia, Wilson, & Attwell, 2018) which suggest synaptic input to occur in the processes of NG2 cells.

Additionally, calcium transients were recorded during myelin sheath establishment in the zebrafish. Calcium transient properties were found to be linked to sheath development (Krasnow et al., 2018). Newly forming myelin sheaths exhibit local changes in the intracellular calcium concentration. The calcium transient duration and frequency determine myelin behavior. High amplitude, long lasting and low frequency calcium transients favor myelin sheath retractation. On the contrary, myelin sheath growth is correlated to short and high frequency calcium transients (Baraban, Koudelka, & Lyons, 2018; Krasnow et al., 2018). The myelination is suggested to depend on calcium signaling. Since the NG2 cells also receives synaptic input which triggers calcium transient in the

processes of NG2 cells. Calcium signaling seems to play a role in the behavior of oligodendroglia lineage cells.

1.3.3 The role of calcium signaling in NG2 cell fate

As a second messenger protein, calcium is crucial for downstream signaling. Calcium has the ability to change the conformation of proteins by modifying their electrostatic field. It regulates kinases which in turn act on gene expression. Calcium entry through AMPARs induces immediate early gene activation. As well, neuroligands increase the phosphorylation of ERKs and CREB in a calcium dependent manner in O2A progenitors (Pende, Holtzclaw, Curtis, Russell, & Gallo, 1994). Calcium can act through different pathways as PKC, CREB, CamKII, or CamKIV to modify NG2 cell proliferation (Soliven, 2001). Indeed, ERK and CREB activation are involved in the regulation of transcription of genes linked to proliferation and differentiation (Soliven, 2001).

In NG2 cells, calcium signaling was linked to different properties as migration, proliferation, and differentiation. For example, the Golli proteins potentiate calcium signaling in NG2 cells and affect their migration, maturation, and morphology. Calcium transients tend to decrease the exploration behavior of NG2 cells, such as migration and processes motility (Paez et al., 2007, 2009). In addition, Golli proteins deletion affects oligodendrocyte maturation and their morphology (Fulton et al., 2010).

Calcium signaling in NG2 cells must play a role in NG2 cell fate through cell cycle modulation. The cell cycle is regulated by cyclin-dependent kinases (CDKs): either by the CDK activating kinases (CAKs) or by the CDK inhibitors (CKIs) which, respectively, favor or inhibit the cell cycle progression. Through its downstream pathways, calcium regulates the CDKs (Yang, Xiong, & Yao, 2013). Expression of the p27 CKI increases after AMPARs activation and stops the cell cycle of NG2 cells (Ghiani et al., 1999).

Through the modulation of the activity of various kinases and CDKs, calcium plays a crucial role in regulating the cell cycle progression. Calcium signaling induced by synaptic input in NG2 cells might play a role in regulating the cell cycle progression.

1.4 Aim of the study

OPCs, also known as NG2 cells, can proliferate and differentiate into myelin-producing oligodendrocytes throughout life. While it has been established that neuronal activity influences the speed and degree of axon myelination, the factors mediating activity-dependent control of NG2 cell fate have not been resolved yet. Direct neuronal synaptic input onto NG2 cells is the main candidate to regulate NG2 cell fate in response to neuronal activity. Glutamatergic input integration is mainly mediated by AMPARs in NG2 cells. During the postnatal period, AMPARs contain the GluA2 subunit, which renders AMPARs calcium impermeable. However, later in life, NG2 cells downregulate the expression of the GluA2 subunit. Thus, the decline of the proliferation rate of NG2 cells observed during the transition from the postnatal to the adult period is mirrored by an increase in calcium permeability of synaptic AMPARs.

In this thesis, we aimed at experimentally addressing the hypothesis that the GluA2 subunit plays a role in the oligodendroglia lineage cells fate by deleting the GluA2 subunit in NG2 cells in the perinatal period and following the fate of NG2 cells and oligodendrocytes. In order to follow NG2 cells fate and delete the GluA2 subunit in NG2 cells, we use a transgenic mouse line, where GluA2 subunit is deleted and a fluorescent reporter is expressed when Cre is conditionally expressed under the NG2 promotor. NG2 cells fate mapping is followed by immunohistochemistry and cell counting.

To pursue our main goal, we pursue the following aims:

- Aim 1: Determine the role of the GluA2 subunit on NG2 cell proliferation.
  We assess the different parts of the cell cycle of NG2 cells using specific markers. In addition, we investigate the role of GluA2 subunit on cell death with the caspase-3 marker.

- Aim 2: Determine the role of the GluA2 subunit on differentiation.
  NG2 cell differentiation is followed in the early and late postnatal days to account for a delayed effect of GluA2 subunit deletion on the number of oligodendrocytes.

- Aim 3: Determine the role of the GluA2 subunit on myelinating properties of oligodendrocytes.

We investigate myelin properties by measuring the internodes length in the early and late postnatal period.

- Aim 4: Determine the role of the GluA2 subunit on motor learning.
  The physiological role of the GluA2 subunit in NG2 cells is investigated in the running wheel motor learning task through the assessment of the NG2 cell proliferation, the motor learning performance and the myelinating oligodendrocyte properties.

2 Materials and methods

2.1 Animals

In order to assess the role of GluA2 subunit in NG2 cells, we conditionally deleted the GluA2 subunit in NG2 cells. With this aim, we used a triple transgenic mouse line, crossing three different transgenic mice lines: NG2creER^{TM}BAC, GluRB$^{lox/lox}$, ROSA26/EYFP (Figure 2.1).

The NG2creER^{TM}BAC mouse line was produced with the BAC modification technique, where the nls-cre cDNA was inserted after the first exon of the *ng2* gene (Zhu et al., 2011). In the NG2CreER^{TM}BAC mouse line, the Cre system is induced under the NG2 promotor by the presence of tamoxifen. When tamoxifen conditionally induces Cre expression in NG2 cells, they are defined as recombined NG2 cells.

The GluRB$^{lox/lox}$ mouse line consists of gene-targeted mice with a floxed GluRB gene (*Gria2*) at the exon 11 (Shimshek et al., 2006). Both, GluRB and GluA2 designate the second subunit of AMPARs. Heterozygous mice, GluA2$^{wt/lox}$, were inter-bred to obtain homozygous GluA2$^{lox/lox}$ and GluA2$^{wt/wt}$, required for our experiments. When Cre recombination takes place in GluA2$^{lox/lox}$ animals, the floxed sequence on the exon 11 is cut out and NG2 cells stop expressing the GluA2 subunit. In the case of GluA2$^{wt/wt}$ mice, the GluA2 subunit is still expressed.

The ROSA26/EYFP reporter mouse line, produced by Srinivas et al. in 2001, make the use of the ubiquitously expressed ROSA26 locus (Srinivas et al., 2001). The enhanced yellow fluorescent protein (EYFP) cDNA is inserted after the ROSA26 locus. Thanks to the insertion of a loxP-flanked stop sequence before the EYFP sequence, the YFP expression will exclusively report Cre expressing cells. Cre expression leads to the constant EYFP expression by cutting the loxP-flanked stop sequence before the EYFP sequence. Recombined NG2 cells and their progeny will express EYFP. Homozygous and heterozygous ROSA26/EYFP mice were used in the following study.

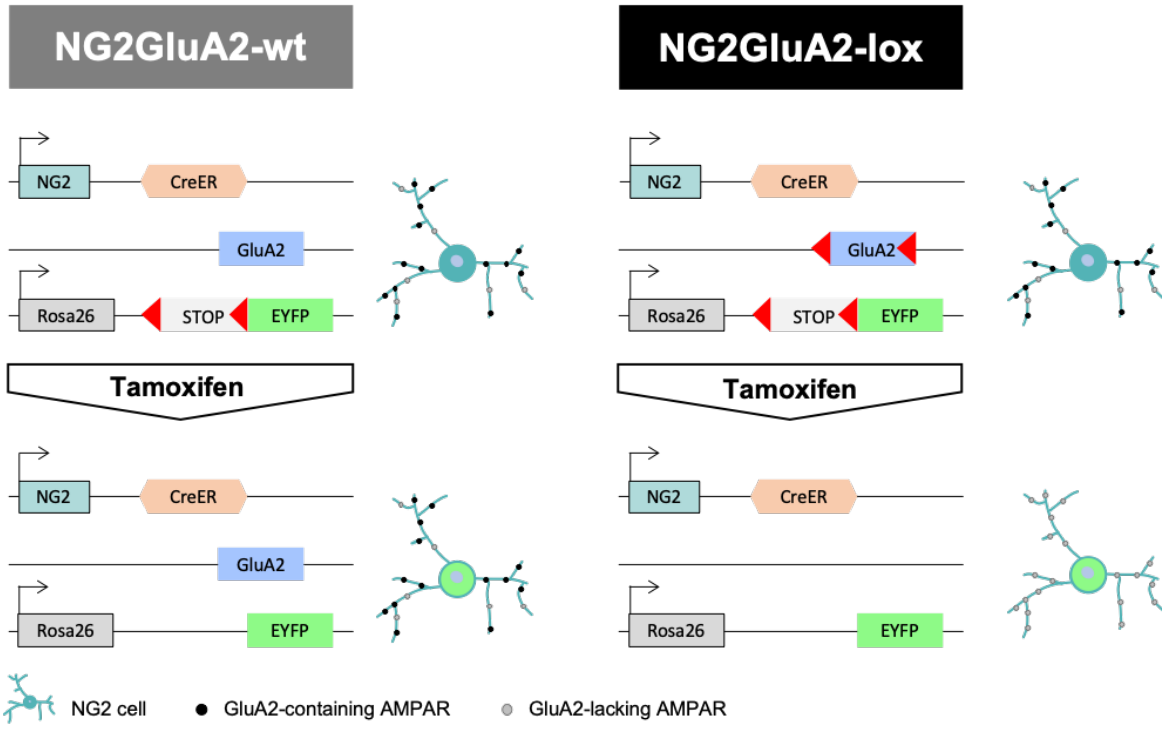

Figure 2.1. GluA2 subunit deletion in NG2 cells expressing the EYFP reporter. Genetic disposition of the mice described as NG2GluA2-wt and NG2GluA2-lox. Tamoxifen application induces the cytoplasmic YFP reporter expression in the recombined NG2 cells of both mice groups: NG2GluA2-wt and NG2GluA2-lox. Tamoxifen induces GluA2 deletion only in the recombined NG2 cells of NG2GluA2-lox mice.

Another triple mouse line was used to look at the internode length of the GluA2 deleted NG2 cells. In order to label the myelin, we chose a mouse reporter line with a membrane bound fluorescent reporter. We replaced the R26EYFP reporter mouse line with the mT/mG reporter mouse line (Figure 2.2). The mT/mG mouse line expresses the membrane tagged tdTomato (mT) ubiquitously. Under Cre activity, recombined NG2 cells express the membrane tagged EGFP (Enhanced green fluorescent protein) (mG). This mouse line was created by Muzumdar et al. in 2007 with the gene targeting technology at the ROSA26 locus. The homozygous and heterozygous mT/mG expressing mice were included in our experiments.

The mice were kept in an animal facility with a 12 hours dark/light cycle. They had access to food and water *ad libitum*. The experiments were performed from E17 until the fifth week of life, in accordance to the guidelines of the Bonn University Medical School Care Committee.

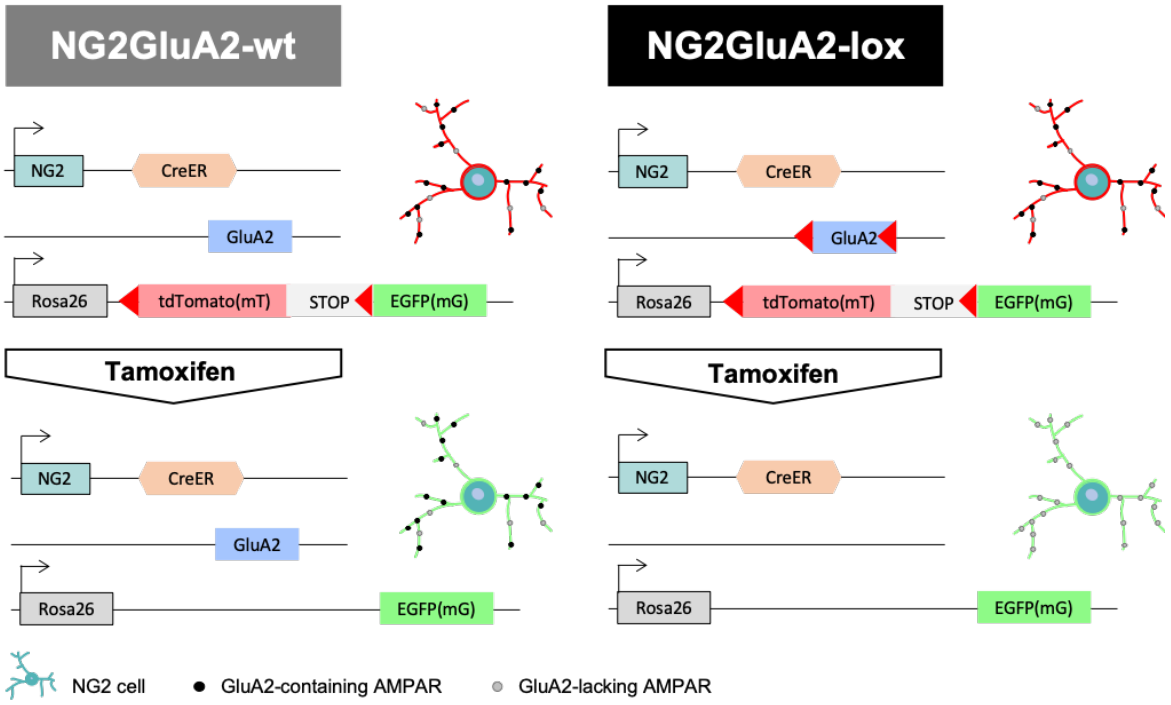

Figure 2.2. GluA2 subunit deletion in NG2 cells expressing the membrane GFP reporter. Genetic disposition of the mice described as NG2GluA2-wt and NG2GluA2-lox. Before tamoxifen expression all the cells express the membranous tdTomato fluorescence. After, tamoxifen application, recombined NG2 cells express the membranous GFP reporter in both mice groups: NG2GluA2-wt and NG2GluA2-lox. Tamoxifen induces GluA2 deletion exclusively in the recombined NG2 cells of NG2GluA2-lox mice.

2.2 Solutions

2.2.1 Slicing solution

For slice preparation, we use the modified artificial cerebrospinal fluid (mACSF) composed of 87 mM NaCl, 2.5 mM KCl, 1.25 mM Na_2HPO_4, 7 mM $MgCl_2$, 0.5 mM $CaCl_2$, 25 mM $NaHCO_3$, 25 mM Glucose, and 75 mM Sucrose (pH 7.4, 95 % CO2, 5 % O2).

2.2.2 Fixative solution

A solution of paraformaldehyde (PFA) at 4 % and a periodate-lysine-paraformadehyde (PLP) fixative solution was used for the tissue fixation. 4 % PFA (pH 7.4) was dissolved in 1 mM Phosphate buffer saline (PBS). The PLP fixative solution (pH 7.4) is composed of 3 % PFA, 75 mM L-Lysine, 10 mM INaO4 dissolved in 0.1 M

phosphate buffer. The 0.1 M Phosphate buffer (pH 7.4) is composed of 0.1 mM Na_2HPO_4 and 0.02 mM NaH_2PO_4.

2.2.3 Staining solution

Buffers used for staining was the Tris-Buffered saline (TBS) 0.1 mM (pH 7.6) composed of 100 mM TRIS and 154 mM NaCl, or the PBS 10 mM (pH 7.4) composed of 6.5 mM Na_2HPO_4, 1.9 mM NaH_2PO_4, 150 mM NaCl.

2.2.4 Tamoxifen solution

Tamoxifen (TMX) (Sigma-Aldrich) solution of a 10 mg/mL final concentration was prepared by dissolving 20 mg of tamoxifen powder in a 2 mL solution composed of 99.5 % corn oil and 0.5 % EtOH followed by 15 minutes of sonification at 25° C.

2.2.5 BrdU solution

BrdU (Sigma-Aldrich) solution with a concentration of 16.2 mg/mL was prepared by dissolving 16.2 mg BrdU powder in 1 mL 0.9 % NaCl solution followed by 15 minutes sonification at room temperature.

2.2.6 EdU solution

For each administration, 5-ethynyl-2'-deoxyuridine (EdU) (Invitrogen) was freshly dissolved in tap water to obtain a 0.2 mg/mL EdU solution.

2.3 Antibodies

2.3.1 Primary antibodies

Antigen	Host species	Working concentration	Catalogue number	Manufacturer (city, country)
NG2	Rabbit	1:500	AB5320	MerckMillipore (Darmstadt, Germany)
APC (CC1)	Mouse	1:100	OP80	
AN2	Rat	1:250	130-097-455	Miltenyi Biotech (Bergisch Gladbach, Germany)

GFP	Chicken	1:1000	A10262	Thermo Fisher Scientific (Waltham, MA, US)
BrdU	Rat	1:150	MCA2060	Bio-Rad (Hercules, CA, US)
PCNA	Mouse	1:500	M0879	Agilent-Dako (Santa Clara, CA, US)
Cleaved Caspase-3	Rabbit	1:400	10/2017	Cell Signaling (Danvers, MA, US)
Ki67	Rabbit	1:50	ab16667	Abcam (Cambridge, UK)
Contactin associated protein (Caspr)	Rabbit	1:500	ab34151	

2.3.2 Secondary antibodies

Target Species	Host species	Fluophore or Biotin	Working concentration	Catalogue Number	Manufacturer (city, country)
Rabbit	Goat	Rhodamine RedX	1:150	111-295-144	Jackson ImmunoResearch
Rabbit	Goat	Alexa649	1:150	111-495-144	
Rat	Goat	Biotin	1:500	111-065-167	
Rat	Goat	Alexa568	1:150	A-11077	Thermo Fisher Scientific (Waltham, MA, US)
Chicken	Goat	Alexa488	1:200	A-11039	
Mouse	Goat	Alexa647	1:250	A-21236	
Rabbit	Goat	Alexa647	1:150	A-21244	
Mouse	Goat	Alexa405	1:200	A-31553	
Mouse	Donkey	Alexa647	1:200	A-31571	

2.3.3 Dye / cell marker

Dye or Cell marker	Working concentration	Catalogue Number	Manufacturer (city, country)
Streptavidin Dylight649	1:500	BLD-405224	Biozol (Eching, Germany)
Hoechst 33342	10 mg/mL	14553	Sigma Aldrich
Click-iT™ EdU Imaging kit (AlexaFluor647)	-	C10340	Thermo Fisher Scientific (Waltham, MA, US)

2.4 Images acquirement with Confocal Microscopy

2.4.1 Confocal imaging principle.

Confocal microscopy relies on laser technology to illuminate a specific point location in the sample and avoid illumination of the whole sample. Hence, confocal microscopy avoids scattering and over-exposition.

The laser illuminates one specific point at a time in the sample. Lasers with different wavelength emission are used dependent on the wavelength required to excite specific fluorophores. The laser is guided through the microscope's light channel with dichroic mirrors that reflect or transmit the light depending on the wavelength. The scanning system directs the light beam to scan the sample point by point. Once a fluorophore is excited by the light beam, it absorbs the energy and gets excited. When returning to its resting state, the fluorophore emits fluorescence. The emitted light is captured through the objective and goes through the microscope light path, the dichroic mirror is selected to allow the emission fluorescence to pass through it. The pinhole excludes scattered photons and therefore selects photons emitted at the focal plane. Finally, the photomultiplier amplifies and translates the light intensity to electricity which is converted and depicted by the imaging software. (Figure 2.3).

The laser follows a linear scanning in the two-dimensional plane, scanning each point of the x axis for the same line in the y axis. To increase the image quality, each line is scanned several times to average the fluorescence recorded at each point of the sample. The different fluorescent channels are recorded sequentially and not simultaneously to avoid crosstalk in between channels. Finally, the entire depth of the sample is scanned by imaging several planes throughout the whole depth of the sample, with constant intervals between planes to create a Z-stack.

In order to increase the speed of our scanning process, we also used the spinning disk confocal technology. By using a collector disk containing several micro lenses, the laser beam is divided into several paths to illuminate several points on the sample. The pinhole disk, aligned to the collector disk, filters the fluorescence transmitted to the detector, which in this case is a CCD camera (Figure 2.3). The spinning disk confocal

gives the opportunity to scan several points at once with the same resolution as a confocal system. It increases the scanning speed.

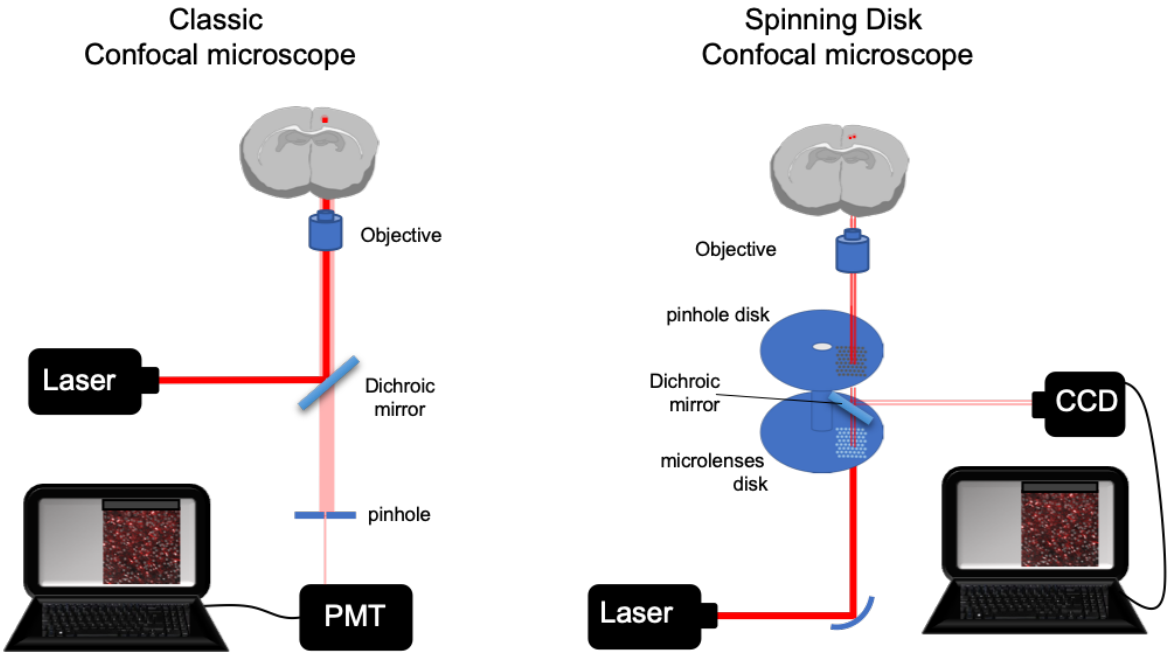

Figure 2.3. Confocal imaging principle. The confocal microscope principle is depicted on the left and the spinning disk confocal principle is depicted on the right. In both set ups, the laser is the illumination source. In the confocal paradigm, the laser beam is guided through the microscope to pass through the objective and hit the sample at one single spot. In the spinning disk confocal set up, the laser beam is split in several beams by the microlense disk and these laser beams are guided to the objective and strikes multiple points on the sample. The light emitted by the sample is then guided through the microscope to pass through the pinhole or the pinhole disk, to discard the scattered light and to only keep the emitted light from the focal plane. Finally, the emitted light is collected by the PMT in the confocal conformation or by a CCD camera in the spinning disk confocal conformation. To convert the light to binary image.

2.4.2 Image acquisition

Three different setups were used for the confocal imaging, the Nikon A1 plus confocal, the Leica SP8 AOTF confocal and the spinning disk confocal VisiScope CSU-W1 associated with the Zeiss Axio Observer microscope. These setups are described in the following chapters.

The region of interest was located using the 5x, 10x and 20x objectives. Images used for cell counting were acquired using the 40x objective. Internodes image acquirement was realized with 60x objective. We used a sequential acquisition of the different laser lines, with a minimal average of two per line.

2.4.2.1 Nikon system

The 405 nm, 488 nm, 561 nm and 640 nm lasers illuminated the sample. The fluorescence is collected by the Photomultiplier Tube (PMT). The images are depicted by the NIS-elements software.

2.4.2.2 Leica system

The lasers illuminating the sample are the 405 nm, 488 nm, 552 nm and 638 nm. The fluorescence is collected with HyD detectors and one PMT. The images are then depicted by the LAS AF v3.x software.

2.4.2.3 Zeiss system

The 405 nm, 488 nm, 561 nm and 640 nm lasers illuminate the sample. The fluorescence is collected by the Two pco.edge sCMOS camera through the DAPI, GFP, mCherry and Cy5 filters. The images are then depicted by the VisiView software.

2.5 Behavioral methods

2.5.1 Rotarod

The rotarod is used to measure the motor coordination of the mice. The mouse is placed on a horizontal suspended rotating cylinder. The cylinder rotation follows an increasing speed, from 4 rotation per minute (RPM) to 40 RPM over a time period of 5 minutes. Falling from the rotarod is a consequence of motor coordination failure, to follow the speed imposed by the rotating cylinder. Hence, the time spent on the cylinder indicates the general motor coordination of the mice. In order to assess the motor coordination of the mice, at PND 23, we used the rotarod from UgoBasile.

2.5.2 Running wheel

The mouse motor activity is recorded with the Scurry mouse activity wheel (Model 80821S, Lafayette Instrument) mounted with a Scurry Mouse Activity counter (Model 86110, Lafayette Instrument), equipped with an I/R sensor, which counts the number of rods per minute that pass in front of the sensor. The counter is linked to the Scurry interface for animal activity (Model 86100, Lafayette Instrument) which then sends the

information to the Scurry Activity Monitoring Software (Model 86185, Lafayette Instrument) (Figure 2.4). Depending on the number of rods in the wheel, the Scurry Activity Monitoring Software calculates the number of wheel turn per minute. The regular wheel is composed of 38 rods. The rods are removable, which allows for the creation of a complex wheel. By removing the rods, we create a wheel composed of 22 rods, with a complex pattern of rods and empty spaces. The switch between the regular wheel and the complex wheel pattern induces an adaptation of the motor scheme previously programmed to run for the regular wheel. Assessing the mouse running speed evolution in the complex wheel allows us to observe the learning ability of the mouse and their adapting motor skills.

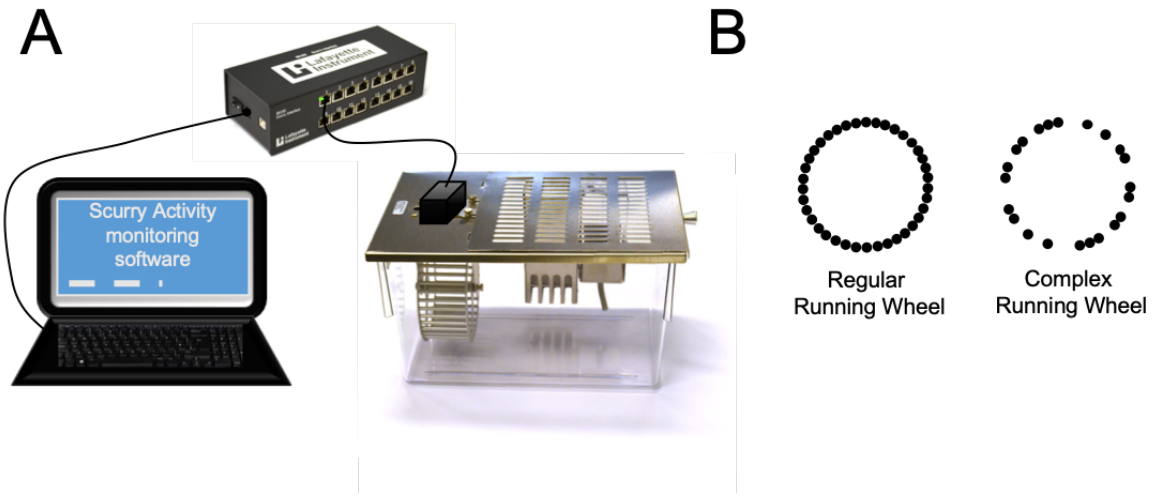

Figure 2.4. Material for Running wheel experiment. A. Running wheel Set up. The Scurry mouse misstep wheel cage is mounted with the Scurry Mouse Activity counter on top of the wheel. The counter is connected to the Scurry interface for animal activity and sends information to the Scurry Activity Monitoring Software installed on a laptop. B. The regular wheel presents 38 rods, regularly distributed on the wheel and the complex wheel is composed of 22 rods unequally distributed.

2.6 Experimental procedure to follow the fate of GluA2 deleted NG2 cells.

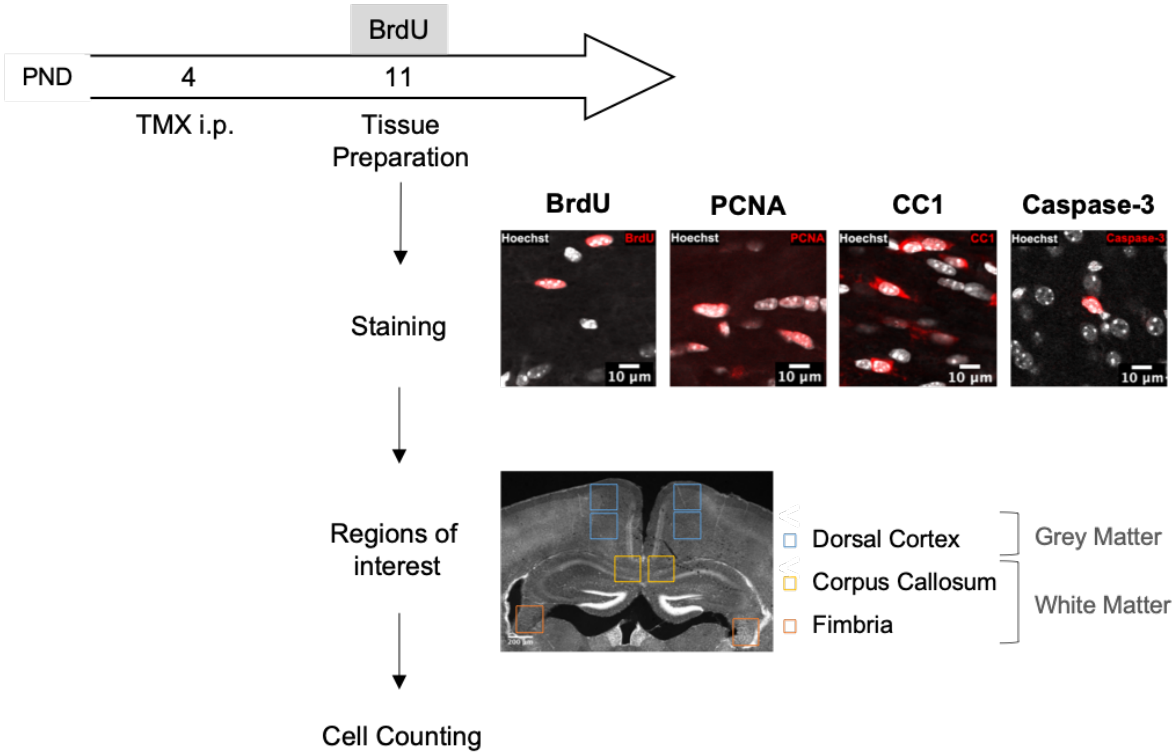

Figure 2.5. Experimental procedure to follow the fate of GluA2 deleted NG2 cells. On PND 4, the mice from both groups NG2GluA2-wt and NG2GluA2-lox, received an intraperitoneal injection of tamoxifen. Seven days later, on PND 11, the mice received an intraperitoneal injection of BrdU then the tissue was collected two hours after the last BrdU injection. Several quadruple stainings were applied to detect the NG2 cells fate: BrdU, PCNA, CC1 and Caspase-3. The NG2 cells fate was assessed in the dorsal cortex to represent the grey matter and the corpus callosum and fimbria to represent the white matter. Finally, the cells were counted using the Fiji software.

2.6.1 Tamoxifen administration

In order to induce Cre-recombination in NG2 cells and delete the GluA2 subunit, the NG2GluA2-wt and NG2GluA2-lox quadruple mouse lines with the EYFP reporter were injected with tamoxifen. Postnatal mice on PND 4 or PND 8 received an intraperitoneal injection of 50 µL Tamoxifen (10 mg/mL).

2.6.2 BrdU administration

To assess the proliferation of NG2 cells with an external marker for the proliferation, we followed two different injections protocols. In the first protocol, the mice received an intraperitoneal injection of 300 mg/KgBW BrdU, 2 hours before tissue preparation. In the

second protocol, the mice received three identical BrdU injections: 24 hours, 10 hours, and 2 hours before tissue preparation.

2.6.3 Tissue preparation

2.6.3.1 Slice fixation

Depending on the experimental group, on PND 11 or PND 18, the mice were anesthetized with isoflurane and then quickly decapitated with a small rodent guillotine. The brain was quickly placed in ice cold oxygenated mACSF. The brain was placed on a cold plate to remove the olfactory bulb and the cerebellum with a razor blade. It was glued to the vibratome plate on the caudal part with the frontal part facing up. The plate was then placed in the vibratome with the rostral part being first cut. 400 µm thick frontal slices were cut with the vibratome (Leica VT1200S, Leica Biosystems and Microm HM650V, Thermo Fisher Scientific) in ice cold mACSF. Once cut, the slices containing the middle part of the corpus callosum and the hippocampus were transferred in a small petri dish and immersed in the PLP-PFA fixative solution for 12 hours.

2.6.3.2 Slice resection

After fixation, the slices were washed three times in TBS for ten minutes. To obtain 50 µm thick slices, the 400 µm thick slices were embedded in 3 % Agar (Sigma Aldrich). The agar block resection of 50 µm thick slices was accomplished with a vibratome (Leica VT1000S).

2.6.4 Immunohistochemistry

Thin slices of 50 µm from the same animal were placed by two per well in a 24-well plate. The antibodies were applied subsequently on the free-floating sections in a total of 500 µL solution on a shaker. Primary antibodies were applied overnight at 4°C and secondary antibodies were applied for three hours at 35°C in TBS or PBS with a concentration ranging from 0.04 % to 0.2 % Triton100X. Between antibody applications, we processed a washing step, during which the slices were rinsed three times for ten minutes in TBS or PBS.

For all following staining, we finished with a DNA labeling. We applied the dye Hoechst 33342 in PBS for 20 minutes at room temperature with a concentration of 0.02 mg/mL. After this step, slices were mounted with vectashield (Vector Laboratories) or Aqua-poly/mount (Polysciences).

2.6.4.1 Quadruple BrdU labeling

To assess the proliferation of NG2 cells, we labeled the BrdU positive cells in the recombined (YFP+) and non-recombined (YFP-) NG2 cell population with the following protocol.

In order to identify the NG2 cells, the primary antibody rabbit-anti-NG2 was applied overnight at 4°C with a concentration of 1:500. On the next day, after a washing step in TBS, the secondary antibody RhodamineRedX-goat-anti-rabbit was applied at 35°C for three hours with a concentration of 1:150.

Next, we labeled the recombined cells. After a washing step in TBS, the primary antibody chicken-anti-GFP was applied overnight at 4°C with a concentration of 1:1000. On the next day, after the washing step in TBS, the secondary antibody Alexa488-goat-anti-chicken was applied for three hours at 35°C with a concentration of 1:200.

Finally, we identified the cells in S-phase by labeling BrdU tagged cells. After a washing step in TBS, we proceeded to an antigen retrieval step. Slices were immersed in 2N HCl for 30 minutes. After a washing step in TBS, the primary antibody rat-anti-BrdU was applied overnight at 4°C with a concentration of 1:150. On the next day, after the washing step in TBS, the secondary antibody Biotin-goat-anti-rat was applied for three hours at 35°C with a concentration of 1:500. This step was followed by a washing step in TBS and the application of the streptavidin Dylight649 for three hours at 35°C with a concentration of 1:500.

2.6.4.2 Quadruple PCNA labeling

The PCNA labeling allowed us to identify the cycling cells in the G1, S, G2 and M phase. We followed the same protocol as for the quadruple BrdU labeling (section 2.6.4.1). Only the BrdU labeling step was replaced by the PCNA labeling.

After the NG2 and YFP staining, we applied the mouse-anti-PCNA primary antibody overnight at 4°C with a concentration of 1:500. On the next day, after a washing step, the Alexa647-goat-anti-mouse secondary antibody was applied for three hours at 35°C with a concentration of 1:250.

2.6.4.3 Quadruple CC1 labeling

To identify the recombined cells that differentiated into oligodendrocytes, we labeled the cells expressing the CC1 marker. We followed the same protocol as for the quadruple BrdU labeling (section 2.6.4.1) with the exception of the BrdU labeling that was replaced by the CC1 labeling.

After the NG2 and YFP staining, we started with a pre-step of antigen retrieval. The slices were bathed in 200 mL citrate buffer and microwaved for one minute at full power (110 P) followed by four minutes at low power (20 P). After cooling down for 30 minutes, we applied a washing step and the first antibody mouse-anti-APC with a concentration of 1:100 was applied overnight at 4°C. The next day, the washing step was applied, followed by the application of the secondary antibody Alexa647-goat-anti-mouse or the Alexa647-donkey-anti-mouse for three hours at 35°C with a concentration of 1:200.

2.6.4.3.1 Quadruple Caspase-3 labeling

Following the NG2 cells fate, we assessed the cell death in this population by labeling the cleaved-caspase-3. We followed the same protocol as for the quadruple BrdU labeling with the exception of the BrdU labeling (section 2.6.4.1) that was replaced by the cleaved caspase-3 labeling.

To identify NG2 cells, we applied the primary antibody, rat-anti-AN2 overnight at 4°C with the 1:250 concentration. After a washing step, on the next day, the secondary antibody, Alexa568-goat-anti-rat was applied for three hours at 35°C.

Next we applied the YFP staining as explained in the BrdU labeling protocol.

Finally, to identify the NG2 cells undergoing cell death, after a washing step, we applied the first antibody, rabbit-anti-cleaved caspase-3, overnight at 4°C with the 1:400 concentration. On the next day, following a washing step, we applied the secondary antibody, Alexa647-goat-anti-rabbit for three hours at 35°C with a concentration of 1:150.

2.6.5 Images acquirement

The NG2 cells fate was observed in three different regions of interest: within grey matter, the dorsal cortex and in white matter, the corpus callosum and the fimbria (Figure 2.5). Per animal, we scanned the regions of interest on four different 50 µm thick slices. We acquired z-stacks on a confocal microscope with an optical resection of 2.5 µm, to view all cells present in the slice. Images were acquired in 8 bits or 16 bits, with 1024 pixels per 1024 pixels. The laser intensity was adjusted to the fluorescence intensity to avoid oversaturation. Lasers were used, depending on the secondary antibody or the dye present in the sample (Nikon : 405 nm, 488 nm, 561 nm, and 640 nm ; Leica SP8 : 405 nm, 488 nm, 552 nm, and 638 nm ; VisiScope : 405 nm, 488 nm, 561 nm, and 640 nm).

2.6.6 Cell Counting

For each plane, the cells were counted with the Fiji software. The CellCounter plug-in was used to mark positive cells for the different markers and to keep track of the total count. First, we identified the NG2+ and YFP+ cells. Then, we identified the double positive cells for the NG2 and YFP markers. Next, we identified the BrdU, PCNA or cleaved-caspase3 positive cells. The last count was to identify the double positivity between the cell fate marker and the NG2, YFP or double positive NG2-YFP cells.

2.6.6.1 Identification of NG2 cells

NG2+ cells were identified by NG2 immunolabeling which labels the cell membrane. NG2 cell morphology is characterized by thin sparse stellate processes, arranged around a small cell body. As described by Nishiyama et al. in 1996, NG2 cell morphology in the grey matter and in the white matter differs. In the corpus callosum, NG2 cells display an oval like cell body shape contrasting with the round cell body found in the cortex (Figure 2.6). In the white matter, NG2 cells seem to be compressed in-between axonal fibers, and the flattened shape of the cell body follows the white matter tract direction.

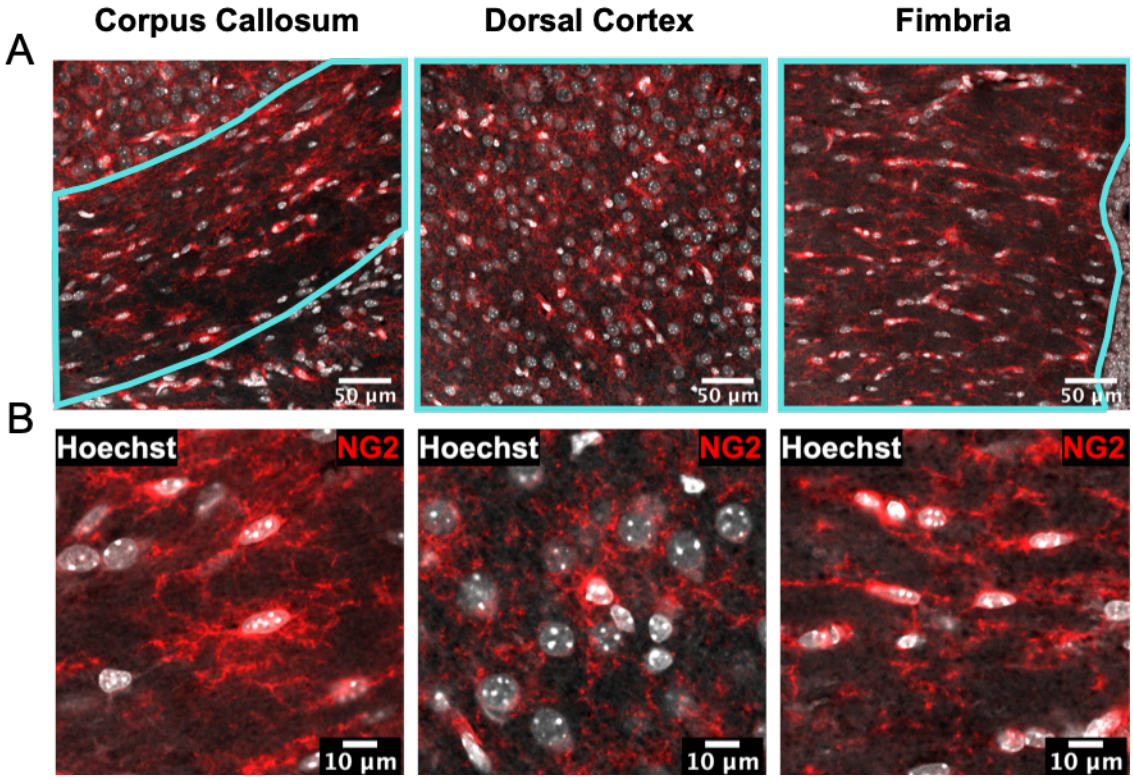

Figure 2.6. NG2 cell morphology in the grey matter compared to the white matter. A. Outlined regions of interest in cyan, for each type of assessed brain region areas. B. Confocal scan of NG2 (red) and Hoechst 33342 (grey) labeling highlighting the different NG2 cell morphology between the grey and white matter areas.

2.6.6.2 Mitotic figures identification

In order to define NG2 cells in mitotic phases, we relied on DNA labeling with the Hoechst 33342 dye in combination with NG2 labeling. During the mitotic phase, we identified NG2 cells in metaphase, anaphase and telophase (Figure 2.7). In metaphase, NG2 cells showed an increased cytoplasmic volume and a stronger NG2 membrane labeling with compacted DNA in the center. In anaphase, NG2 cells show a strong NG2 cell labeling around the cell body, with separated compact DNA in each respective pole. During telophase, NG2 daughter cells are separated by a common central membrane strongly labeled with the NG2 staining. NG2 daughter cells contain compacted DNA that then starts decompaction.

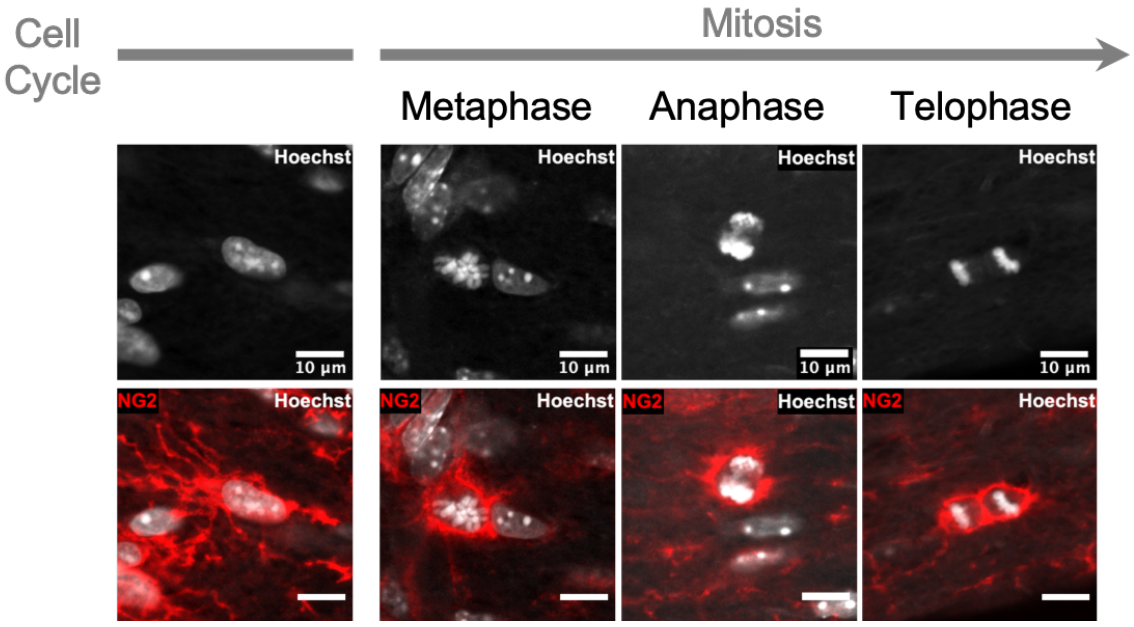

Figure 2.7. Mitotic figures in NG2 cells. The top row represents the DNA labeling with Hoechst 33342 dye. The bottom row represents the co-labeling of the NG2 marker and Hoechst 33342 dye. The morphology of NG2 cells is shown for the three following mitotic phases: the metaphase, the anaphase, and the telophase. The images preceding these phases, shows the NG2 cell morphology and its DNA when it is not in the mitotic phase.

2.6.7 Analysis

The fraction of NG2 cells from the different experiments was obtained using at least the count of two different slices per animals and per region. Our inclusion criteria is a minimum of 50 NG2+YFP+ cells per animal. For the same animal and region, the total amount of cells was summed up in each slice.

2.6.7.1 NG2 cell fate mapping with BrdU labeling

The proliferative fraction of the NG2 recombined cells was obtained by dividing the number of NG2+YFP+BrdU+ cells by the number of NG2+YFP+ cells. For the non-recombined NG2 cells, we divided the number of NG2+YFP-BrdU+ cells by the number of NG2+YFP- cells.

In order to increase our statistical power, we combined the animals that received a single BrdU injection 2 hours before tissue preparation with animals that received 3 times 150µL of BrdU injection before tissue preparation. To combine both groups, we normalized each proliferative fraction obtained for each animal by the NG2GluA2-wt

average fraction in both types of experiment respectively. After normalization, we compared separately the normalized fraction for each region and each fraction type between the NG2GluA2-wt and NG2GluA2-lox group. In Prism, we statistically tested the difference with unpaired t-test.

2.6.7.2 NG2 cell fate mapping using PCNA as marker

The PCNA positive fraction was obtained by dividing the number of NG2+YFP+PCNA+ cells by the total NG2+YFP+ cells in each animal for the regions concerned. The difference between the NG2GluA2-wt and NG2GluA2-lox group was assessed by comparing the mean values of each group with an unpaired t-test in Prism.

2.6.7.3 NG2 cell density

For each slice, we calculated the number of planes and the areas we selected to be counted. The area was then multiplied by the number of planes in the z-stack. We summed up the total area of each slice and then the cell density was calculated with the number of cells divided by the counted area per animal. Per group, we obtained the average cell density. We tested the statistical difference between the NG2GluA2-wt and NG2Glua2-lox group, using the online platform QuickCalcs from Graphpad.

2.6.7.4 NG2 cell differentiation

We calculated the differentiation with the fraction of CC1+ cells and NG2+ cells amongst the YFP+ population. A minimum of 100 YFP+ counted cells per animal was our inclusion criteria in this experiment. We tested the difference between the two groups for each category of population (NG2+CC1+, NG2+CC1-, NG2-CC1+, NG2-CC1-) in each regions of interest with the online platform QuickCalcs from Graphpad.

2.7 Experimental procedure to determine the role of GluA2 on internode length.

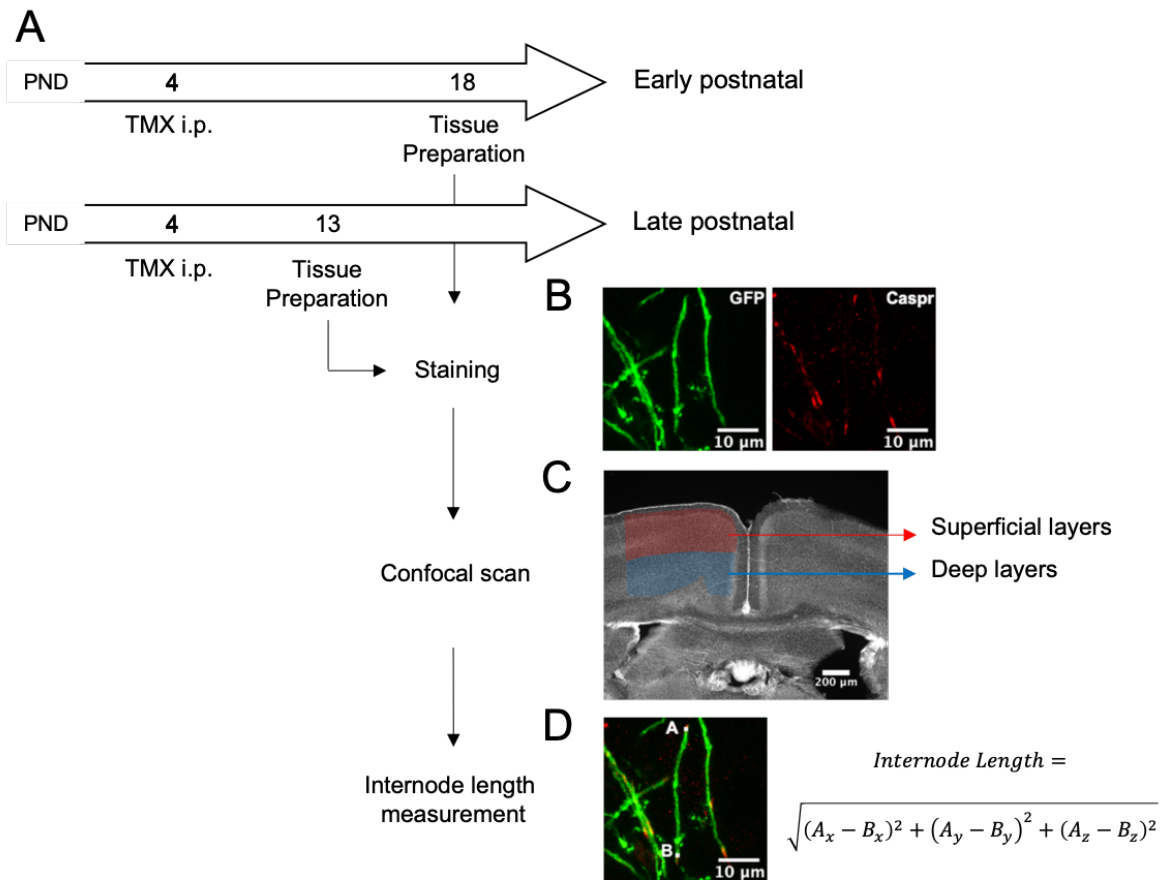

Figure 2.8. Experimental procedure to estimate internode length in the early and late postnatal period, of NG2GluA2-wt and NG2GluA2-lox mice. A. On PND 4, mice from the NG2GluA2-wt and NG2GluA2-lox groups received an intraperitoneal injection of tamoxifen. To analyze the impact of GluA2 deletion at an early and later postnatal stage, we fixed the brain slices containing the region of interest at PND 13 or PND 18. B. Maximum projection of GFP, Caspr and Hoechst 33342 labeling. 50 µm thick slices were processed through our immunohistochemistry protocol to be stained for GFP and Caspr. C. Example scan of the Hoechst 33342 labeling. Confocal scans were acquired in the superficial and deep layers of the dorsal cortex with an optical resection of 1 µm. D. Maximum projection of four optical resection. Using the Fiji software, we marked the beginning (point A) and the end (point B) of the internode using Caspr as a reference to detect the endings of the internodes. The exact location was extracted in Fiji and exported to excel, to calculate the distance in-between both points with the indicated formula. Internodes were estimated to be a straight segment.

2.7.1 Tamoxifen administration

Cre recombination in NG2 cells and GluA2 subunit deletion, was induced in the quadruple mouse line with the mT/mG reporter with tamoxifen injection at the PND 4. Postnatal mice received an intraperitoneal injection of 25 µL Tamoxifen (10 mg/mL).

2.7.2 Tissue preparation

On PND 13 or PND 18, we prepared the slices as previously mentioned in the NG2 cell fate experimental procedure. Fixation was achieved with 4 % PFA solution. We selected the anterior part of the corpus callosum and the frontal cortex.

2.7.3 Immunohistochemistry

We followed the same procedure as the NG2 cell fate experiment, 50 µm thick slices were placed by two in a well. We sequentially labeled Caspr, GFP and at last the DNA with the dye Hoechst 33342.

First, to identify the paranodes, we applied the primary antibody, rabbit-anti-Caspr, overnight at 4°C with a concentration of 1:500. The next day, we applied a washing step followed by application of the secondary antibody, Rhodamine-Red-X-goat anti-rabbit, for three hours at 35°C with a concentration of 1:150.

Secondly, we applied the GFP staining as previously described in the quadruple BrdU labeling (section 2.6.4.1).

Finally, we labeled the DNA, to identify the cell nucleus, with Hoechst 33342 as described previously in the experimental protocol, to follow NG2 cells fate (section 2.6.4.1).

2.7.4 Image acquirement

Images were acquired across all layers of the cortex, with a minimum of two scans per animal. In order to measure the internodes, we used a higher objective magnification and a smaller optical resection for better resolution. Z-stacks of 1 µm optical resection were acquired with a 63x objective, on a confocal microscope. Images were acquired in 8 bits or 16 bits with 2048 pixels per 2048 pixels. We scanned sequentially the 405 nm, the

488 nm and the 561 nm laser. The laser intensity was adjusted to the fluorescence intensity to avoid oversaturation. A line average of two was applied.

2.7.5 Internode length measurement

To measure the length of the internodes, we tagged both endings of the internodes marked by the Caspr and recorded the coordinates in the “ROI manager” of Fiji. We extracted the coordinates in excel and made the following calculation to estimate the length of each internode.

$$Internode\ Length = \sqrt{(A_x - B_x)^2 + (A_y - B_y)^2 + (A_z - B_z)^2}$$

2.7.6 Analysis

At least 20 internodes were measured per animal. The internode lengths from all animals, were pulled together in each mouse group respectively. From both the, NG2GluA2-wt and the NG2GluA2-lox datasets, we calculated the mean ± SEM in Excel. In IgorPro, we plotted the Cumulative Distribution Frequency (CDF) based on all internode lengths pulled together for each group. We statistically tested the mean differences between groups in Prism. The Kolmogorov-Smirnov test was realized in IgorPro. With a level of significance of $p<0.05$, distribution of both groups was considered to be different, when the D value was greater than the critical value (C value).

2.8 Experimental procedure to determine the role of GluA2 on NG2 cell fate and oligodendrocyte properties after a motor task.

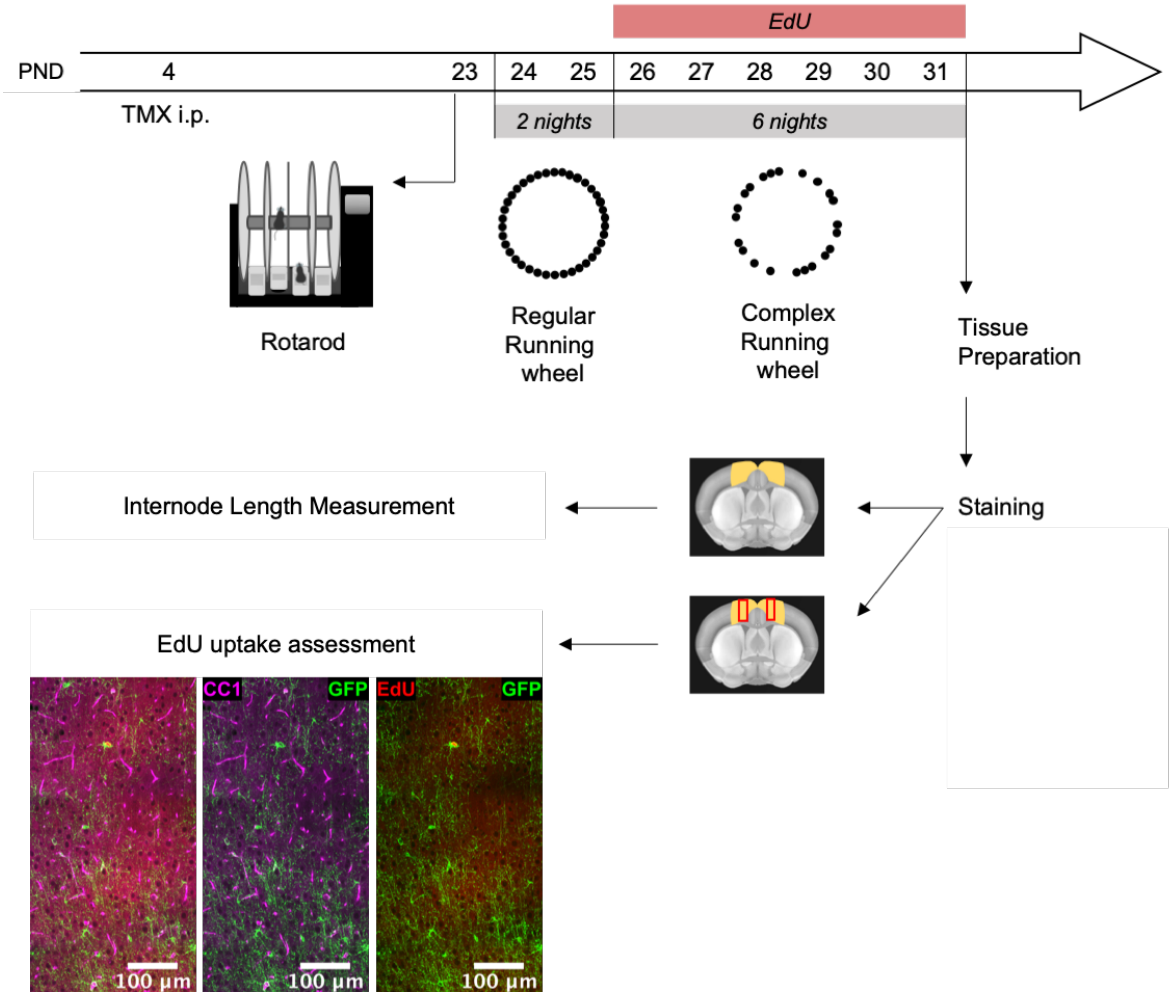

Figure 2.9. Experimental procedure to determine the role of GluA2 on NG2 cell fate and oligodendrocyte properties after a motor learning task. On PND 4, a tamoxifen intraperitoneal injection induced NG2 cell recombination in the transgenic mice containing the mT/mG reporter. On PND 23, the motor coordination of the NG2GluA2-wt and NG2GluA2-lox mice was assessed, and they were placed in a wheel cage with a regular wheel for two consecutive days and nights. On PND 25, the regular wheel was exchanged with a complex wheel for six consecutive days and nights. Concomitantly, mice received EdU administered through tap water. On PND 31, the mouse brain was collected, so that the tissue could be labeled by immunohistochemistry with the CC1 marker, the GFP reporter, the Caspr marker and the EdU marker. Images were acquired with a spinning confocal disk. For the internodes' length measurement, images were scanned in the motor cortex with a 63x objective. For the EdU uptake assessment, mosaic stack images were scanned through all layers of the motor cortex with a 40x objective.

2.8.1 Tamoxifen administration

Cre recombination in NG2 cells and GluA2 subunit deletion was induced in the quadruple mouse line using the mT/mG reporter, with a tamoxifen injection on PND 4. Postnatal mice received an intraperitoneal injection of 25 µL Tamoxifen (10 mg/mL).

2.8.2 Assessment of motor coordination with the rotarod

Motor coordination of the mice was assessed on PND 23. The protocol is depicted in Figure 2.10. The mice were habituated to the room for 15 minutes in their cage prior to experiments. Then, during the habituation phase, mice were placed on the rotarod, turning at a constant speed of 5 RPM for five minutes. In between each rotarod session, the mice were placed in the resting cage for ten minutes. Then, the mice encountered three trial sessions of five minutes, each interposed with resting phases. The trial phase consisted of five minutes acceleration between 4 RPM and 40 RPM. We noted the latency to fall and the falling speed, to assess motor coordination performance.

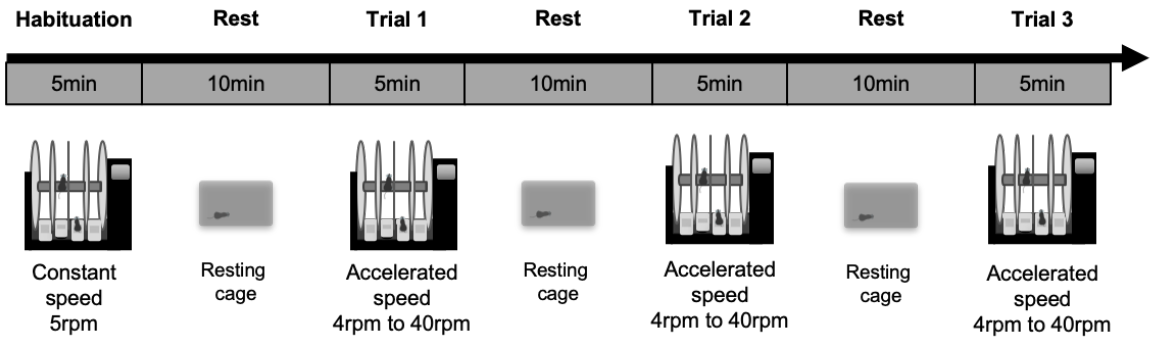

Figure 2.10. Rotarod experimental timeline. Timeline of the rotarod protocol to assess the motor coordination of the mice. The protocol starts with a habituation phase to the rotarod. It is followed by three cycles of five minutes of rotarod sessions and ten minutes of resting phase in a cage.

2.8.3 Motor learning task with the running wheel

On the same day, after the motor coordination assessment, mice were housed in a cage with free access to a regular wheel. Every night, during the active phase, we recorded four parameters: the average speed (m/min), the maximum speed (m/min), the total distance (m), and the total time spent on the wheel (min). After two nights in the regular wheel, we exchanged the regular wheel with a complex wheel, composed of 22

rods. On the third night until the eighth night, we recorded the mouse activity in the complex wheel (Figure 2.9).

2.8.4 EdU administration

During the six days of complex wheel, EdU 0.2 mg/mL was presented in the tap water and renewed every two days (Figure 2.9). We measured the EdU consumption by weighing the mouse water bottles before and after EdU presentation.

2.8.5 Tissue preparation

On the next day, following the eighth night in the wheel cage, we followed the same tissue preparation as previously described. The tissue fixation was realized with 4 % PFA.

2.8.6 Immunohistochemistry

We sequentially labeled the paranodes with the Caspr marker, internodes with the GFP reporter, oligodendrocytes with the CC1 marker and proliferative cells with the EdU marker.

We followed the same experimental procedure as described in the internode length experimental protocol to label the Caspr marker and the GFP marker (section 2.7.3).

After GFP staining and a washing step, we applied a solution of 2 % non-fat dry milk in 0.3 % triton in PBS for 30 minutes. Immediately afterwards, the primary antibody mouse-anti-APC was applied overnight at 4°C with a concentration of 1:100. On the next day, after a washing step, we applied the secondary antibody, Alexa405-goat-anti-mouse, for three hours at 35°C with a concentration of 1:200.

Finally, we labeled the EdU marker. A pre-step of 30 minutes in 0.2 % triton PBS solution was necessary for permeabilization. After washing the slices two times in PBS, we applied a mix of 430 µL of Reaction buffer, 20 µL of CuSO4, 1.25 µL of AlexaFluor 647 Azide, and 50 µL of additive buffer (prediluted 1:10) from the Click-iT^{TM} EdU Imaging kit containing AlexaFluor647. Then, the slices were mounted to acquire confocal scans.

2.8.7 Image acquirement

Confocal images were acquired with the Visiscope microscope (section 2.4.2). The internodes were scanned with a 63x objective. The proliferative fractions were calculated via cell counting stitched images, from the superficial to deep layers of the motor cortex, imaged with a 40x objective.

2.8.8 Analysis

2.8.8.1 Motor coordination with rotarod

In Excel, we calculated the average falling speed and latency to fall per group. We statistically tested the difference between NG2GluA2-wt and NG2GluA2-lox groups in Prism.

2.8.8.2 Running wheel experiment

All parameters were measured at night during the 12 hours active phase, also known as the dark phase. Raw data provided the running distance (m) for each minute. Per night, we analyzed four parameters in the running wheel experiment. The total time spent on the wheel was measured by summing up every minute where the running speed exceeded 0 m/min. The total traveled distance (m) was measured by summing up the distance travelled each minute. The average speed was measured by dividing the total running distance by the total time spent on the wheel. The maximum running speed was measured by selecting the highest running speed in the period of one minute time. Finally, we calculated the mean ± SEM for each parameter per group and plot it in IgorPro. We statistically tested the difference between NG2GluA2-wt and NG2GluA2-lox groups in Prism.

2.8.8.3 Myelination analysis

At least 70 internodes were measured per animal. The internode lengths from all animals were pulled together in each mouse group respectively. From both, NG2GluA2-wt and NG2GluA2-lox dataset, we calculated the mean ± SEM in Excel. In IgorPro, we plotted the CDF based on internode lengths from both mice groups. We statistically tested the mean differences between groups in Prism. The Kolmogorov-Smirnov test was

realized in IgorPro. With a level of significance of $p<0.05$, distribution of both groups was considered to be different, when the D value was greater than the critical value (C value).

Additionally, in Fiji, we measured the bright GFP+ area below the longitudinal fissure. We measured the area surface and the length with the Fiji ROI manager. For comparison, we calculated the mean ± SEM in Excel for both, NG2GluA2-wt and NG2GluA2-lox mice groups and tested the statistical differences in Prism.

2.8.8.4 Proliferative fraction

The cells were counted in Fiji with the “Cell Counter” Plugin. The EdU fraction was calculated in excel for each cell category per animal: CC1-YFP-, CC1-YFP+, CC1+YFP+, CC1+YFP-. We calculated the mean ± SEM in both groups NG2GluA2-wt and NG2GluA2-lox and plot the data in IgorPro. Statistical tests were applied between both groups in Prism.

3 Results

3.1 Increased proliferation in GluA2 deficient NG2 cells

GluA2 deletion (GluA2 KO) in NG2 cells renders AMPARs permeable to calcium. Therefore, the calcium transient induced by glutamatergic input in NG2 cells is expected to be increased. In the adult period, the GluA2 subunit expression is decreased compared to the postnatal period (Ziskin et al., 2007). In parallel, the NG2 cells proliferation rate is decreased in the adult period compared to the postnatal period (Dimou & Gallo, 2015). Since the decrease of GluA2 subunit expression seems to be correlated to a slower proliferation rate of the NG2 cell population, we hypothesized that GluA2 deletion in NG2 cells will decrease NG2 cell proliferation. We chose to study NG2 cell fate in the early postnatal period, when the NG2 cell population exhibits the highest proliferation and differentiation rate.

3.1.1 Increased DNA replication in GluA2 deficient NG2 cells.

First, we assessed the role of the GluA2 subunit on the proliferative fraction of NG2 cells during the first postnatal week (PNW). The GluA2 subunit was selectively deleted in NG2 cells using a mouse model where Cre was expressed under the NG2 promotor, *Gria2* coding for the GluA2 subunit was floxed and, the YFP reporter was expressed under the *ROSA26* gene. Therefore, injecting the NG2GluA2-lox animals with tamoxifen induced a deletion of the GluA2 subunit and the YFP reporter expression in NG2 cells exclusively. Presence of the YFP reporter account for NG2 cell recombination (Figure 3.1 A). In order to asses NG2 cell proliferation during the first PNW, NG2GluA2-lox and NG2GluA2-wt animals received a tamoxifen injection on the fourth postnatal day (PND 4). The proliferative fraction measurement was based on the BrdU uptake method, seven days after GluA2 deletion. Cells taking up BrdU are undergoing DNA replication in the S phase of the cell cycle. Therefore, NG2 cells expressing BrdU are classified as proliferative NG2 cells. We focused our investigations on three different areas of the mouse brain: the

corpus callosum and the fimbria as white matter areas, and the dorsal cortex as grey matter area. We compared the white matter to the grey matter area because NG2 cells in the white matter area shows a higher proliferation rate. Intraperitoneal BrdU injection was performed in both NG2GluA2-wt and NG2GluA2-lox animals (Figure 3.1 B). Two experimental groups were included in this study. The first experimental group received a single BrdU injection two hours prior to tissue collection. Because the fraction of BrdU uptake was very low with a two hours exposure time (NG2+YFP+ cell population : Corpus Callosum : NG2GluA2-wt: 0.051 ± 0.013, n = 7; NG2GluA2-lox: 0.091 ± 0.017, n = 7 ; Fimbria : NG2GluA2-wt: 0.092 ± 0.017, n = 7; NG2GluA2-lox: 0.148 ± 0.02, n = 7 ; Dorsal Cortex : NG2GluA2-wt: 0.025 ± 0.006, n = 7; NG2GluA2-lox: 0.037 ± 0.004, n = 7 ; NG2+YFP- cell population : Corpus Callosum : NG2GluA2-wt: 0.054 ± 0.015, n=7; NG2GluA2-lox: 0.096 ± 0.015, n = 7 ; Fimbria : NG2GluA2-wt: 0.089 ± 0.018, n = 7; NG2GluA2-lox: 0.127 ± 0.015, n = 7 ; Dorsal Cortex : NG2GluA2-wt: 0.023 ± 0.006, n = 7; NG2GluA2-lox: 0.032 ± 0.004, n = 7), we increased the period of BrdU exposition. The second experimental group received three BrdU injections within 24 hours, with the last injection two hours prior to tissue collection (NG2+YFP+ cell population : Corpus Callosum : NG2GluA2-wt: 0.15 ± 0.06, n = 3; NG2GluA2-lox: 0.26 ± 0.017, n = 5 ; Fimbria : NG2GluA2-wt: 0.311 ± 0.067, n = 4; NG2GluA2-lox: 0.412 ± 0.04, n = 5 ; Dorsal Cortex : NG2GluA2-wt: 0.054 ± 0.009, n = 5; NG2GluA2-lox: 0.071 ± 0.018, n = 5 ; NG2+YFP- cell population : Corpus Callosum : NG2GluA2-wt: 0.19 ± 0.09, n = 3; NG2GluA2-lox: 0.31 ± 0.03, n = 5 ; Fimbria : NG2GluA2-wt: 0.29 ± 0.06, n = 4; NG2GluA2-lox: 0.41 ± 0.03, n = 5 ; Dorsal Cortex : NG2GluA2-wt: 0.06 ± 0.02, n = 5; NG2GluA2-lox: 0.06 ± 0.02, n = 5). To increase our statistical power, we pooled the results from the first and second experiments mentioned above. Following immunohistochemistry labeling and confocal imaging in the regions of interest (Figure 3.1 B), we counted the number of BrdU+ cells in the recombined (NG2+YFP+) and the non-recombined (NG2+YFP-) NG2 cells (Figure 3.1 C). The YFP expression in NG2 cells indicates Cre-recombination and GluA2 deletion for the NG2GluA2-lox animals. In NG2GluA2-wt animals, the GluA2 subunit is not deleted after injecting tamoxifen because the *Gria2* gene is not floxed (Figure 3.1 A). Therefore, GluA2 deletion occurs only in the YFP+, recombined NG2 cells, of the NG2GluA2-lox animals.

The NG2 cell proliferative fraction for the YFP+ cells (BrdU+NG2+YFP+/ NG2+YFP+) of the NG2GluA2-lox and NG2GluA2-wt group was normalized on the NG2 cell proliferative fraction for the YFP+ cells of the NG2GluA2-wt group. The fraction of BrdU uptake in the recombined NG2 cell population was increased in the NG2GluA2-lox group (corpus callosum: 1.766 ± 0.196, n = 12; fimbria: 1.434 ± 0.145, n = 12) compared to the NG2GluA2-wt group (corpus callosum: 1.000 ± 0.203, n = 10; fimbria: 1.000 ± 0.134, n = 11) in both white matter areas (unpaired t-test in corpus callosum: p = 0.014; fimbria: p = 0.040) (Figure 3.1 D).

Despite the absence of recombination reporter expression, the NG2 cell proliferative fraction of the YFP- cells was increased in the NG2GluA2-lox group (corpus callosum: 1.729 ± 0.170, n = 12; fimbria: 1.425 ± 0.104, n = 12) compared to the NG2GluA2-wt group (corpus callosum: 1.000 ± 0.229, n = 10; fimbria: 1.000 ± 0.140, n = 11) in both white matter areas (unpaired t-test in corpus callosum: p = 0.017; fimbria: p = 0.023) (Figure 3.1 E). Independently of the YFP reporter expression indicating Cre-recombination, the BrdU expression in NG2 cells was increased in the entire population of NG2 cells of the NG2GluA2-lox group in white matter areas.

In summary, GluA2 deletion in early postnatal NG2 cells increases their proliferation in the white matter areas.

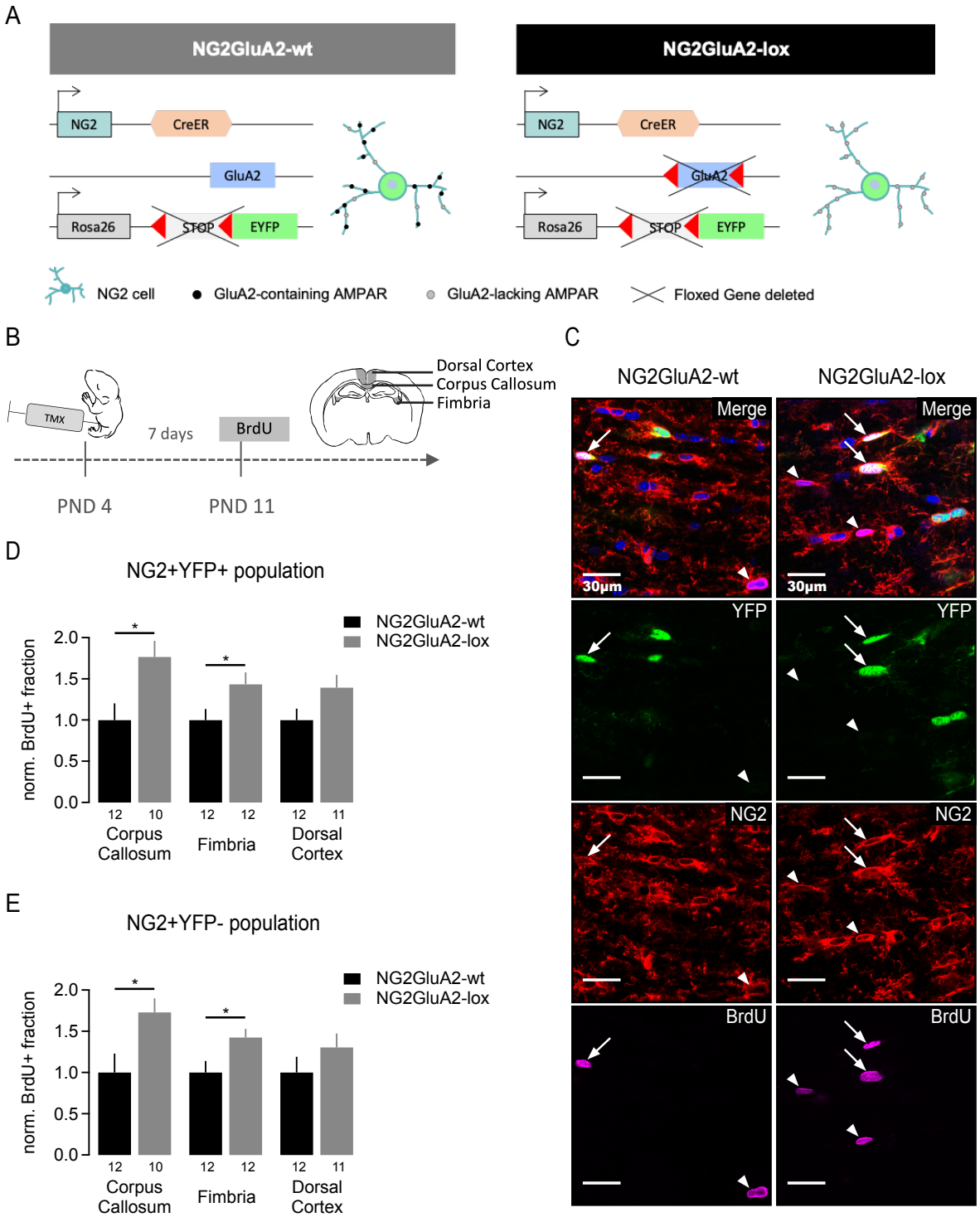

Figure 3.1 Increased BrdU uptake in NG2 cells of NG2GluA2-lox animals. A. Scheme of the transgenic mouse model. Conditional Cre activation under the NG2 promotor induces the deletion of the stop codon before the YFP coding sentence. Therefore, the reporter YFP is expressed after Cre activation when tamoxifen is injected. Only in the NG2GluA2-lox animals, GluA2 coding sentence is deleted after Cre activation. B. Experimental procedure: IP injection of tamoxifen (10 mg/mL) on PND 4 followed by IP injection of BrdU (16,2 mg/mL) on PND 11, two hours before tissue fixation. C. Confocal scans indicating YFP (green, reporter for recombination), NG2 (red),

and BrdU (purple) labeling in the corpus callosum of NG2GluA2-wt and NG2GluA2-lox mice. Scale bar = 30 µm._D. Normalized BrdU+ fraction in the NG2+YFP+ population. E. Normalized BrdU+ fraction in the NG2+YFP- population.

3.1.2 Unchanged cell cycle growth fraction after GluA2 deletion in NG2 cells.

To extend our understanding of the role of the GluA2 subunit on NG2 cells fate, we measured the NG2 cells growth fraction with the endogenous PCNA marker in the recombined NG2 cell population (NG2+YFP+). PCNA is expressed in actively cycling cells (Kukley et al., 2008; Sasaki, Kurose, & Ishida, 1993). The PCNA expression was assessed in both NG2GluA2-wt and NG2GluA2-lox mice groups, seven days after tamoxifen injection at the PND 4 (Figure 3.2 A). We counted the number of PCNA+ cells in the recombined NG2 cell population (NG2+YFP+) in the white matter areas. The growth fraction was calculated amongst the recombined NG2 cell population (PCNA+NG2+YFP+/NG2+YFP+). The calculated growth fraction was around 50 % in both, the NG2GluA2-wt (corpus callosum: 0.50 ± 0.10, n = 4; fimbria: 0.53 ± 0.07, n = 6) and NG2GluA2-lox group (corpus callosum: 0.59 ± 0.11, n = 3; fimbria: 0.56 ± 0.04, n = 3; unpaired t-test in corpus callosum: p = 0.53; fimbria: p = 0.81) (Figure 3.2 C). Half of the recombined NG2 cells are actively cycling and the deletion of GluA2 does not affect this fraction. The GluA2 subunit does not seem to play a role in the entrance of NG2 cells into the cell cycle.

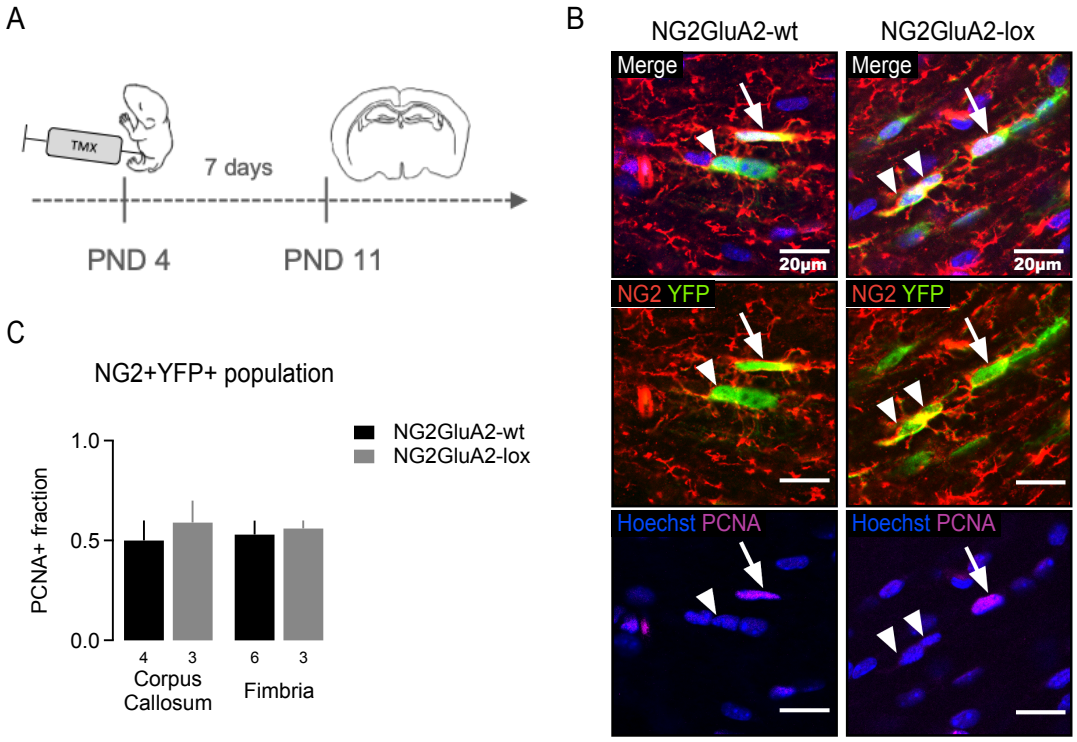

Figure 3.2. GluA2 deletion does not affect NG2 cells growth fraction. A. Experimental timeline: tamoxifen application on PND 4, followed by the PCNA fraction assessment, seven days later. B. Exemplary images scans of NG2+YFP+ cells in the corpus callosum positive (arrow) or negative (arrowhead) for PCNA in NG2GluA2-wt and NG2GluA2-lox mice. Scale bar = 20 µm. C. Growth fraction of NG2+YFP+ cell population in the corpus callosum and the fimbria for both NG2GluA2-wt and NG2GluA2-lox groups.

3.1.3 NG2 cell mitotic fraction is unaffected by GluA2 deletion in NG2 cells.

The increase in the BrdU positive cell fraction in the NG2 cell population suggested that also the mitotic fraction should be increased in the absence of GluA2. We investigated the fraction of NG2 cells in a mitotic phase after GluA2 deletion at PND 4 in the same confocal images acquired for the BrdU uptake experiment. We focused on three phases of mitosis: the metaphase, the anaphase, and the telophase (see section 2.6.6.2); when the DNA configuration alone is sufficient to identify the cells in mitotic phase. In the Figure 3.3.D, arrowheads mark NG2 cells in telophase. In the recombined (NG2GluA2-wt: corpus callosum: 0.035 ± 0.019, n = 4; fimbria: 0.046 ± 0.011, n = 4; NG2GluA2-lox: corpus callosum: 0.053 ± 0.010, n = 4; fimbria: 0.027 ± 0.012, n = 4 ; Unpaired t-test: corpus callosum: p = 0.16, fimbria: p = 0.29) and non-recombined NG2 cell population (NG2GluA2-wt: corpus callosum: 0.041 ± 0.013, n = 4; fimbria: 0.042 ± 0.014, n = 4;

NG2GluA2-lox: corpus callosum: 0.031 ± 0.011, n = 4; fimbria: 0.055 ± 0.012, n = 4 ; Unpaired t-test: corpus callosum: p = 0.58, fimbria: p = 0.51), the fraction of mitotic figures was similar in both groups NG2GluA2-wt and NG2GluA2-lox. This fraction represents less than 10 % of the population (Figure 3.3. B and C). The increase in the fraction of NG2 cells in S phase, taking up BrdU, does not result in an increase in the mitotic NG2 cell fraction.

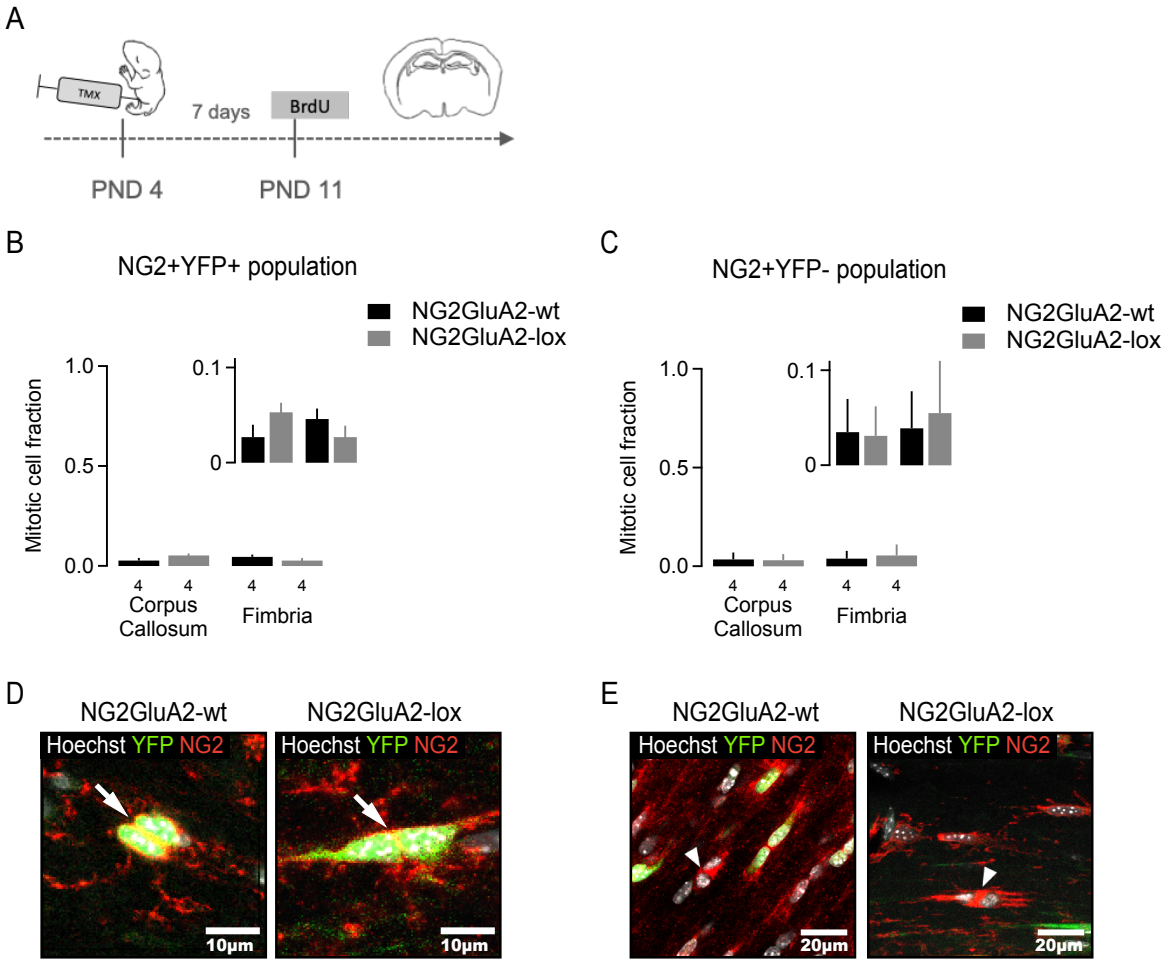

Figure 3.3. Mitotic NG2 cell fraction is not altered after GluA2 deletion. A. Experimental procedure: IP injection of tamoxifen on PND 4 followed by IP injection of BrdU on PND 11, two hours before tissue fixation. B. Mitotic cell fraction in the NG2+YFP+ cell population in the white matter areas of the NG2GluA2-wt and NG2GluA2-lox groups. C. Mitotic cell fraction in the NG2+YFP- cell population in the white matter areas of the NG2GluA2-wt and NG2GluA2-lox groups. D. and E. Exemplary confocal frame scan in the corpus callosum of NG2GluA2-wt and NG2GluA2-lox mice. Hoechst (grey), YFP (green), and NG2 (red) labeling reveal in D. a recombined NG2 cell in telophase (arrow), Scale bar = 10 µm, and E. a non-recombined NG2 cell in telophase (arrowhead). Scale bar = 20 µm.

3.1.4 Differential regulation of proliferation by the GluA2 subunit during development

The dynamics of NG2 cells proliferation and differentiation depend on developmental periods (Dimou & Gallo, 2015). In the adult, NG2 cell proliferation is decreased compared to the postnatal period (Dimou & Gallo, 2015). During this period, NG2 cells originate from different generation waves (Hill & Nishiyama, 2014). It is possible that GluA2 deletion affects NG2 cells differently depending on the origin of the NG2 cells. Focusing on the early postnatal period when the NG2 cell population strongly proliferates and differentiates (Akiko Nishiyama et al., 1999), we assessed the effect of GluA2 deletion on NG2 cell proliferation for the three NG2 cell generation waves. GluA2 was respectively deleted in the embryo at E17, in the first postnatal week (PNW) at PND 4, and in the second PNW at PND 8. Results from the GluA2 deletion on E17 are not presented as the number of NG2GluA2-lox animals collected during the experiments was too low to interpret the data. Neither during the first nor the second postnatal week, GluA2 deletion significantly affected NG2 cell BrdU uptake. However, during the first PNW, a trend to an increase of BrdU uptake in NG2 cells was observed (NG2GluA2-wt: corpus callosum: 1.00 ± 0.29, n = 7; fimbria: 1.00 ± 0.21, n = 7; dorsal cortex: 1.00 ± 0.23, n = 7; NG2GluA2-lox: corpus callosum: 1.39 ± 0.34, n = 7; fimbria: 1.52 ± 0.22, n = 7; dorsal cortex: 1.20 ± 0.17, n = 7 ; Unpaired t-test: corpus callosum: $p = 0.40$, fimbria: $p = 0.11$, dorsal cortex: $p = 0.50$). On the contrary, during the second PNW, GluA2 deletion appeared to reduce BrdU uptake in NG2 cells. (NG2GluA2-wt: corpus callosum: 1.00 ± 0.18, n = 6; fimbria: 1.00 ± 0.22, n = 4; dorsal cortex: 1.00 ± 0.44, n = 6 ; NG2GluA2-lox: corpus callosum: 0.99 ± 0.27, n = 5; fimbria: 0.71 ± 0.15, n = 5; dorsal cortex: 0.59 ± 0.12, n = 5 ; Unpaired t-test: corpus callosum: $p = 0.98$, fimbria: $p = 0.30$, dorsal cortex: $p = 0.43$) (Figure 3.4).

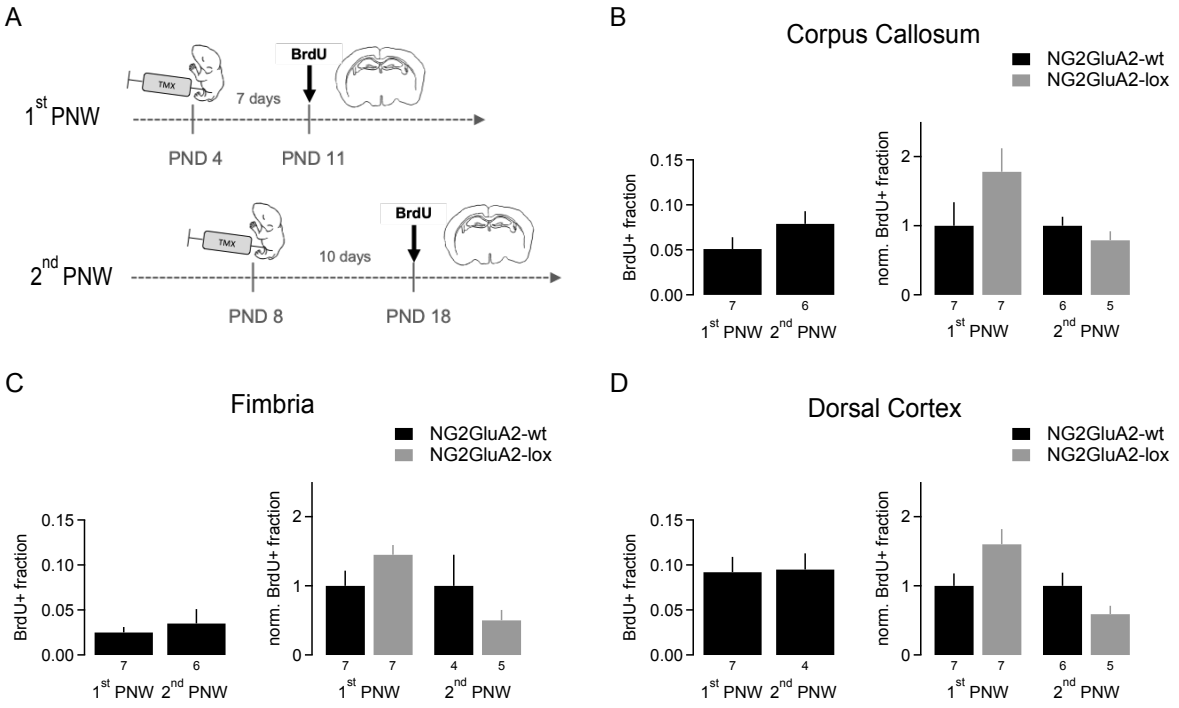

Figure 3.4. GluA2 deletion tends to affect NG2 cells BrdU uptake depending on their origin. A. Experimental timeline for both experimental groups, first PNW and second PNW. NG2 cell recombination was induced on PND 4 or PND 8 by Tamoxifen injection and, followed by the application of BrdU on PND 11 or PND 18. B, C, D. BrdU+ fraction in the NG2GluA2-wt group and normalized BrdU+ fraction in the recombined NG2 cell population for the different regions of interest: corpus callosum (B), fimbria (C), and dorsal cortex (D).

3.2 Role of GluA2 deletion on density of oligodendrocyte lineage cells.

Ablation of the GluA2 subunit selectively in NG2 cells increases the fraction of proliferative NG2 cells. To measure the impact of the increase in NG2 cell proliferation on the oligodendroglia lineage cell population, we investigated the impact of GluA2 deletion in NG2 cells on the NG2 cell density and the oligodendrocyte population.

3.2.1 GluA2 deletion in NG2 cells affects the NG2 cell density in a region dependent manner.

We quantified the number of NG2 cells, the number of YFP+ cells, and the number of NG2+YFP+ cells in the white and grey matter area. The white matter area was represented by the corpus callosum and the fimbria. The grey matter area was represented by the dorsal cortex. We quantified the number of NG2 cells in confocal images of brain sections from NG2GluA2-wt and NG2GluA2-lox mice that had been

treated with tamoxifen at PND 4 and with BrdU at PND 11 (Figure 3.5 A). Because NG2 cell proliferation is increased in the NG2GluA2-lox group, increased proliferation due to GluA2 ablation in the NG2GluA2-lox group suggested an increase in NG2 cell density in the NG2GluA2-lox group. However, the NG2 cell population, identified as NG2+ cells, in the NG2GluA2-lox group did not show an increased density compared to the NG2GluA2-wt group (NG2GluA2-wt group: corpus callosum: 272.1 ± 87.1 cells/mm^3, n = 5; fimbria: 272.2 ± 76.5 cells/mm^3, n = 5; dorsal cortex: 82.0 ± 7.7 cells/mm^3, n = 5; NG2GluA2-lox: corpus callosum: 302.0 ± 114.9 cells/mm^3, n = 3; fimbria: 217.4 ± 32.9 cells/mm^3, n = 4; dorsal cortex: 74.0 ± 2.3 cells/mm^3, n = 5; unpaired t-test: corpus callosum: p = 0.84 ; fimbria: p = 0.57 ; dorsal cortex: p = 0.37) (Figure 3.5 C). In parallel, the fraction of NG2 cells amongst the recombined cell population (YFP+) was not affected by the GluA2 deletion in NG2 cells (Corpus callosum: NG2GluA2-wt: 0.63 ± 0.04, n = 10; NG2GluA2-lox: 0.58 ± 0.04, n = 12; unpaired t-test: p = 0.39; Fimbria: NG2GluA2-wt: 0.60 ± 0.03, n = 11; NG2GluA2-lox: 0.56 ± 0.03, n = 12; unpaired t-test: p = 0.36; Dorsal cortex: NG2GluA2-wt: 0.83 ± 0.04, n = 12; NG2GluA2-lox: 0.82 ± 0.04, n = 12; unpaired t-test: p = 0.86) (Figure 3.5 B). Moreover, the recombined NG2 cell population identified as NG2+YFP+ cells, where the GluA2 subunit was deleted in the NG2GluA2-lox group shows a similar cell density compared to the NG2GluA2-wt group in the white matter (NG2GluA2-wt: corpus callosum: 64.9 ± 26.2 cells/mm^3, n = 5; fimbria: 58.3 ± 13.5 cells/mm^3, n = 5; dorsal cortex: 22.1 ± 2.2 cells/mm^3, n = 5; NG2GluA2-lox: corpus callosum: 130.3 ± 48.4 cells/mm^3, n = 3; fimbria: 95.0 ± 10.6 cells/mm^3, n = 4; dorsal cortex: 42.8 ± 2.1 cells/mm^3, n = 5; unpaired t-test: corpus callosum: p = 0.37; fimbria: p = 0.07; dorsal cortex: p = 0.0001) (Figure 3.5 D). Furthermore, the recombined cell population originating from NG2 cells lacking the GluA2 subunit in the NG2GluA2-lox group shows a similar cell density compared to the NG2GluA2-wt group in the white matter (NG2GluA2-wt: corpus callosum: 142.3 ± 69.4 cells/mm^3, n = 5; fimbria: 110.8 ± 25.0 cells/mm^3, n = 5; dorsal cortex: 31.7 ± 4.2 cells/mm^3, n = 5; NG2GluA2-lox: corpus callosum: 283.9 ± 114.9 cells/mm^3, n = 3; fimbria: 197.2 ± 43.4 cells/mm^3, n = 4; dorsal cortex: 58.0 ± 8.1 cells/mm^3, n = 5; unpaired t-test: corpus callosum: p = 0.30; fimbria: p = 0.11; dorsal cortex: p = 0.02) (Figure 3.5 E).

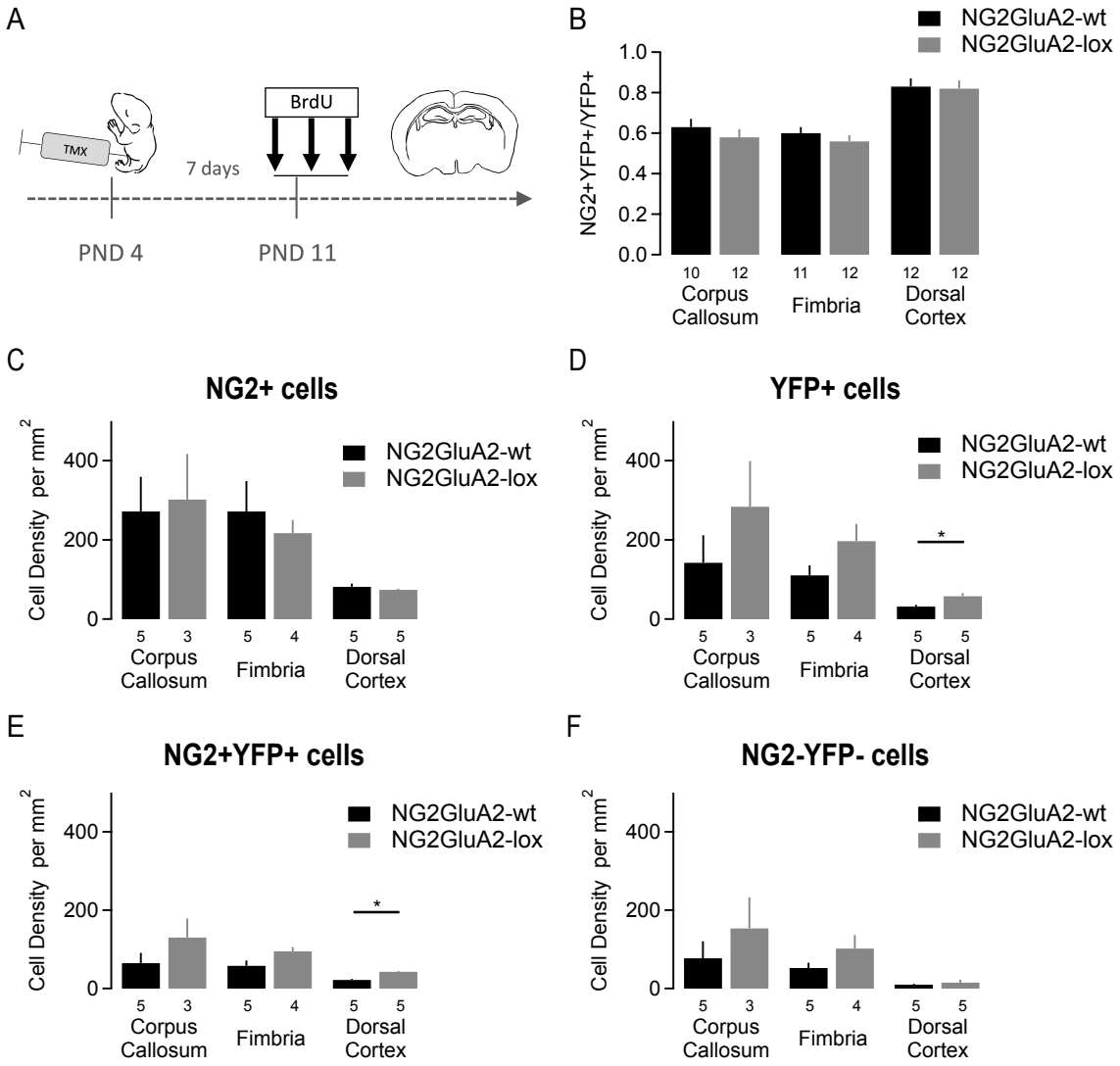

Figure 3.5. GluA2 deletion affects NG2 cell density. A. Experimental procedure with NG2 cells recombination on PND 4 and triple BrdU injection for 24 hours prior immunohistochemistry on PND 11 to obtain the data in panels B to F. B. Proportion of NG2 cells in the recombined cell population. C. NG2+ cell density. D. YFP+ cell density. E. NG2+YFP+ cell density. F. NG2-YFP+ cell density.

Finally, we isolated the recombined cell population negative for the NG2 marker. NG2-YFP+ cell population are the oligodendrocytes coming from the recombined NG2 cells where the GluA2 subunit was deleted in the NG2GluA2-lox group. The NG2-YFP+ cell density is similar in the NG2GluA2-lox and NG2GluA2-wt groups. (NG2GluA2-wt: corpus callosum: 77.4 ± 43.5 cells/mm3, n = 5; fimbria: 52.5 ± 13.3 cells/mm3, n = 5; dorsal cortex: 9.6 ± 2.3 cells/mm3, n = 5; NG2GluA2-lox: corpus callosum: 153.6 ± 79.3 cells/mm3, n=3; fimbria: 102.2 ± 34.6 cells/mm3, n = 4; dorsal cortex: 15.2 ± 7.1

cells/mm3, n=5; unpaired t-test: corpus callosum: p = 0.56 ; fimbria: p = 0.26 ; dorsal cortex: p = 0.47) (Figure 3.5 F). Only in the dorsal cortex, the cell density of YFP+ recombined cells and of NG2+YFP+ cells were significantly increased in the NG2GluA2-lox group compared to the NG2GluA2-wt group (Figure 3.5.D, E).

3.2.2 Cell death remains stable in the NG2 cell population after GluA2 ablation.

The finding that the NG2 cell density was not increased in the absence of the GluA2 subunit was unexpected since we observed an increase in NG2 cell proliferation. To understand the effect of the GluA2 subunit deletion on the cell fate of the oligodendroglia lineage, we assessed cell death in this population. Previous studies from Pitman et al. in 2020 reported an increase in NG2 cell death four days after the ablation of the Cav1.2 subunit in those cells. After the conditional GluA2 deletion on PND 4, we assessed the fraction of NG2 cell death with the cleaved caspase-3 marker, four days after recombination (Figure 3.6.A, B). There were no YFP+ recombined NG2 cells positive for this marker in both NG2GluA2-wt (n = 3) and NG2GluA2-lox (n = 3) groups. Only a small number of caspase-3 cells was present in the brain area investigated, under 3 cells/mm^3 (Figure 3.6.D). Also, amongst the non-recombined NG2 cell population, the fraction of caspase-3 positive cells was low, below 0.003 % (Figure 3.6.C). Therefore, GluA2 deletion in early postnatal NG2 cells does not lead to NG2 cell death.

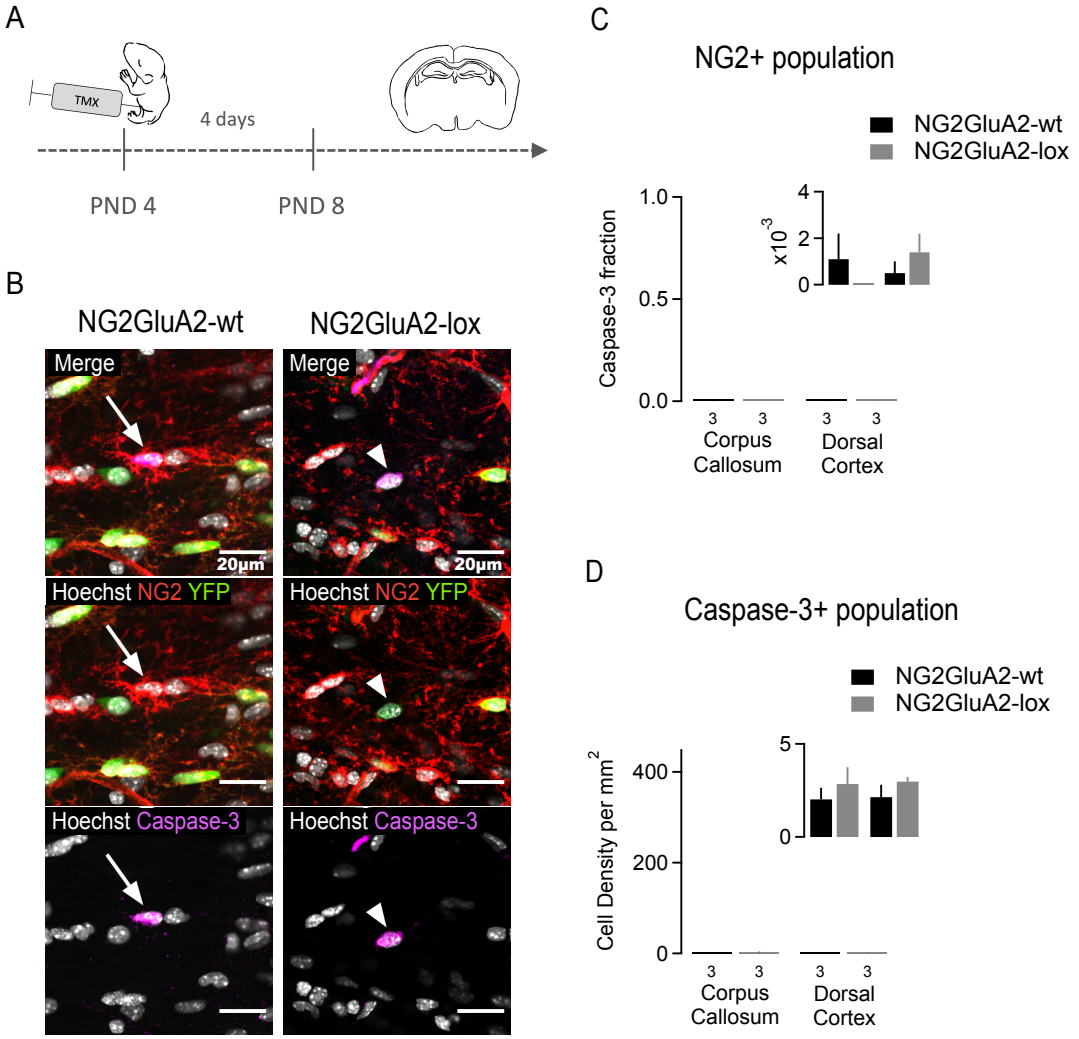

Figure 3.6. GluA2 deletion does not increase the number of Caspase-3 positive cells. A. Experimental timeline: tamoxifen application on PND 4, followed by the quadruple cleaved caspase-3 labeling, four days later. B. Exemplary confocal scans in the corpus callosum of NG2GluA2-wt and NG2GluA2-lox slices for Hoechst 33342 (grey), NG2 (red), YFP (green) and caspase-3 (purple) labeling. Example of NG2+Caspase-3+ cell (arrow) and NG2-YFP+Caspase-3+ cell (arrowhead). Scale bar = 20 µm. C. Caspase-3+ fraction (NG2+Caspase-3+/NG2+) within the NG2 cell population in the white matter areas. D. Caspase-3+ cell density in the white matter areas.

3.3 Differentiation is unaltered in GluA2 deleted NG2 cells.

Finally, to further examine of the role of the GluA2 subunit in the regulation of the cell fate of the oligodendroglia lineage, we assessed the effect of the absence of GluA2 on NG2 cell differentiation in the early (PND 11) and advanced phases of differentiation (PND 20). The GluA2 subunit deletion increases the proliferation of NG2 cells with the

NG2 cell density to remain stable, this condition supposes the supernumerary NG2 cells produced by an increase of proliferation to differentiate into oligodendrocytes rather than remain as NG2 cells. The differentiation into oligodendrocyte was assessed by immunohistochemistry with the CC1 marker on PND 11, the same time point at which we detected an increased proliferation. The fraction of NG2-CC1+ cells in the YFP+ recombined population was similar in the NG2GluA2-wt (corpus callosum: 0.33 ± 0.06, n = 4; fimbria: 0.22 ± 0.01, n = 3) and NG2GluA2-lox groups (corpus callosum: 0.32 ± 0.11, n = 4; fimbria: 0.20 ± 0.06, n = 3) in each region investigated (unpaired t-test; corpus callosum: p = 0.94 ; fimbria: p = 0.76). In parallel, we assessed the fraction of NG2+CC1- cells in the YFP+ recombined cell population. It was similar between both experimental groups, NG2GluA2-wt (corpus callosum: 0.57 ± 0.06, n = 4; fimbria: 0.67 ± 0.05, n = 3) and NG2GluA2-lox (corpus callosum: 0.58 ± 0.08, n = 4; fimbria: 0.67 ± 0.11, n = 3) (unpaired t-test; corpus callosum: p = 0.92; fimbria: p = 1). Furthermore, we observed the same outcome at a later time point, during the PND 18 - PND 20 time period, seven to nine days after the detected increase in proliferation. On PND 20, the fraction of YFP+ recombined oligodendrocytes and NG2+ cells was also similar between the NG2GluA2-wt (NG2-CC1+ fraction: corpus callosum: 0.80 ± 0.02, n = 4; fimbria: 0.61 ± 0.07, n = 4 ; dorsal cortex: 0.47 ± 0.05, n = 4; NG2+CC1- fraction: corpus callosum: 0.17 ± 0.02, n = 4; fimbria: 0.31 ± 0.06, n = 4 ; dorsal cortex: 0.50 ± 0.05, n = 4) and NG2GluA2-lox groups (NG2-CC1+ fraction: corpus callosum: 0.73 ± 0.04, n = 4; fimbria: 0.61 ± 0.06, n = 4 ; dorsal cortex: 0.51 ± 0.03, n = 4; NG2+CC1- fraction: corpus callosum: 0.21 ± 0.03, n = 4; fimbria: 0.28 ± 0.06, n = 4 ; dorsal cortex: 0.46 ± 0.02, n = 4). The NG2-CC1+ fraction was calculated to ensure that NG2 cells produced after PND 11 had time to completely differentiate into oligodendrocytes. On PND 20, the fraction of YFP+ recombined oligodendrocytes in the NG2GluA2-lox group remained identical to the NG2GluA2-wt group (unpaired t-test: corpus callosum: p = 0.17; fimbria: p = 1).

However, the recombined cell population (YFP+) is also composed of double positive NG2 and CC1 cells (NG2+CC1+), and double negative NG2 and CC1 cells (NG2-CC1-). In the early or late postnatal period, both NG2GluA2-wt and NG2GluA2-lox group display similar fraction of NG2+CC1+ fraction (PND11: corpus callosum: NG2GluA2-wt: 0.014 ± 0.008, n = 4 ; NG2GluA2-lox: 0.007 ± 0.004, n = 4; unpaired t-test: p = 0.46; fimbria: NG2GluA2-wt: 0.013 ± 0.008, n = 3; NG2GluA2-lox: 0.010 ± 0.010, n = 3; unpaired

t-test: p = 0.83; PND 18-20: corpus callosum: NG2GluA2-wt: 0.005 ± 0.002, n = 4; NG2GluA2-lox: 0.003 ± 0.001, n = 4; unpaired t-test: p = 0.48; fimbria: NG2GluA2-wt: 0.008 ± 0.003, n = 4; NG2GluA2-lox: 0.004 ± 0.002, n = 4; unpaired t-test: p = 0.30; dorsal cortex: NG2GluA2-wt: 0.009 ± 0.005, n = 4; NG2GluA2-lox: 0.006 ± 0.002, n = 4; unpaired t-test: p = 0.69) and NG2-CC1- fraction (PND11: corpus callosum: NG2GluA2-wt: 0.12 ± 0.03, n = 4; NG2GluA2-lox: 0.10 ± 0.04, n = 4; unpaired t-test: p = 0.74; fimbria: NG2GluA2-wt: 0.06 ± 0.01, n = 3; NG2GluA2-lox: 0.13 ± 0.07, n = 3; unpaired t-test: p = 0.36; PND 18-20: corpus callosum: NG2GluA2-wt: 0.033 ± 0.01, n = 4; NG2GluA2-lox: 0.058 ± 0.01, n = 4; unpaired t-test: p = 0.13; fimbria: NG2GluA2-wt: 0.09 ± 0.02, n = 4; NG2GluA2-lox: 0.10 ± 0.02, n = 4; unpaired t-test: p = 0.95; dorsal cortex: NG2GluA2-wt: 0.03 ± 0.01, n = 4; NG2GluA2-lox: 0.03 ± 0.01, n = 4; unpaired t-test: p = 0.89).

In addition to the effect of the GluA2 deletion on the oligodendroglia cell lineage, we examined the fate of early postnatal NG2 cells marked by YFP reporter on PND 4. In the corpus callosum, on PND 11, 30 % of NG2 cells differentiated into oligodendrocytes, and 55 % remained as NG2 cells. One week later, on PND 18 - 20, 75 % of NG2 cells differentiated into oligodendrocytes, and only 20 % remained as NG2 cells (Figure 3.7). The early postnatal differentiation rate depends on the brain region. It is increased in the white matter compared to the grey matter. Moreover, in the white matter regions, the differentiation of the NG2 cells is more important in the corpus callosum than in the fimbria at this time point of development (Figure 3.7).

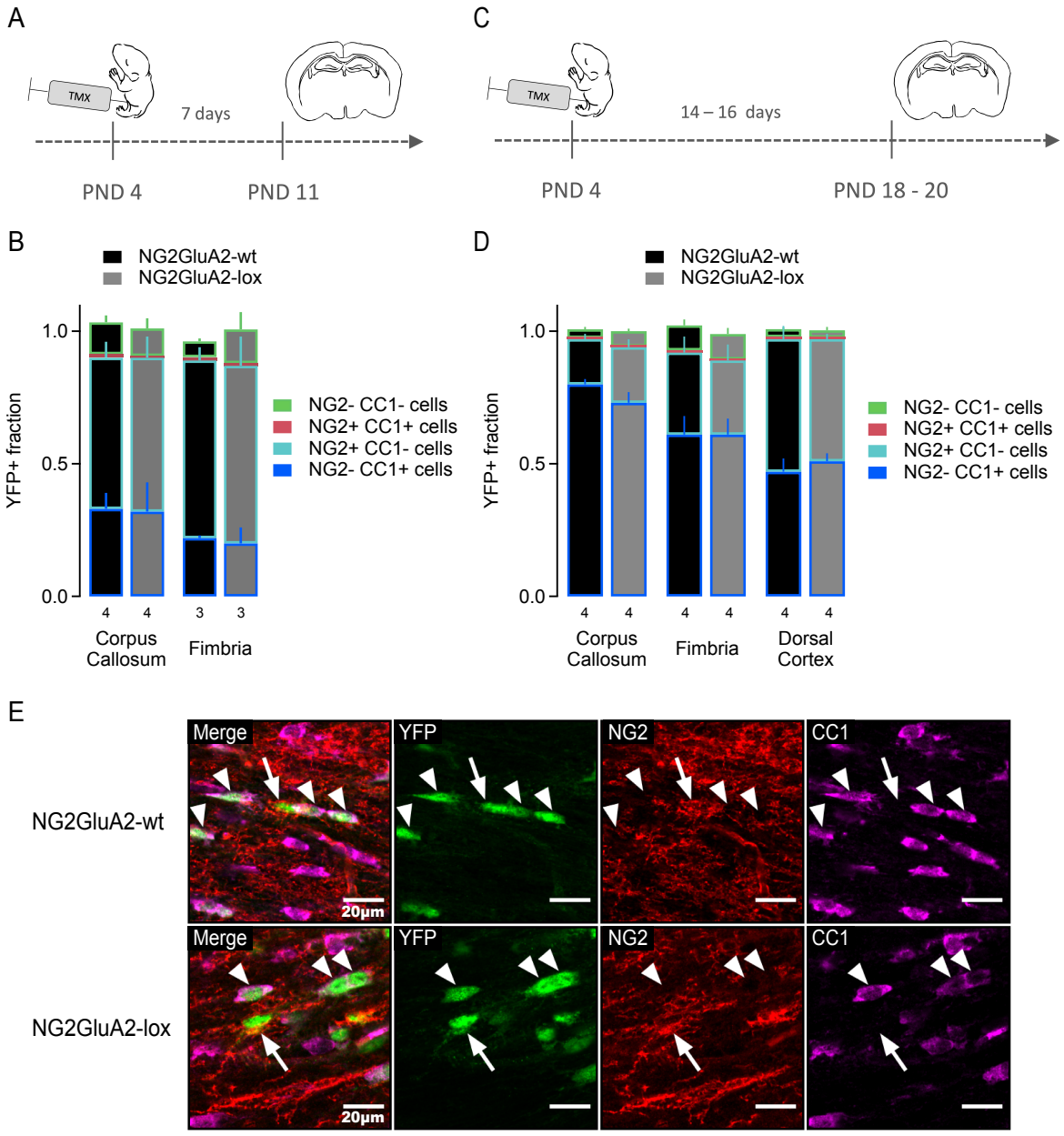

Figure 3.7 GluA2 deletion does not affect the differentiation rate of NG2 cells. A. Experimental timeline: tamoxifen injection on PND 4 followed by immunohistochemistry on PND 11. B. Fraction of NG2+CC1-, NG2-CC1+, NG2+CC1+, and NG2-CC1- cells in the YFP+ recombined population in the corpus callosum and the fimbria on PND 11. C. Experimental timeline: tamoxifen injection on PND 4 followed by immunohistochemistry on PND 18 to PND 20. D. Fraction of NG2+CC1-, NG2-CC1+, NG2+CC1+, and NG2-CC1- cells in the YFP+ recombined population in the corpus callosum, the fimbria and the dorsal cortex. E. Exemplary confocal scans of NG2GluA2-wt and NG2GluA2-lox mice brain sections. Identification of NG2+YFP+ cells (arrow) and CC1+YFP+ cells (arrowhead) with YFP (green), NG2 (red), and CC1 (purple) immunohistochemistry on PND 20 in the corpus callosum. Scale bar = 20µm.

Overall, GluA2 deletion in the early postnatal days leads to an increase in DNA replication in white matter NG2 cells but does not affect the proliferative NG2 cell fraction, the number of mitotic NG2 cells, the fraction of apoptotic NG2 cells, and the differentiation rate. The density of NG2 cells and of oligodendrocytes remains unchanged 7 days or 16 days after the deletion of GluA2.

3.4 Dysregulation of the oligodendrocyte internode length by GluA2 deletion.

Myelination is dependent on NG2 cell differentiation into oligodendrocytes which relies on neuronal activity (Demerens et al., 1996). It has been postulated that calcium signaling induced by neuronal synaptic input in NG2 cells would play a role in the guidance of oligodendrocyte myelination to achieve neuronal activity dependent myelination (Sun et al., 2016). A modification of the synaptic signaling machinery, as the deletion of the AMPARs GluA2 subunit in NG2 cells, may affect oligodendrocyte properties after differentiation. Myelination pattern is determined by the number of myelin sheaths produced by oligodendrocytes, the thickness of the myelin and the internode length which defines the length of the myelinated axon segment. In this study, we investigated one property of the myelinating oligodendrocytes, the internode length, after GluA2 deletion in NG2 cells. In the following experiments, the reporter mouse model was exchanged for membranous GFP reporter instead of the cytoplasmic YFP used in the previous experiments (Figure 3.8 A). The membranous GFP reporter by labelling the membrane of the oligodendrocytes provide a precise measurement of the internode length (Figure 3.8 C). We measured the internode length in the dorsal cortex.

3.4.1 Early postnatal internode length is shortened by GluA2 deletion in NG2 cells.

In order to decipher the role of the GluA2 subunit in the onset of myelination, we assessed the internode length of recombined oligodendrocytes in both NG2GluA2-wt and NG2GluA2-lox mice. GluA2 deletion was induced on PND 4 and the internodes were measured on PND 13, during the onset of myelination. Internodes of recombined oligodendrocytes were identified with the expression of membranous GFP (Figure 3.8.B). The cumulative distribution frequencies (CDF) of internode lengths differed between the

NG2GluA2-wt and NG2GluA2-lox groups (Kolmogorov-Smirnov test: $P < 0.01$) (Figure 3.8 D). In the NG2GluA2-lox group 6.3 % of measured internodes were shorter than 15 µm, meanwhile in the NG2GluA2-wt group less than 1 % of internodes were in this range. In the early period of myelination, internodes measured in the NG2GluA2-lox tissue (46.55 ± 1.99 µm, n = 142, 5 animals) were shorter than the ones measured in the NG2GluA2-wt tissue (54.45 ± 1.65 µm, n = 161, 5 animals) (Figure 3.8 D). GluA2 deletion selectively affected the shorter internodes (NG2GluA2-wt: 37.21 ± 0.88 µm, n = 76; NG2GluA2-lox: 30.49 ± 1.16 µm, n = 85; unpaired t-test: $p < 0,0001$) and not the longer internodes (NG2GluA2-wt: 69.87 ± 1.79 µm, n = 85; NG2GluA2-lox: 70.48 ± 2.17 µm, n = 57; unpaired t-test: $p = 0.83$) (Figure 3.8 E and F). Since myelination is known to start with long internodes, the shorter internodes are considered immature internodes. Hence, GluA2 deletion in NG2 cells shortens immature internodes or delays the process of internode elongation.

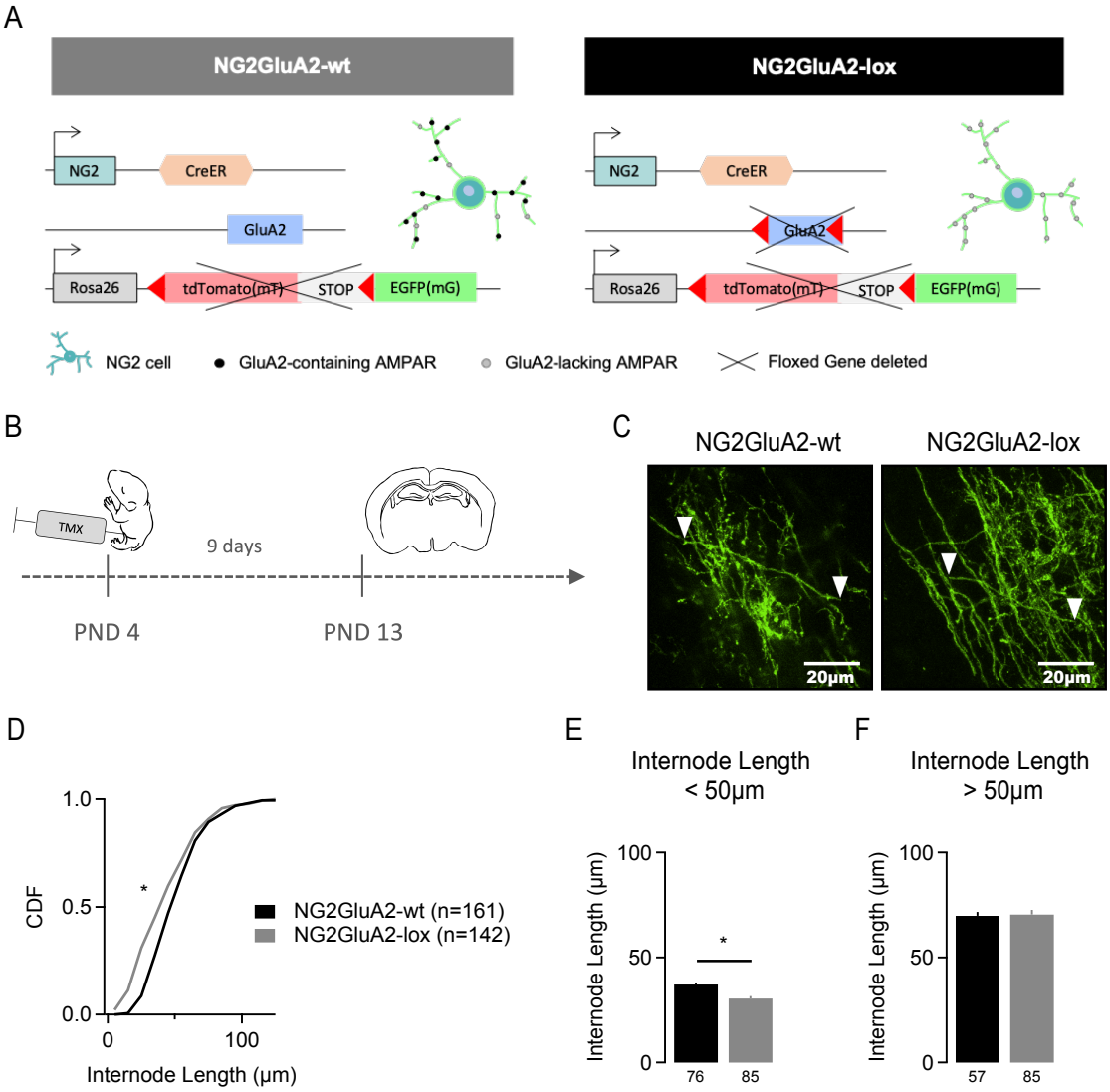

Figure 3.8. Shortened internodes after GluA2 deletion in NG2 cells at PND 13. A. Scheme of the transgenic mouse model. Conditional Cre activation under the NG2 promotor induces the deletion of the TdTomato and stop codon sentence before the GFP coding sentence. Therefore, the membranous reporter GFP is expressed after Cre activation when tamoxifen is injected. Only in the NG2GluA2-lox animals, GluA2 coding sentence is deleted after Cre activation. B. Experimental timeline with tamoxifen injection on PND 4, followed by membrane GFP labeling on PND 13. C. Exemplary scans of the membrane GFP labeling to measure the internode length for both NG2GluA2-wt and NG2GluA2-lox mice. Arrowheads indicate the endings of one measured internode. Scale bar = 20 µm. D. CDF of the internode length. E. Average of the internode length shorter than or equal to 50 µm. F. Average of the internode length longer than 50 µm.

3.4.2 Late postnatal internode length is unchanged by GluA2 deletion in NG2 cells.

Since the GluA2 deletion affects the internode length in the early stage of myelination, we assessed whether this effect would persist later in development. We chose to investigate the internode length on PND 20 when the myelination is still ongoing but already partly established. In order to exclusively measure mature internodes, we labeled the contactin-associated protein (Caspr) as a marker for established nodes of Ranvier. Internodes were defined as GFP expressing myelin flanked by two Caspr markers (Fig. 3.9 B). The cumulative distribution frequency (Kolmogorov-Smirnov test: p=0.08) and the average of the internode length were similar between the NG2GluA2-lox group and the NG2GluA2-wt group (NG2GluA2-wt: 37.45 ± 1.33 µm, n = 159, 3 animals; NG2GluA2-lox: 39.14 ± 1.04 µm, n = 186, 4 animals; unpaired t-test: p = 0.31) (Figure 3.9). The length of mature internodes on PND 20 is not affected by the deletion of the GluA2 subunit in early postnatal NG2 cells.

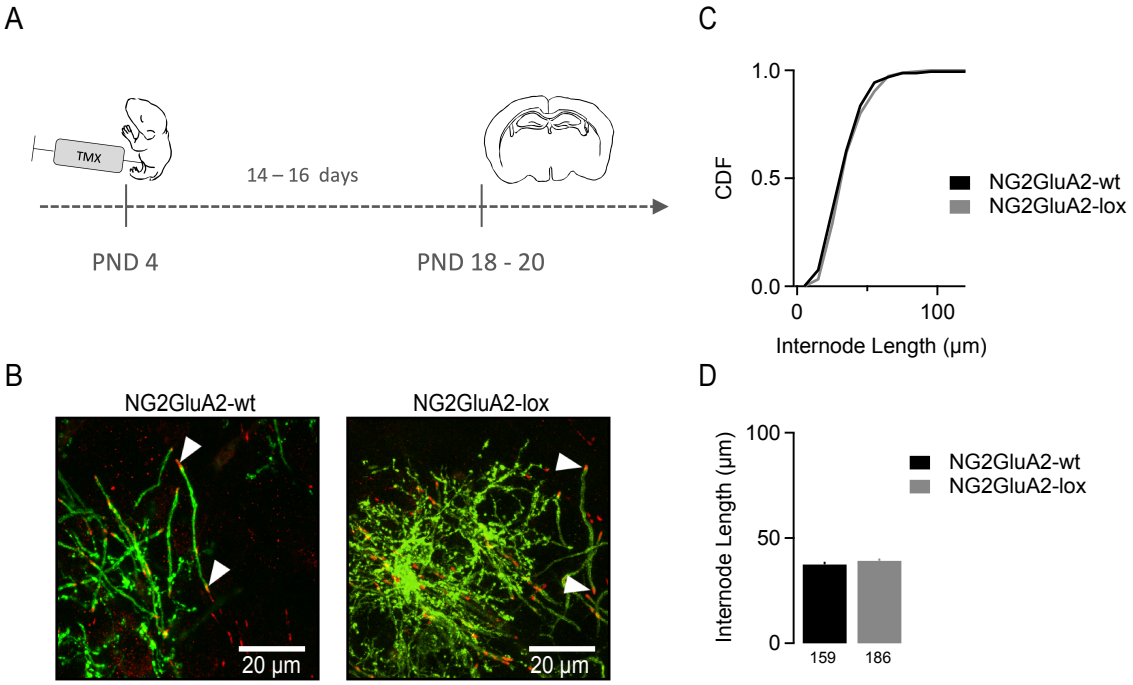

Figure 3.9 Unchanged internode length on PND 20 after GluA2 deletion. A. Experimental timeline with a single tamoxifen injection on PND 4, followed by membrane GFP labeling between PND 18 and PND 20. B. Exemplary scans of the internode length measurement with the GFP-labeled internode (green) and the Caspr-labeled node of Ranvier (red) marked by the arrowheads on PND 18–20 for both NG2GluA2-wt and NG2GluA2-lox mice. Scale bar = 20 µm. C. CDF of the internode length. D. Average of the internode length.

3.4.3 GluA2 subunit deletion affects the internode length differently regarding their position in the cortex layer.

Because the myelination process first takes place in the deep layers of the cortex and then in the superficial layers, we divided the measured internodes regarding their location in the superficial or deep layers of the cortex for both early and late postnatal myelination phases. In the early postnatal myelination phase, the internodes were shorter in the NG2GluA2-lox group in the deep (NG2GluA2-lox: 47.04 ± 2.55 µm, n = 112; NG2GluA2-wt: 52.76 ± 1.67 µm, n = 117; unpaired t-test: p = 0.04) and superficial layers (NG2GluA2-lox: 46.56 ± 3.68 µm, n = 27; NG2GluA2-wt: 58.95 ± 4.04 µm, n = 44; unpaired t-test: p = 0.04) in comparison to the NG2GluA2-wt group. The effect of the absence of GluA2 in NG2 cells on the internode length did not depend on the location of axons in the cortex (Figure 3.10).

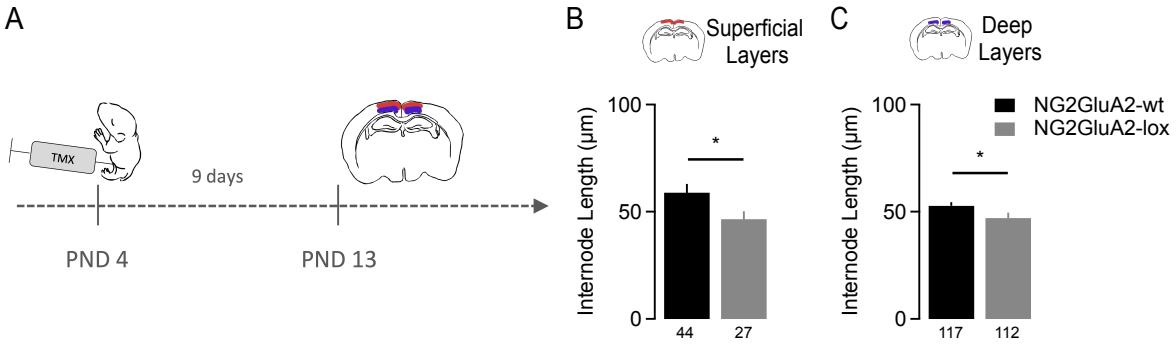

Figure 3.10. GluA2 deletion affects the internode length in dependence of their position in the cortical layer on PND 13. A. Experimental timeline with tamoxifen injection on PND 4, followed by membrane GFP labeling on PND 13. B. Internode length average in the superficial cortical layers on PND 13. C. Internode length average in the deep cortical layers on PND 13.

However, in the late postnatal myelination phase, the internodes in the deep layers were elongated in the NG2GluA2-lox group (46.59 ± 2.62 µm, n = 49) compared to the NG2GluA2-wt group (39.51 ± 2.06 µm, n = 90, unpaired t-test: p = 0.04). The internodes located in the superficial layers were not affected by the GluA2 deletion in the late postnatal myelination phase (NG2GluA2-wt: 34.76 ± 1.40 µm, n = 69; NG2GluA2-lox: 36.48 ± 0.97 µm, n = 137, unpaired t-test: p = 0.32) (Figure 3.11). GluA2 deletion in NG2 cells induces a shortening of the internode length in the early postnatal myelination phase independently of the axon location. However, in the late postnatal myelination phase, GluA2 deletion in NG2 cells induces an elongation of the internodes only in the deep

layers of the cortex. For the latter, the effect of the GluA2 subunit deletion in NG2 cells depend on the axon location in the cortex.

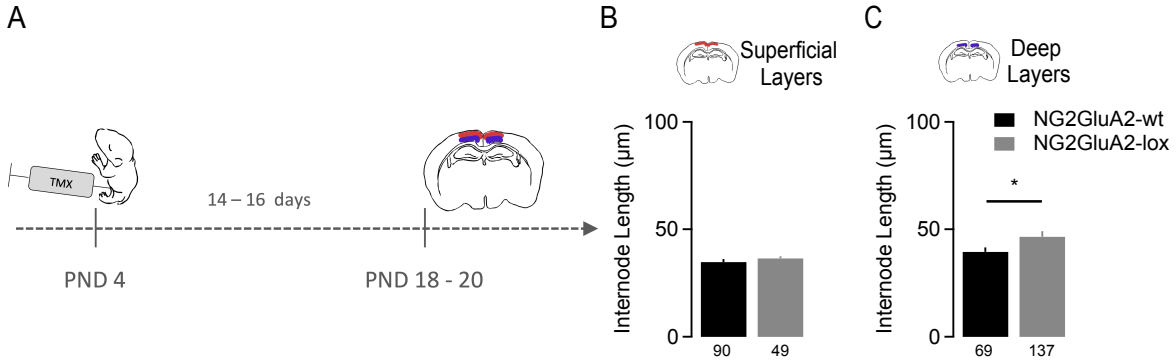

Figure 3.11 GluA2 deletion affects the internode length in dependence of their position in the cortical layer on PND 20. A. Experimental timeline with a single injection on PND 4, followed by membrane GFP labeling between PND 18 and PND 20. B. Internode length average in the superficial cortical layers between PND 18 and PND 20. C. Internode length average in the deep cortical layers between PND 18 and PND 20.

3.5 GluA2 deletion in NG2 cells in the context of motor learning activity.

GluA2 deletion in NG2 cells affects NG2 cells proliferation and the internode length during the myelination onset. To further investigate the critical role of the GluA2 subunit in the fate of NG2 cells and its physiological consequences, we assessed the role of GluA2 deletion in myelination and NG2 cell proliferation during a motor learning paradigm known to recruit the oligodendroglia lineage cells in the motor cortex area. This paradigm stimulates NG2 cells proliferation and oligodendrocytes generation (McKenzie et al., 2014).

3.5.1 Motor skills are not affected by GluA2 deletion.

First, we ensured the motor skills not to be affected by the GluA2 deletion. To assess the motor skills, we measured the falling speed and the latency to fall during an increasing speed protocol on the rotarod. The NG2GluA2-lox mice (falling speed: 24.95 ± 2.44 RPM, n = 8; Latency to fall: 170.71 ± 20.32 s, n = 8) presented the same performance as the NG2GluA2-wt mice (falling speed: 28.57 ± 2.71 RPM, n = 7; Latency to fall: 201.76 ± 22.77 s, n = 7) (Unpaired t-test, falling speed: $p = 0.34$; latency to fall: $p = 0.33$) (Figure 3.12). Therefore, we consider the GluA2 deletion in young NG2 cells to have no impact on motor skills.

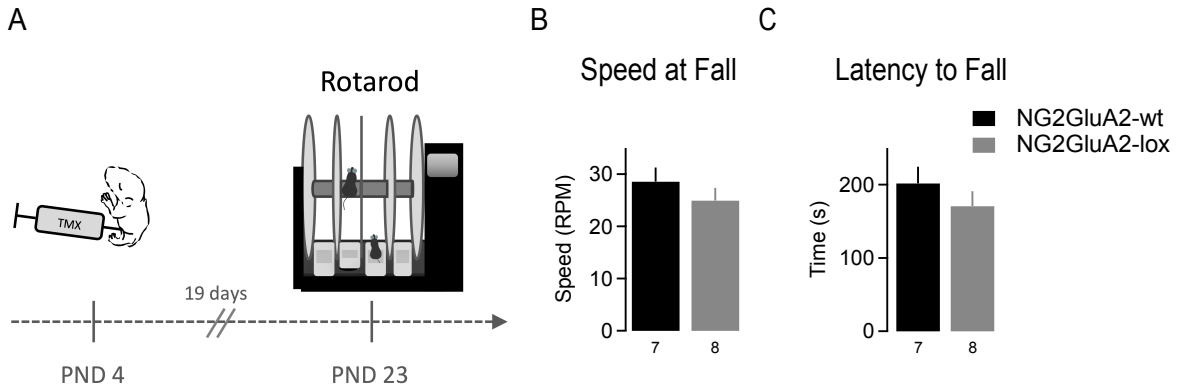

Figure 3.12. Unaltered motor skills after postnatal GluA2 deletion in NG2 cells. A. Experimental timeline: assessment of the motor ability on PND 23, 19 days after NG2 cell recombination on PND 4. B. Speed at fall of the NG2GluA2-wt and NG2GluA2-lox mice. C. Latency to fall for the NG2GluA2-wt and NG2GluA2-lox mice.

3.5.2 Motor learning is impaired by GluA2 deletion in NG2 cells.

It has been proven that motor learning paradigm in a running wheel increases NG2 cells proliferation and oligodendrocytes generation. We use this paradigm to assess the role of the GluA2 subunit in the fate of NG2 cells and overall in the mouse behavior. The motor learning paradigm is composed of two phases: the habituation for two days in a regular wheel followed by six days of motor learning in a complex wheel (Figure 3.13.A). The regular wheel is composed of 32 rungs while the complex wheel is composed of 22 unevenly spaced rungs (Figure 3.13.A). In the regular wheel, NG2GluA2-wt and NG2GluA2-lox group display a similar performance for the four parameters investigated (Average speed : NG2GluA2-wt group: 8.2 ± 1.3 m/min, n = 9; NG2GluA2-lox group: 8.1 ± 1.5 m/min, n = 10; unpaired t-test: p = 0.96 ; Maximum speed : NG2GluA2-wt group: 16.5 ± 1.6 m/min, n = 9; NG2GluA2-lox group: 16.4 ± 1.9 m/min, n = 10; unpaired t-test: p = 0.97 ; Running time : NG2GluA2-wt group: 128.7 ± 26.4 min, n = 9; NG2GluA2-lox group: 125.3 ± 24.6 min, n = 10; unpaired t-test: p = 0.93 ; Running distance : NG2GluA2-wt group: 1245.4 ± 384.4 m, n = 9; NG2GluA2-lox group: 1279.5 ± 452.9 m, n = 10; unpaired t-test: p = 0.96) (Figure 3.13). GluA2 deletion in NG2 cells does not affect the motor performance in the running wheel. As previously seen in the rotarod, NG2GluA2-wt and NG2GluA2-lox mice show similar motor performances. Then, the mice must adapt from running in the regular wheel to running in the more difficult, complex wheel. The adaptation to the complex wheel is fast, neither the average speed (NG2GluA2-wt group

R2: 18.04 ± 2.30 m/min, n = 8; C1: 16.48 ± 1.51 m/min, n = 8; unpaired t-test: p = 0.58; NG2GluA2-lox group R2: 17.04 ± 2.11 m/min, n = 10; C1: 17.42 ± 1.64 m/min, n = 9; unpaired t-test: p = 0.89) nor the maximum speed (NG2GluA2-wt group R2: 0.27 ± 1.91 m/min, n = 8; C1: 9.29 ± 1.39 m/min, n = 8; unpaired t-test: p = 0.99; NG2GluA2-lox group R2: 9.69 ± 1.66 m/min, n = 10; C1: 9.14 ± 1.35 m/min, n = 9; unpaired t-test: p = 0.80) were decreased between the last day of regular wheel (R2) and the first day of complex wheel (C1) in both groups (Figure 3.13.B, C).

We assessed the performance of the mice over time with the average speed and maximum speed recording during the active phase. Over time, the mice boost their ability to run in the complex wheel. A motor learning occurs when the average speed and maximum speed are increased on the last day of training (C6) compared to the first day (C1). The average speed (C1: 9.29 ± 1.39 m/min, n = 8; C6: 13.87 ± 2.06 m/min, n = 7; unpaired t-test: p = 0.08) and maximum speed (C1: 16.48 ± 1.51 m/min, n = 8; C6: 23.45 ± 1.33 m/min, n = 7; unpaired t-test: p = 0.005) increased on the last day compared to the first day of complex wheel in the NG2GluA2-wt group. However, the NG2GluA2-lox group presented a similar average speed (C1: 9.14 ± 1.35 m/min, n = 9; C6: 11.28 ± 2.31 m/min, n = 6; unpaired t-test: p = 0.41) and maximum speed (C1: 17.42 ± 1.64 m/min, n = 9; C6: 21.33 ± 2.22 m/min, n = 6; unpaired t-test: p = 0.17) between the first and last day of complex wheel (Figure 3.13.B, C). The NG2GluA2-lox mice group failed to improve their performance during a motor learning task in contrast to the NG2GluA2-wt mice group. The difference in speed performance between both groups does not depend on a training difference. Normalized running time and distance, of the last day on the first day of complex wheel revealed that the mice from both groups spent a similar time on the wheel (NG2GluA2-wt: 2.09 ± 0.77, n = 7; NG2GluA2-lox: 1.16 ± 0.24, n = 6; unpaired t-test: p = 0.31) and ran a similar distance (NG2GluA2-wt: 3.64 ± 1.42, n = 7; NG2GluA2-lox: 1.46 ± 0.39, n = 6; unpaired t-test: p = 0.20) (Figure 3.13.D, E).

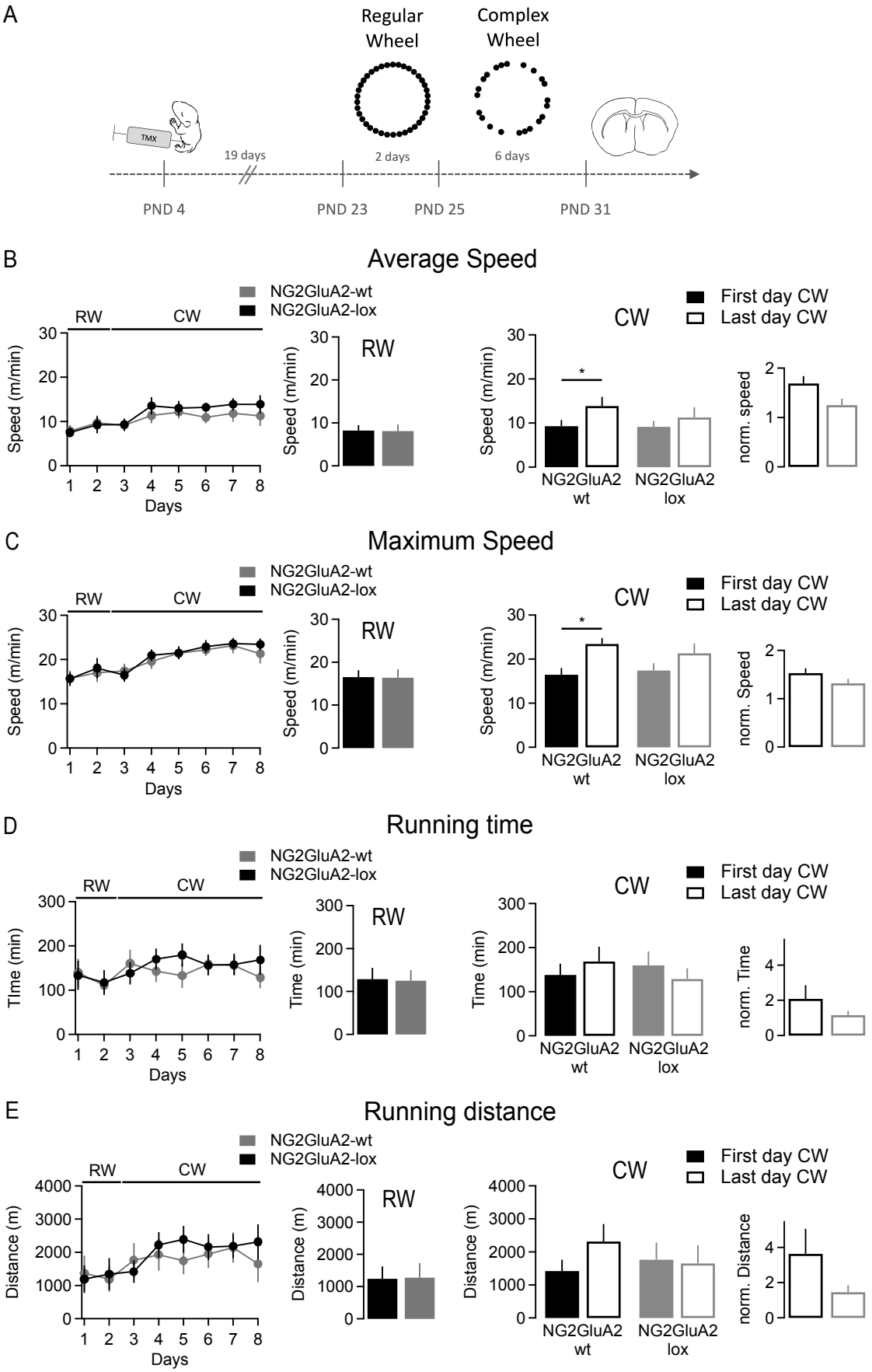
A
Regular Wheel
Complex Wheel
TMX
19 days
2 days
6 days
PND 4
PND 23
PND 25
PND 31
B
Average Speed
NG2GluA2-wt
NG2GluA2-lox
RW
CW
Speed (m/min)
Days
First day CW
Last day CW
norm. speed
NG2GluA2 wt
NG2GluA2 lox
C
Maximum Speed
norm. Speed
D
Running time
Time (min)
norm. Time
E
Running distance
Distance (m)
norm. Distance

Figure 3.13 GluA2 deletion decreases motor skill learning. A. Experimental timeline for the motor skill learning paradigm after NG2 cell recombination on PND 4. B, C, D, E. From left to right: Performance overtime in the regular wheel (RW: Day 1, Day 2) and the complex wheel (CW : Day3 to Day 8) in the NG2GluA2-wt and NG2GluA2-lox group. Comparison of NG2GluA2-wt and NG2GluA2-lox performances in the RW. Comparison of NG2GluA2-wt and NG2GluA2-lox performances in the complex wheel for the first and last day of CW. Comparison of the Normalized performances of the last day of CW on the first day of CW in the NG2GluA2-wt and NG2GluA2-lox group. B. Average speed. C. Maximum speed. D. Running time. E. Running distance.

In parallel, we normalized the performance of the last day of complex wheel on the first day of complex wheel for both groups. NG2GluA2-wt and NG2GluA2-lox comparison indicated a higher performance in the NG2GluA2-wt group only for the average speed (NG2GluA2-wt: 1.69 ± 0.15, n = 7; NG2GluA2-lox: 1.25 ± 0.13, n = 6; unpaired t-test: p = 0.05) (Figure 3.13.B). In conclusion, the early postnatal GluA2 deletion in NG2 cells prevents a fast motor learning in the motor learning paradigm.

3.5.3 GluA2 subunit deletion in NG2 cells did not alter the internode length in the motor cortex during a motor learning paradigm.

We investigated whether the difference in the motor learning performance between the NG2GluA2-wt mice and the NG2GluA2-lox mice is related to different myelination properties in the motor cortex. A lower performance in the wheel motor learning paradigm suggested an impairment of the myelin properties in the motor cortex as we measured shorter internode length in the NG2GluA2-lox mice during early myelination. The internode length averages were similar in NG2GluA2-wt and NG2GluA2-lox groups (NG2GluA2-wt: 32.25 ± 1.45 µm, n = 6; NG2GluA2-lox: 32.85 ± 0.91 µm, n = 6; unpaired t-test: p = 0.73) (Figure 3.14.C) independent of the cortex layer (superficial layer, NG2GluA2-wt: 30.94 ± 1.36 µm, n = 94; NG2GluA2-lox: 28.54 ± 1.33 µm, n = 61; unpaired t-test: p = 0.23; middle layer, NG2GluA2-wt: 30.52 ± 0.80 µm, n = 328; NG2GluA2-lox: 31.97 ± 0.79 µm, n = 310; unpaired t-test: p = 0.35; deep layer, NG2GluA2-wt: 36.93 ± 1.88 µm, n = 95; NG2GluA2-lox: 39.33 ± 2.59 µm, n = 38; unpaired t-test: p = 0.48) (Figure 3.14.D). In addition, the cumulative distribution frequency of the internode length in NG2GluA2-wt and NG2GluA2-lox appeared to be similar (Kolmogorov-Smirnov test: p = 0.99) (Figure 3.14.B).

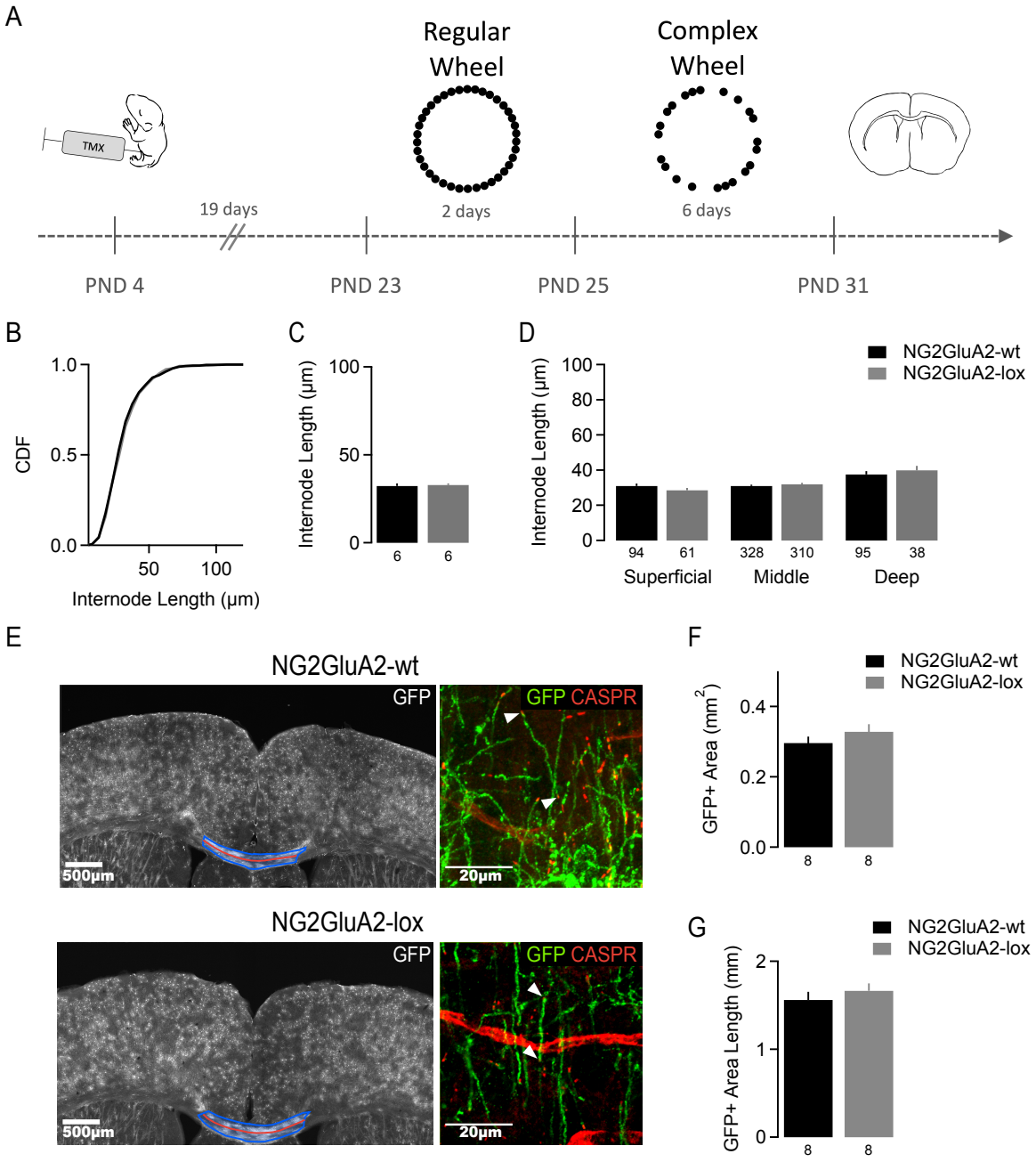

Figure 3.14. Unchanged internodes length and myelination spread after GluA2 subunit deletion in NG2 cells during the wheel motor learning paradigm. A. Experimental timeline: GFP, Caspr labelling, and, measurement of internode length on PND 31 after GluA2 deletion on PND 4 and motor learning task from PND 23 and PND 31. B. Cumulative distribution frequency of the internode length. C. Internode length average in NG2GluA2-wt and NG2GluA2-lox group. D. Internode length average per group in respect of their distribution in the motor cortex. E. Left: Exemplary confocal scans to measure the spread of GFP+ fluorescence in the corpus callosum. In blue, the GFP+ area measurement, in red, the GFP+ area length measurement. Scale bar: 500 µm. Right: Exemplary confocal scans to measure the internode length in the motor cortex. Scale bar = 20 µm. F. Area of GFP+ cells in the corpus callosum G. Length of the GFP+ cells area in the corpus callosum.

Motor coordination depends on the connection of the two hemispheres going through the corpus callosum (Bloom and Hynd, 2005). We measured the spread of the GFP+ area in the corpus callosum to account for the myelination ability of the recombined oligodendrocyte population. The myelination speed in the corpus callosum was assessed by measuring the length and the area of the GFP+ fluorescence (Figure 3.14.E). These parameters were similar in both groups (NG2GluA2-wt: GFP+ area: 0.30 ± 0.02 mm^2, n = 8; GFP+ area length: 1.56 ± 0.09 mm, n = 8; NG2GluA2-lox: GFP+ area: 0.33 ± 0.02 mm^2, n = 8; GFP+ area length: 1.67 ± 0.08 mm, n = 8; unpaired t-test: GFP+ area: p = 0.27 ; GFP+ area length: p = 0.42) (Figure 3.14.F, G).

Therefore, we conclude that the early postnatal GluA2 deletion in NG2 cells does not affect the internode length in the motor cortex and the myelination speed in the corpus callosum during a motor learning paradigm.

3.5.4 GluA2 subunit deletion in NG2 cells does not affect NG2 cell proliferation after a wheel motor learning task.

Wheel motor learning paradigm increases NG2 cells proliferation which suggests the GluA2 subunit in NG2 cells to play a role. Therefore, we assessed the cell proliferation known to take place mostly in NG2+ cells (Dawson et al., 2003). Proliferation was assessed with EdU, an analog of thymidine, incorporated into DNA during DNA synthesis. EdU was administered in drinking water during the six consecutive days of the complex wheel. We measured the EdU+ fraction of four different cell populations as described in the following description. The EdU+CC1-GFP- cells (NG2GluA2-wt: motor cortex: 0.68 ± 0.040, n = 5; corpus callosum: 0.27 ± 0.06, n = 4; NG2GluA2-lox: motor cortex: 0.65 ± 0.07, n = 5; corpus callosum: 0.40 ± 0.04, n = 4) and EdU+CC1-GFP+ cells (NG2GluA2-wt: motor cortex: 0.29 ± 0.037, n = 5; corpus callosum: 0.22 ± 0.04, n = 4; NG2GluA2-lox: motor cortex: 0.32 ± 0.07, n = 5; CC1-GFP+: 0.19 ± 0.06, n = 4) represented proliferating non-recombined NG2 cells and proliferating recombined NG2 cells, respectively. The EdU+CC1+GFP- cells (NG2GluA2-wt: motor cortex: 0.027 ± 0.008, n = 5; corpus callosum: 0.27 ± 0.04, n = 4; NG2GluA2-lox: motor cortex: 0.026 ± 0.008, n = 5; corpus callosum: 0.29 ± 0.04, n = 4) and EdU+CC1+GFP+ cells (NG2GluA2-wt: motor cortex: 0.006 ± 0.003, n = 5; corpus callosum: 0.12 ± 0.02, n = 4; NG2GluA2-lox: motor cortex: 0.004 ± 0.002, n = 5; corpus callosum: 0.12 ± 0.02, , n = 4) represented, respectively,

newly formed oligodendrocytes and newly formed oligodendrocytes originating from recombined NG2 cells. The four different categories of cells presented similar EdU fraction in the NG2GluA2-wt group for the two regions investigated, the corpus callosum and the motor cortex. GluA2 deletion did not affect the fraction of NG2 cells nor oligodendrocytes taking up EdU in the motor cortex or corpus callosum during the motor learning paradigm (NG2GluA2-wt : motor cortex: CC1+GFP+: 0.012 ± 0.007, n = 5; CC1-GFP+: 0.16 ± 0.018, n = 5; corpus callosum: CC1+GFP+: 0.36 ± 0.08, n = 5; CC1-GFP+: 0.48 ± 0.10, n = 5; NG2GluA2-lox: motor cortex: CC1+GFP+: 0.014 ± 0.009, n = 5; CC1-GFP+: 0.18 ± 0.034, n = 5; corpus callosum: CC1+GFP+: 0.35 ± 0.05, n = 5; CC1-GFP+: 0.46 ± 0.13, n = 5) (Figure 3.15.B, C). The proliferation and generation of new oligodendrocytes during motor learning is not affected by GluA2 deletion in early postnatal NG2 cells.

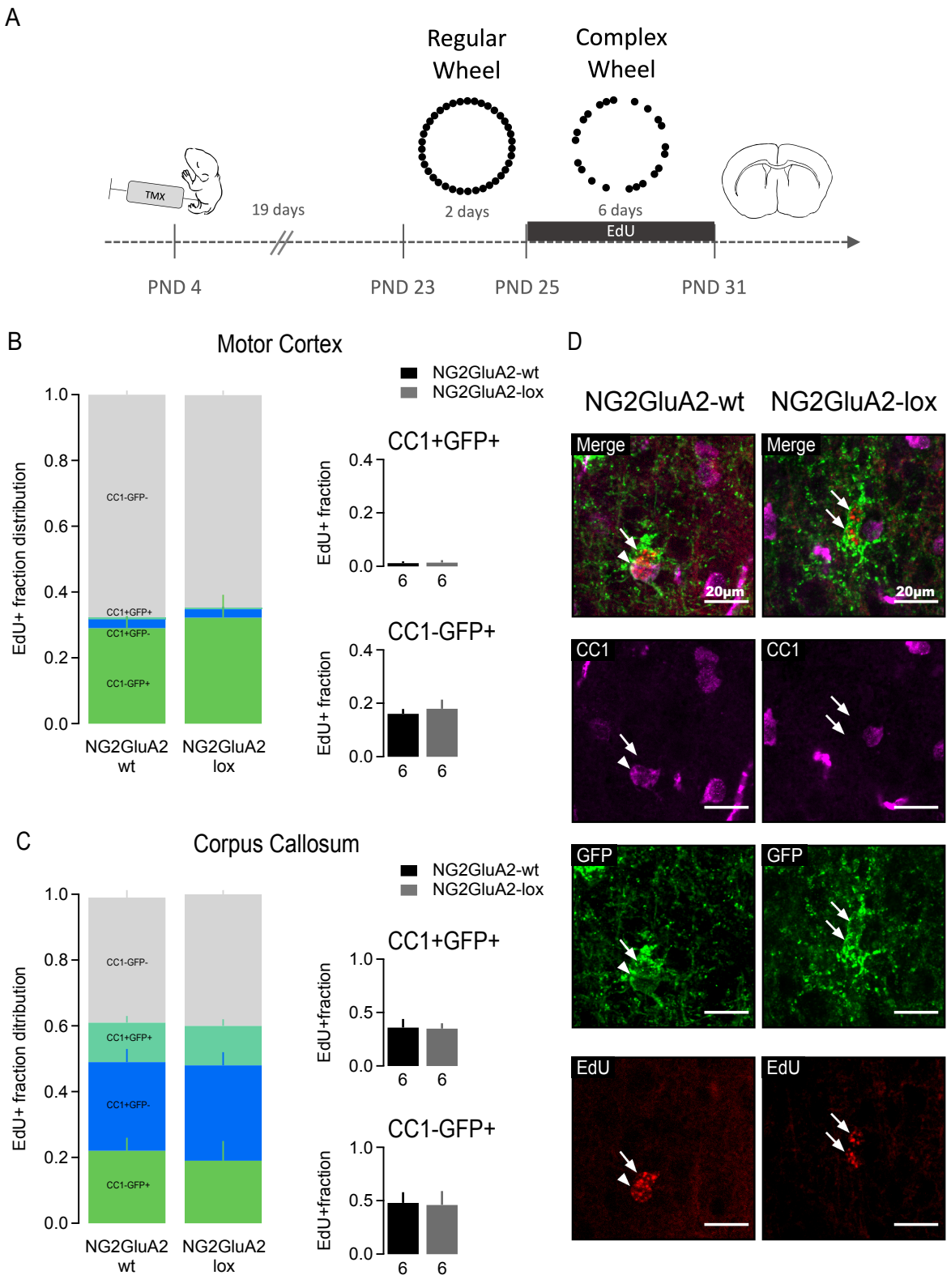

Figure 3.15. Proliferation of NG2 cells is not affected by motor learning paradigm after GluA2 deletion. A. Experimental timeline: NG2GluA2-wt and NG2GluA2-lox mice receive EdU on PND 25 and during six days of complex wheel after NG2 cell recombination on PND 4. B.C. Left: Fraction of the oligodendrocyte cell population in the EdU+ cell population. Right: EdU+

fraction in the CC1+GFP+ and CC1-GFP+ cell population respectively in the motor cortex (B) and the corpus callosum (C). D. Exemplary scans after EdU quadruple labeling in NG2GluA2-wt and NG2GluA2-lox group. Scale bar = 20 µm.

In the motor cortex, the largest fraction of EdU+ cells are NG2 cells. Meanwhile, in the corpus callosum, the largest fraction are oligodendrocytes. This indicates that, independently of the experimental group, there is a high fraction of newly formed oligodendrocytes in the corpus callosum after motor learning, that is not observed in the motor cortex.

4 Discussion

Amongst glia cells, only NG2 cells receives direct synaptic input from neurons. During NG2 cell division, the maintenance of neuronal synaptic input to NG2 cell (Kukley et al., 2008) suggest an essential role of this connection in NG2 cell function. Although neuron–NG2 cell synaptic communication is known to be essential to myelinogenesis (Demerens et al., 1996), the mechanism through which the neuronal synaptic input regulates the fate of NG2 cells remains unknown. As AMPARs are mainly responsible for the glutamatergic synaptic input integration in NG2 cells, we investigated the role of AMPARs in the regulation of NG2 cells fate. The calcium signaling pathway is a candidate through which the AMPARs activation can regulate NG2 cells fate. Calcium permeability in AMPARs depends on the expression of the GluA2 subunit, with GluA2-lacking AMPARs being permeable to calcium and GluA2-containing AMPARs impermeable to calcium (Cull-candy et al., 2006). Moreover, the expression of the GluA2 subunit is differentially regulated through the development. It has been shown that during brain development, GluA2 subunit in NG2 cell is downregulated (Ziskin et al., 2007) which suggest an increase in calcium permeability through AMPARs. In parallel, NG2 cell proliferation slows down during brain development. Therefore, we suggested that the calcium signal induced by synaptic input in NG2 cells might be linked to the proliferation rate of NG2 cells through the expression of the GluA2 subunit in NG2 cells. Since a low proliferation rate in NG2 cells is correlated with the downregulation of the GluA2 subunit, we hypothesized GluA2 deletion in NG2 cells to decrease NG2 cells proliferation. Deciphering the role of GluA2 subunit in NG2 cells fate reveals four main findings. First, GluA2 subunit in postnatal NG2 cells regulates the cell cycle of NG2 cells through DNA synthesis regulation. Second, GluA2 subunit in early postnatal NG2 cells regulates the myelination speed. Third, NG2 cell population is a heterogeneous cell population across the brain region area and the developmental stage. Fourth, GluA2 subunit in postnatal NG2 cells plays a role in the motor cognitive learning.

Role of GluA2 subunit in cell cycle of NG2 cells

Our main hypothesis suggested a decrease in NG2 cells proliferation after GluA2 deletion in postnatal NG2 cells. Our results suggest the opposite. Postnatal GluA2 deletion in NG2 cells increases the fraction of NG2 cells BrdU uptake (Figure 3.1). BrdU is known as a proliferation marker. This thymidine analogue is inserted in DNA during DNA replication. The insertion of BrdU being linked to DNA replication during cell proliferation, our results suggests that rendering AMPARs calcium permeable, through GluA2 deletion in postnatal NG2 cells, increases NG2 cell proliferation. Recent studies suggest as well that GluA2 subunit in NG2 cells plays a role in their proliferation (Chen et al., 2018; Khawaja et al., 2021). In agreement with our finding, NG2 cell proliferation was increased when NG2 cells were transduced with a retrovirus expressing modified GluA2 subunit in postnatal NG2 cells in vivo leading to an increase of AMPARs calcium permeability (Chen et al., 2018). Later in the adult period when AMPARs are permeable to calcium and lack the GluA2 subunit, an overexpression of the GluA2 subunit, using a transgenic mouse line, increases NG2 cell proliferation (Khawaja et al., 2021). In contrary to the postnatal period, rendering AMPARs impermeable to calcium favors NG2 cell proliferation in the adult period. GluA2 deletion in postnatal or adult NG2 cells plays a role in NG2 cells proliferation. However, the study from Kougioumtzidou et al. in 2017 showed the opposite. Using a germline knock-out of the GluA2 subunit, they found that GluA2 subunit deletion in NG2 cells had no effect on the proliferation of NG2 cells in the postnatal period (Kougioumtzidou et al., 2017). This result could be due to compensatory mechanisms occurring during embryonic development to compensate the lack of calcium signaling through AMPARs. The results in the studies presented above suggest that the role of GluA2 subunit on the proliferation of NG2 cells is dependent on the brain developmental stage.

Surprisingly, in our study, increased BrdU uptake occurs in all NG2 cells independently of the reporter expression which determines the deletion of the GluA2 subunit in NG2 cells for the NG2GluA2-lox mice. This finding suggests that factors released from the NG2 cells with GluA2 deletion must be responsible for the changes observed in wild-type NG2 cells. Indeed, NG2 cells have the ability to release neuromodulators as growth factors (Parolisi & Boda, 2018). We hypothesize that this released neuromodulators could affect the surrounding NG2 cells fate.

Finally, GluA2 subunit deletion in postnatal NG2 cells had no effect on the growth fraction of NG2 cells population that defines the fraction of cells actively cycling.

Increased BrdU uptake in NG2 cells does not define a proliferation increase in NG2 cell.

Cells uptake BrdU while undergoing DNA synthesis. The main cause of DNA synthesis in a cell is preparation for cell division leading to cell proliferation. An increase in the fraction of cells BrdU uptake is most commonly related to a proliferation increase in this cell population. In accordance to an increased NG2 cell proliferation we expected to find evidences to confirm that the increase in BrdU uptake correlates with an increase in proliferation. Within the NG2 cell population, we suppose three different fate for the NG2 cells newly created. First, the daughter cells remain as NG2 cells. Second, they differentiate into oligodendrocytes. Third, they undergo apoptosis. The three possibilities were investigated and none of these categories were increased after GluA2 deletion in postnatal NG2 cells. The increase in BrdU uptake in NG2 cell population suggesting an increase in cell proliferation is not supported by an increase of the oligodendrocyte lineage cell population in their progenitor (Figure 3.5), maturated (Figure 3.7) or apoptotic cell category (Figure 3.6). In addition, in the case that BrdU uptake describe an increase in cell proliferation, the number of cells undergoing mitosis should be increased as well. The mitotic phase describes the last phase of the cell cycle when the cell undergoes cell division to create two daughter cells. However, the fraction of mitotic NG2 cells remained unchanged after GluA2 deletion in the postnatal NG2 cells (Figure 3.3). The latter suggest the increased BrdU uptake in NG2 cells to show an increase in DNA synthesis which does not relate to proliferation cell increase. The postnatal GluA2 deletion in NG2 cells increases DNA synthesis in NG2 cells.

Several studies have examined the role of calcium in cell cycle regulation and have found that calcium signaling regulates cell cycle progression (Kahl & Means, 2003). Calcium acts through its effectors, such as calcineurin, calmodulin, and calmodulin kinases, which in turn regulate cyclins and cyclin kinases implicated in cell cycle regulation (Humeau et al., 2018; Kahl & Means, 2003). For example, calcium inhibits the transcription factor inhibition implicated in DNA synthesis and cell cycle progression (Humeau et al., 2018; Pennycook et al., 2020). This same transcription factor plays a role in the DNA replication

during the S phase of the cell cycle (Pennycook et al., 2020). Therefore, deletion of the GluA2 subunit which renders all AMPARs permeable to calcium might directly affect the cell cycle progression of NG2 cells. BrdU uptake takes place during the S phase of the cell cycle when the DNA is replicated. GluA2 deletion in NG2 cells might elongate the S phase duration and therefore the time for BrdU uptake during DNA replication. Therefore, an elongation of the S phase could explain an increase in BrdU uptake fraction although the cell proliferation remains unchanged after postnatal GluA2 deletion. Further investigations on the cell cycle dynamic of NG2 cells will be necessary to decipher the role of GluA2 subunit in NG2 cells.

GluA2 subunit in NG2 cells regulates oligodendrocytes internode length

Calcium signalling in the myelin sheath is correlated to the length of myelin sheath also described as internodes. Internode elongation takes place only when the frequency of calcium events reached a certain threshold in the internode (Krasnow et al., 2018). As well, a high increase in calcium signalling, as long-lasting calcium bursts, shorten the internode length (Krasnow et al., 2018). GluA2 deletion in postnatal NG2 cells increases calcium signalling due to glutamatergic synaptic input through GluA2-lacking AMPARs in NG2 cells. Deletion of GluA2 subunit in postnatal NG2 cells increases the frequency of shorter internodes in oligodendrocytes during the second postnatal week (Figure 3.8). This effect is no longer present in the third postnatal week. GluA2 deletion in postnatal NG2 cells, rather, increased the internode length in the deep cortical layers (Figure 3.9). The increased internode length in the third postnatal week seems to reveal a compensatory mechanism following the shortening of the internode length during the myelination onset. In addition, the internodes length after a learning motor task remain unaffected by the GluA2 deletion in early postnatal NG2 cells (Figure 3.14). Our results suggest GluA2 subunit deletion in early NG2 cells to shorten immature internodes during the myelination onset in the development. Therefore, GluA2 subunit in NG2 cells regulates myelination onset during the early phase of myelination in the development.

Shorter immature internodes suggest a delay in the elongation of the internodes or a delay in the maturation of newly formed oligodendrocytes. If the differentiation of NG2 cells into oligodendrocyte is delayed, the elongation or immature internodes would be delayed as

well. However, GluA2 deletion in postnatal NG2 cells did not change the differentiation rate of NG2 cells (Figure 3.7). Internodes shortening due to GluA2 deletion in NG2 cells was unexpected because oligodendrocytes do not express the GluA2 subunit (Kula, Chen, & Kukley, 2019). Absence of the GluA2 subunit in oligodendrocytes suggest that the regulation of the internode elongation might take place in the NG2 cells stage. Calcium through its effectors has the ability to regulate gene expression (Clapham, 2007). Since GluA2 subunit deletion in NG2 cells modify the calcium signaling in NG2 cells, we hypothesize GluA2 subunit deletion to delay myelination through gene expression regulation. In reference to our results, GluA2 subunit in NG2 cells plays a role in the myelination regulated by calcium signaling in NG2 cells only in the early postnatal period.

Internode lengths depend on their location in the cortex

Our data suggest a difference in internode lengths between the deep and superficial layers of the cortex (Figure 3.10). In 2014, Tomassy et al. described the internode length from the superficial layers to be shorter than the deep layers (Tomassy et al., 2014). In our case, only the internodes measured during the third and the fifth postnatal weeks, at PND 31, seems to be in accordance with this finding. At the onset of myelination, the superficial layers seemed to present longer internodes than in the deep layers. This could be the consequence of the myelination sequence, when longer internodes are first established followed by the shorter internodes (Young et al., 2013). Along this line, the internode length measured on the third postnatal week were shorter than the internodes measured during the myelination onset. The internode length variation in dependence of the cortex layer and the age of the mice was in accordance with the literature (Tomassy et al., 2014).

GluA2 deletion in NG2 cells impaired the learning motor performance.

The motor learning task gives us the opportunity to assess the role of the GluA2 subunit in physiological conditions requiring myelin plasticity. This learning paradigm depends on the generation of oligodendrocytes in the primary motor cortex and the corpus callosum. Myrf (myelin regulatory factor) deletion in NG2 cells prevents the production of newly formed oligodendrocytes and Myrf deficient mice perform worse on the complex

wheel than their wild-type litter mates (McKenzie et al., 2014). Since the GluA2 subunit regulates the cell cycle of NG2 cells and plays a role in early myelination, we expected the GluA2 deletion in postnatal NG2 cells to impact the performance of the mice in the complex running wheel. Indeed, while control mice showed an increase in their running performance, GluA2 deletion in NG2 cells prevented the improvement of running performance over the training period. Therefore, motor learning in the complex wheel is dependent on the expression of GluA2-containing AMPARs in NG2 cells. Learning a motor task relies partly on adaptative myelination performed by newly formed oligodendrocytes. However, internodes length in the motor cortex and myelination spread in the corpus callosum was not affected by GluA2 deletion in early postnatal NG2 cells. Impairment of the learning motor task performances is not due to a shortening of the internode's length.

NG2 cells proliferation has been shown to be increased during a motor learning paradigm using the complex running wheel (McKenzie et al., 2014). Since the GluA2 deletion in postnatal NG2 cells affected the cell cycle, we expected to see an impairment of the proliferation of NG2 cells during the learning motor paradigm in the cortex area implicated in the motor behavior. However, after running six days in the complex wheel, the mice deficient for GluA2 in postnatal NG2 cells did not show signs of an altered cell cycle. As well, the fraction of newly generated oligodendrocytes was not affected by the GluA2 deletion in the corpus callosum or the motor cortex. Surprisingly, GluA2 deletion did not alter NG2 cell proliferation. Nevertheless, the GluA2 deletion effect on NG2 cell proliferation might have been diluted in the overall increase of NG2 cell proliferation due to motor learning (McKenzie et al., 2014). Another explanation for the absence of NG2 cell proliferation could be the selected time window to assess the proliferation after the motor learning task starts. McKenzie et al. in 2014 showed that NG2 cell proliferation was increased only on the fourth day after the complex wheel experiment started. The next day, on the fifth day, the NG2 cell proliferation rate was comparable to non-running mice (McKenzie et al., 2014). Therefore, the NG2 cell proliferation increase due to motor learning motor paradigm in the complex wheel might have occurred in a short time window that we missed, since we measured the proliferation on the sixth day after the introduction of the complex wheel.

Role of GluA2 subunit in NG2 cells is dependent on the time and location of its expression in NG2 cells.

NG2 cell population is heterogeneous. During the development but also depending on their brain area location, NG2 cells adapt their properties (Vigano & Dimou, 2015). While the necessity to populate the brain with NG2 cells and provide myelination decreases with aging, the cell cycle of NG2 cells elongates its duration (Dimou & Gallo, 2015). In the same direction, NG2 cells in the grey matter surrounded by neuronal cell bodies, may not have the same function as NG2 cells in the white matter surrounded by axons calling for myelination. The discrepancies obtained in our results in the white matter versus the grey matter and along the developmental period support the fact that NG2 cell population is heterogeneous. GluA2 subunit deletion in postnatal NG2 cells altered the cell cycle of NG2 cells in the white matter only and not in the grey matter. In addition, regarding the heterogeneity during the development, in our study, GluA2 deletion in NG2 cells impact the DNA synthesis when deleted in the first postnatal week but not anymore when it was deleted in the second postnatal week. This result suggests the first postnatal week to be critical for the role of GluA2 subunit in regulating the DNA synthesis in NG2 cells.

Physiological role of GluA2 subunit expression in NG2 cells

Deletion of the GluA2 subunit in postnatal NG2 cells suggested a role for the GluA2 subunit in the myelination speed during the early postnatal period. First, expression of the GluA2 subunit in postnatal NG2 cells speeds up the myelination process through the regulation of internodes elongation. Second, GluA2 subunit expression in postnatal NG2 cells decreases the fraction of NG2 cells showing DNA synthesis. We suggest the fraction of NG2 cells showing DNA synthesis to mirror the duration of DNA replication during the cell cycle of NG2 cells. If this hypothesis is verified, GluA2 subunit expression in NG2 cells would be implicated in speeding up the proliferation process in NG2 cell.

GluA2 deletion in postnatal NG2 cells alters glutamatergic synaptic input integration in NG2 cells. GluA2 deletion in postnatal NG2 cells altered the motor learning performances

in the complex running wheel. This result highlights the role of glutamatergic synaptic input integration in NG2 cells on motor cognitive performances.

In conclusion, GluA2 subunit expression in NG2 cells is necessary for the regulation of myelination onset through glutamatergic synaptic input integration in NG2 cells. In addition, GluA2 subunit in NG2 cells plays a role in cognitive learning processes. Further investigations will be necessary to understand by which mechanism GluA2 subunit in NG2 cells regulates motor learning.

Outlook

GluA2 subunit expression in postnatal NG2 cells have been found to increase the fraction of cells undergoing DNA synthesis. We hypothesized the DNA synthesis increase to be due to S phase elongation. Using a gene encoded tracer expression in GluA2 deleted NG2 cells would help us define the S phase duration. If the S phase is elongated due to the GluA2 subunit deletion, we would like to assess which calcium effectors are implicated in this process.

Regarding the role of GluA2 subunit on the myelination we measured the internode length which represent only one aspect of the myelination. In order to define if GluA2 subunit plays a role in myelin thickness, we should measure the G-ratio of myelin sheath originating from oligodendrocytes generated by GluA2 deleted NG2 cells using the triple transgenic mouse line with the membranous GFP reporter.

GluA2 subunit expression is associated with calcium signaling in NG2 cells. In which type of calcium signaling does GluA2 subunit expression plays a role in NG2 cells? Spontaneous or evoked calcium signaling? Global or local calcium signaling? For this purpose, we could patch-clamp NG2 cells with a fluorescent calcium indicator and record the calcium response amplitude and location in NG2 cells after glutamate uncaging. The triple transgenic mouse model with GluA2 deletion in NG2 cells and a fluorescent reporter for Cre-recombination would be crossed to the NG2DsRed transgenic mouse line to identify GluA2 deleted NG2 cells in slices.

How does GluA2 subunit regulates myelination speed? Which calcium effectors are involved? Which genes are implicated? Performing single RNA sequencing on control or GluA2 deleted oligodendrocyte lineage cells (NG2 cells, pre-oligodendrocytes, oligodendrocytes) identified with the reporter of the triple transgenic mouse line would give us an insight for the identification of the effectors implicated in the role of GluA2 subunit in NG2 cells.

GluA2 subunit expression correlates with higher performances in the learning motor task. To understand how GluA2 subunit expressed in NG2 cells plays a role in motor learning, myelination properties such as myelin thickness or the number of internodes per oligodendrocytes must be investigated.

5 Abstract

Oligodendrocytes precursor cells (OPC), also called NG2 cells, proliferate or differentiate into myelin-producing oligodendrocytes throughout life. Myelination depends on neuronal activity. Although NG2 cells receive neuronal glutamatergic synaptic input throughout the CNS, factors mediating activity-dependent control of the oligodendrocyte lineage cell fate have not been resolved yet. Glutamatergic signalling in NG2 cells is mainly mediated by AMPARs. During the postnatal period, AMPARs are calcium impermeable due to the expression of the GluA2 subunit. Later in the adult period, NG2 cells downregulate the GluA2 subunit, therefore they express GluA2-lacking AMPARs, permeable to calcium. Thus, the decline of the proliferation rate of NG2 cells observed during the transition from the postnatal to the adult period is mirrored by an increase in the calcium-permeability of synaptic AMPA receptors. We hypothesized that the postnatally expressed GluA2 subunit enables the proliferation of NG2 cells by suppressing calcium entry during synaptic activity. Here, we assessed the impact of postnatal GluA2 subunit deletion on the oligodendrocyte lineage cell fate. In order to induce a conditional deletion of the GluA2 subunit in NG2 cells, we crossed the three following mouse lines. NG2CreER mouse line conditionally express Cre under the NG2 promotor. R26REYFP mouse line express the yellow fluorescent protein reporter after Cre expression. GluA2lox mouse line undergoes a deletion of *Gria2* allele responsible for GluA2 expression. First, we followed the oligodendrocyte lineage cell fate with the BrdU and PCNA markers to examine NG2 cell proliferation, the cleaved caspase-3 marker to probe for cell death, and the CC1 marker to analyse differentiation of NG2 cells into oligodendrocytes. We found that GluA2 deletion in early postnatal NG2 cells increased BrdU uptake in NG2 cells without increasing cell density or cell death in the oligodendrocyte lineage cell population. Secondly, we investigated the role of GluA2 subunit on myelination establishment by measuring the internodes length during myelination onset and at a later timepoint during the postnatal phase. GluA2 deletion in NG2 cells shortened immature internodes during myelination onset. Thirdly, the role of the GluA2 subunit in NG2 cells was investigated in a motor

learning task requiring newly formed oligodendrocytes. GluA2 deletion altered the motor learning performance in mice. Although it did not affect the myelination properties investigated or NG2 cells proliferation. Overall, the GluA2 subunit in postnatal NG2 cells regulates DNA synthesis in NG2 cells and myelination onset through the regulation of internode elongation. Our study highlights the prominence of glutamatergic synaptic input integration in postnatal NG2 cells to regulate oligodendrocyte lineage cell fate.

6 List of figures

Figure 1.1 Oligodendrocyte lineage cell markers. 11
Figure 1.2. NG2 cells origins. 12
Figure 1.3. NG2 cell fate and cell cycle. 14
Figure 1.4. Axonal Myelination. 16
Figure 1.5. GluA2 subunit insertion in AMPAR composition. 22
Figure 2.1. GluA2 subunit deletion in NG2 cells expressing the EYFP reporter. 29
Figure 2.2. GluA2 subunit deletion in NG2 cells expressing the membrane GFP reporter. 30
Figure 2.3. Confocal imaging principle. 34
Figure 2.4. Material for Running wheel experiment. 36
Figure 2.5. Experimental procedure to follow the fate of GluA2 deleted NG2 cells. 37
Figure 2.6. NG2 cell morphology in the grey matter compared to the white matter. 42
Figure 2.7. Mitotic figures in NG2 cells. 43
Figure 2.8. Experimental procedure to estimate internode length in the early and late postnatal period, of NG2GluA2-wt and NG2GluA2-lox mice. 45
Figure 2.9. Experimental procedure to determine the role of GluA2 on NG2 cell fate and oligodendrocyte properties after a motor learning task. 48
Figure 2.10. Rotarod experimental timeline. 49
Figure 3.1 Increased BrdU uptake in NG2 cells of NG2GluA2-lox animals. 56
Figure 3.2. GluA2 deletion does not affect NG2 cells growth fraction. 58
Figure 3.3. Mitotic NG2 cell fraction is not altered after GluA2 deletion. 59
Figure 3.4. GluA2 deletion tends to affect NG2 cells BrdU uptake depending on their origin. 61
Figure 3.5. GluA2 deletion affects NG2 cell density. A 63
Figure 3.6. GluA2 deletion does not increase the number of Caspase-3 positive cells. 65
Figure 3.7 GluA2 deletion does not affect the differentiation rate of NG2 cells. 68
Figure 3.8. Shortened internodes after GluA2 deletion in NG2 cells at PND 13. 71

Figure 3.9 Unchanged internode length on PND 20 after GluA2 deletion. 72
Figure 3.10. GluA2 deletion affects the internode length in dependence of their position in the cortical layer on PND 13. 73
Figure 3.11 GluA2 deletion affects the internode length in dependence of their position in the cortical layer on PND 20. 74
Figure 3.12. Unaltered motor skills after postnatal GluA2 deletion in NG2 cells. 75
Figure 3.13 GluA2 deletion decreases motor skill learning. 78
Figure 3.14. Unchanged internodes length and myelination spread after GluA2 subunit deletion in NG2 cells during the wheel motor learning paradigm. 79
Figure 3.15. Proliferation of NG2 cells is not affected by motor learning paradigm after GluA2 deletion. 82

7 References

Allen, N. J., & Lyons, D. A. Glia as Architects of Central Nervous System Formation and Function. *Physiology & Behavior*, 2018, *176*(3), 139–148

Baraban, M., Koudelka, S., & Lyons, D. A. Ca 2 + activity signatures of myelin sheath formation and growth in vivo. *Nature Neuroscience*, 2018, *21*(January), 19–23

Barres, B. A., & Raff, M. C. Proliferation of oligodendrocyte precursor cells depends on electrical activity in axons. *Nature*, 1993, *361*(6409), 258–260

Bercury, K. K., & Macklin, W. B. Dynamics and mechanisms of CNS myelination. *Developmental Cell*, 2015, *32*(4), 447–458

Bergles, D. E., Roberts, J. D., Somogyi, P., & Jahr, C. E. Glutamatergic synapses on oligodendrocyte precursor cells in the hippocampus. *Nature*, 2000, *405*(6783), 187–91

Butt, A. M. Neurotransmitter-mediated calcium signalling in oligodendrocyte physiology and pathology. *Glia*, 2006, *54*, 666–675

Catterall, W. A., Perez-reyes, E., Snutch, T. P., & Striessnig, J. International Union of Pharmacology . XLVIII . Nomenclature and Structure-Function Relationships of Voltage-Gated Calcium Channels, *Pharmacological reviews*, 2005, *57*(4), 411–425

Cheli, V. T., Santiago González, D. A., Spreuer, V., & Paez, P. M. Voltage-gated Ca2+ entry promotes oligodendrocyte progenitor cell maturation and myelination in vitro. *Experimental Neurology*, 2015, *265*, 69–83

Chen, T. J., Kula, B., Nagy, B., Barzan, R., Gall, A., Ehrlich, I., & Kukley, M. In Vivo Regulation of Oligodendrocyte Precursor Cell Proliferation and Differentiation by the AMPA-Receptor Subunit GluA2. *Cell Reports*, 2018, *25*(4), 852–861

Clapham, D. E. Calcium Signaling. *Cell*, 2007, *131*(6), 1047–1058.

Cull-candy, S., Kelly, L., & Farrant, M. Regulation of Ca 2 + -permeable AMPA receptors : synaptic plasticity and beyond, *Current opinion in Neurobiology*, 2006, 288–297

Czopka, T., & Auer, F. New Approaches to Analyse Axon- Oligodendrocyte Communication in vivo, *Neuroforum*, 2017, *23*(4), 175–181

Czopka, T., ffrench-Constant, C., & Lyons, D. A. Individual oligodendrocytes have only a few hours in which to generate new myelin sheaths invivo. *Developmental Cell*, 2013, *25*(6), 599–609

Dawson, M. R. L., Polito, A., Levine, J. M., & Reynolds, R. NG2-expressing glial progenitor cells: An abundant and widespread population of cycling cells in the adult rat CNS. *Molecular and Cellular Neuroscience*, 2003, *24*(2), 476–488

De Biase, L. M., Nishiyama, A., & Bergles, D. E. Excitability and synaptic communication within the oligodendrocyte lineage. *The Journal of Neuroscience*, 2010, *30*(10), 3600–11

Demerens, C., Stankoff, B., Logak, M., Anglade, P., Allinquant, B., Couraud, F., Zalc, B., Lubetzki, C. Induction of myelination in the central nervous system by electrical activity. *Proceedings of the National Academy of Sciences of the United States of America*, 1996, *93*(18), 9887–92

Dimou, L., & Gallo, V. NG2-Glia and Their Functions in the Central Nervous System. *Glia*, 2015, *63*, 1429–1451

Dimou, L., Simon, C., Kirchhoff, F., Takebayashi, H., & Götz, M. Progeny of Olig2-Expressing Progenitors in the Gray and White Matter of the Adult Mouse Cerebral Cortex. *Journal of Neuroscience*, 2008, *28*(41), 10434–10442

Espinosa de los Monteros, A., Zhang, M., & De Vellis, J. O2A progenitor cells transplanted into the neonatal rat brain develop into oligodendrocytes but not astrocytes. *Proceedings of the National Academy of Sciences of the United States of America*, 1993, *90*(1), 50–54

Fannon, J., Tarmier, W., & Fulton, D. Neuronal Activity and AMPA-Type Glutamate Receptor Activation Regulates the Morphological Development of Oligodendrocyte Precursor Cells. *Glia*, 2015, *63*(6), 1021–1035

Ffrech-Constant, C., & Raff, M. Proliferating bipotential glial progenitor cells in adult rat optic nerve. *Nature, 1986, 319, 499-502*

Ford, M. C., Alexandrova, O., Cossell, L., Stange-Marten, A., Sinclair, J., Kopp-Scheinpflug, C., Pecka, M., Attwell, D., Grothe, B. Tuning of Ranvier node and internode properties in myelinated axons to adjust action potential timing. *Nature Communications*, 2015, *6*, 1–14

Fulton, D., Paez, P. M., Fisher, R., Handley, V., Colwell, C. S., & Campagnoni, A. T.

Regulation of L-type Ca++ currents and process morphology in white matter oligodendrocyte precursor cells by golli-myelin proteins. *Glia*, 2010, *58*(11), 1292–1303

Gallo, V., Zhou, J. M., Mcbain, C. J., Wright, P., Knutson, P. L., & Armstrong, R. C. Oligodendrocyte Progenitor Cell Proliferation and Lineage Progression Are Regulated by Glutamate Receptor-Mediated K+ Channel Block. *The Journal of Neuroscience*, 1996, *76*(8), 2659–2670

Ghiani, C. A., Eisen, A. M., Yuan, X., DePinho, R. A., McBain, C. J., & Gallo, V. Neurotransmitter receptor activation triggers p27(Kip1) and p21(CIP1) accumulation and G1 cell cycle arrest in oligodendrocyte progenitors. *Development*, 1999, *126*(5), 1077–1090

Haberlandt, C., Derouiche, A., Wyczynski, A., Haseleu, J., Pohle, J., Karram, K., Trotter, J., Seifert, G., Frotscher, M., Steinhäuser, C., Jabs, R. Gray matter NG2 cells display multiple ca2+-signaling pathways and highly motile processes. *PLoS ONE*, 2011, *6*(3), 1–17

Hill, R. A., & Nishiyama, A. NG2 cells (polydendrocytes): Listeners to the neural network with diverse properties. *Glia*, 2014, *62*(8), 1195–1210

Hill, R. A., Patel, K. D., Goncalves, C. M., Grutzendler, J., & Nishiyama, A. Modulation of oligodendrocyte generation during a critical temporal window after NG2 cell division. *Nature Neuroscience*, 2014, *17*(11), 1518–1527

Hughes, E. G., Kang, S. H., Fukaya, M., & Bergles, D. E. Oligodendrocyte progenitors balance growth with self-repulsion to achieve homeostasis in the adult brain. *Nature Neuroscience*, 2013, *16*(6), 668–76

Humeau, J., Bravo-San Pedro, J. M., Vitale, I., Nuñez, L., Villalobos, C., Kroemer, G., & Senovilla, L. Calcium signaling and cell cycle: Progression or death. *Cell Calcium*, 2018, *70*, 3–15

Jäkel, S., & Dimou, L. Glial Cells and Their Function in the Adult Brain: A Journey through the History of Their Ablation. *Frontiers in Cellular Neuroscience*, 2017, *11*(February), 1–17

Kahl, C. R., & Means, A. R. Regulation of Cell Cycle Progression by Calcium/Calmodulin-Dependent Pathways. *Endocrine Reviews*, 2003, *24*(6), 719–736

Keiner, S., Niv, F., Neumann, S., Steinbach, T., Schmeer, C., Hornung, K., Schlenker, Y.,

Förster, M., Witte, O.W., Redecker, C. Effect of skilled reaching training and enriched environment on generation of oligodendrocytes in the adult sensorimotor cortex and corpus callosum. *BMC Neuroscience*, 2017, *18*(31), 1–13

Kessaris, N., Fogarty, M., Iannarelli, P., Grist, M., Wegner, M., & Richardson, W. D. Competing waves of oligodendrocytes in the forebrain and postnatal elimination of an embryonic lineage. *Nature Neuroscience*, 2006, *9*(2), 173–179

Khawaja, R. R., Agarwal, A., Fukaya, M., Jeong, H.-K., Gross, S., Gonzalez-Fernandez, E., Soboloff, J., Bergles, D.E., Kang, S. H. GluA2 overexpression in oligodendrocyte progenitors promotes postinjury oligodendrocyte regeneration. *Cell Reports*, 2021, *35*(7), 109147

Kougioumtzidou, E., Shimizu, T., Hamilton, N. B., Tohyama, K., Sprengel, R., Monyer, H., Attwell, D., Richardson, W. D. Signalling through AMPA receptors on oligodendrocyte precursors promotes myelination by enhancing oligodendrocyte survival. *ELife*, 2017, *6*, 1–31

Krasnow, A. M., Ford, M. C., Valdivia, L. E., Wilson, S. W., & Attwell, D. Regulation of developing myelin sheath elongation by oligodendrocyte calcium transients in vivo. *Nature Neuroscience*, 2018, *21*(January), 24–28

Kukley, M., Capetillo-Zarate, E., & Dietrich, D. Vesicular glutamate release from axons in white matter. *Nature Neuroscience*, 2007, *10*(3), 311–320

Kukley, M., & Dietrich, D. Kainate receptors and signal integration by NG2 glial cells. *Neuron Glia Biology*, 2009, *5*(1–2), 13–20

Kukley, M., Kiladze, M., Tognatta, R., Hans, M., Swandulla, D., Schramm, J., & Dietrich, D. Glial cells are born with synapses. *The FASEB Journal*, 2008, *22*(8), 2957–2969

Kukley, M., Nishiyama, A., & Dietrich, D. The Fate of Synaptic Input to NG2 Glial Cells: Neurons Specifically Downregulate Transmitter Release onto Differentiating Oligodendroglial Cells. *Journal of Neuroscience*, 2010, *30*(24), 8320–8331

Kula, B., Chen, T. J., & Kukley, M. Glutamatergic signaling between neurons and oligodendrocyte lineage cells: Is it synaptic or non-synaptic? *Glia*, 2019, *67*(11), 2071–2091

Larson, V. A., Zhang, Y., & Bergles, D. E. Electrophysiological properties of NG2+ cells: Matching physiological studies with gene expression profiles. *Brain Research*, 2016, *1638*, 138–160

Li, Q., Brus-Ramer, M., Martin, J. H., & McDonald, J. W. Electrical stimulation of the medullary pyramid promotes proliferation and differentiation of oligodendrocyte progenitor cells in the corticospinal tract of the adult rat. *Neuroscience Letters*, 2010, *479*(2), 128–133

Lin, S., & Bergles, D. E. Synaptic signaling between GABAergic interneurons and oligodendrocyte precursor cells in the hippocampus. Nature Neuroscience, 2004, 7(1), 24–32.

McKenzie, I. A., Ohayon, D., Li, H., De Faria, J. P., Emery, B., Tohyama, K., & Richardson, W. D. Motor skill learning requires active central myelination. *Science*, 2014, *346*(6207), 318–322

Menn, B., Garcia-Verdugo, J. M., Yaschine, C., Gonzalez-Perez, O., Rowitch, D., & Alvarez-Buylla, A. Origin of Oligodendrocytes in the Subventricular Zone of the Adult Brain. *Journal of Neuroscience*, 2006, *26*(30), 7907–7918

Mitew, S., Gobius, I., Fenlon, L. R., Mcdougall, S. J., Hawkes, D., Xing, Y. L., Bujalka, H., Gundlach, A.L., Richards, L.J., Kilpatrick, T.J., Merson, T.D., Emery, B. Pharmacogenetic stimulation of neuronal activity increases myelination in an axon-specific manner. *Nature Communications*, 2018, 9:306, 1–16

Muzumdar, M. D., Tasic, B., Miyamichi, K., Li, L., & Luo, L. A Global Double-Fluorescent Cre Reporter Mouse. *Genesis*, 2007, *45*, 593–605

Naruse, M., Ishizaki, Y., Ikenaka, K., & Tanaka, A. Origin of oligodendrocytes in mammalian forebrains : a revised perspective. *The Journal of Physiological Sciences*, 2017, *67*(1), 63–70

Nishiyama, A., Lin, X. H., Giese, N., Heldin, C. H., & Stallcup, W. B. Co-localization of NG2 proteoglycan and PDGF alpha-receptor on O2A progenitor cells in the developing rat brain. *Journal of Neuroscience Research*, 1996, *43*, 299–314

Nishiyama, Akiko, Chang, A., & Trapp, B. D. NG2+ Glial Cells : A Novel Glial Cell Population in the Adult Brain. *Journal of Neuropathology and Experimental Neurology*, 1999, *58*(11), 1113–1124

Nishiyama, Akiko, Komitova, M., Suzuki, R., & Zhu, X. Polydendrocytes (NG2 cells): multifunctional cells with lineage plasticity. *Nature Reviews. Neuroscience*, 2009a, *10*(1), 9–22

Nishiyama, Akiko, Komitova, M., Suzuki, R., & Zhu, X. Polydendrocytes (NG2 cells):

multifunctional cells with lineage plasticity, 2009b, *10*(January), 9–21

Paez, P. M., Fulton, D. J., Spreuer, V., Handley, V., Campagnoni, C. W., Macklin, W. B., Colwell, C., Campagnoni, A. T. Golli myelin basic proteins regulate oligodendroglial progenitor cell migration through voltage-gated Ca2+ influx. *Journal of Neuroscences*, 2009, *29*(20), 6663–6676

Paez, P. M., Spreuer, V., Handley, V., Feng, J., Campagnoni, C., & Campagnoni, A. T. Increased Expression of Golli Myelin Basic Proteins Enhances Calcium Influx into Oligodendroglial Cells, 2007, *27*(46), 12690–12699

Parolisi, R., & Boda, E. NG2 Glia : Novel Roles beyond Re- / Myelination. *Neuroglia*, 2018, *1*, 151–175

Pende, M., Holtzclaw, L. A., Curtis, J. L., Russell, J. T., & Gallo, V. Glutamate regulates intracellular calcium and gene expression in oligodendrocyte progenitors through the activation of DL-α-amino-3-hydroxy- 5-methyl-4-isoxazolepropionic acid receptors. *Proceedings of the National Academy of Sciences of the United States of America*, 1994, *91*(8), 3215–3219

Pennycook, B. R., Vesela, E., Peripolli, S., Singh, T., Barr, A. R., Bertoli, C., & de Bruin, R. A. M. E2F-dependent transcription determines replication capacity and S phase length. *Nature Communications*, 2020, *11*(3503), 1–12

Pitman, K. A., Ricci, R., Gasperini, R., Beasley, S., Pavez, M., Charlesworth, J., … Young, K. M. The voltage-gated calcium channel CaV1.2 promotes adult oligodendrocyte progenitor cell survival in the mouse corpus callosum but not motor cortex. *Glia*, 2020, *68*(2), 376–392

Pringle, N. P., & Richardson, W. D. A singularity of PDGF alpha-receptor expression in the dorsoventral axis of the neural tube may define the origin of the oligodendrocyte lineage. *Development*, 1993, *117*(2), 525–533

Psachoulia, K., Jamen, F., Young, K. M., & Richardson, W. D. Cell cycle dynamics of NG2 cells in the postnatal and ageing brain, 2010, *5*, 57–67

Redondo, C., Lopez-Toledano, M. A., Lobo, M.V.T., Gonzalo-Gobernado, R., Reimers, D., Herranz, A.S., Paino, C.L., Bazan, E. Kainic Acid Triggers Oligodendrocyte Precursor Cell Proliferation and Neuronal Differentiation From Striatal Neural Stem Cells. *Journal of Neuroscience Research*, 2007, *85*(11), 2352–2359

Rivers, L. E., Young, K. M., Rizzi, M., & Jamen, F. PDGFRA / NG2 glia generate

myelinating oligodendrocytes and piriform projection neurons in adult mice, 2008, *11*(12), 1–24

Sasaki, K., Kurose, A., & Ishida, Y. Flow cytometric analysis of the expression of PCNA during the cell cycle in hela cells and effects of the inhibition of DNA synthesis on it. *Cytometry*, 1993, *14*(8), 876–882

Shimshek, D. R., Bus, T., Grinevich, V., Single, F. N., Mack, V., Sprengel, R., Spergel, D.J., Seeburg, P. H. Impaired reproductive behavior by lack of GluR-B containing AMPA receptors but not of NMDA receptors in hypothalamic and septal neurons. *Molecular Endocrinology*, 2006, *20*(February), 219–231

Snaidero, N., & Simons, M. Myelination at a glance. *Journal of Cell Science*, 2014, *127*(14), 2999–3004

Soliven, B. Calcium signalling in cells of oligodendroglial lineage. *Microscopy Research and Technique*, 2001, *52*(6), 672–679

Srinivas, S., Watanabe, T., Lin, C.-S., William, C. M., Tanabe, Y., Jessell, T. M., & Costantini, F. Cre reporter strains produced by targeted insertion of EYFP and ECFP into the ROSA26 locus. *BMC Developmental Biology*, 2001, *1*(4), 1–8

Sun, W., & Dietrich, D. Synaptic integration by NG2 cells. *Frontiers in Cellular Neuroscience*, 2013, *7*(December), 255

Sun, W., Matthews, E. A., Nicolas, V., Schoch, S., & Dietrich, D. NG2 glial cells integrate synaptic input in global and dendritic calcium signals. *eLIFE*, 2016, 1–25

Tomassy, G. S., Berger, D. R., Chen, H., Kasthuri, N., Hayworth, K. J., Vercelli, A., Seung, H.S., Lichtman, J.W., Arlotta, P. Distinct profiles of myelin distribution along single axons of pyramidal neurons in the neocortex, *Science*, 2014, *344*(6181), 319–324

Vigano, F., & Dimou, L. The heterogeneous nature of NG2-glia. *Brain Research*, 2015, 1–9

Woo-Pin Ge, Xiu-Juan Yang, Zhang, Z., Wang, H.-K., Shen, W., Deng, Q.-D., & Duan, S. Long-Term Potentiation of Neuron- Glia synapses mediated ba Ca-Permeable AMPA receptors. *Science Reports*, 2006, *312*(June), 1533–1537

Xiao, L., Ohayon, D., Mckenzie, I. A., Sinclair-wilson, A., Wright, J. L., Fudge, A. D., Emery, B., Li, H., Richardson, W. D. Rapid production of new oligodendrocytes is required in the earliest stages of motor-skill learning. *Nature Neuroscience*, 2016, *19*(9), 1210–1217

Yang, Q. K., Xiong, J. X., & Yao, Z. X. Neuron-NG2 cell synapses: Novel functions for regulating NG2 cell proliferation and differentiation. *BioMed Research International*, 2013, 1, 18–21

Young, K. M., Psachoulia, K., Tripathi, R. B., Dunn, S. J., Cossell, L., Attwell, D., Tohyama, K., Richardson, W. D. Oligodendrocyte dynamics in the healthy adult CNS: Evidence for myelin remodeling. *Neuron*, 2013, *77*(5), 873–885

Yuan, X., Eisen, A. M., McBain, C. J., & Gallo, V. A role for glutamate and its receptors in the regulation of oligodendrocyte development in cerebellar tissue slices. *Development*, 1998, *125*(15), 2901–2914

Zhu, X., Bergles, D. E., & Nishiyama, A. NG2 cells generate both oligodendrocytes and gray matter astrocytes. *Development*, 2007, *135*(1), 145–157

Zhu, X., Hill, R. A., Dietrich, D., Komitova, M., Suzuki, R., & Nishiyama, A. Age-dependent fate and lineage restriction of single NG2 cells, 2011, *753*, 745–753

Ziskin, J. L., Nishiyama, A., Rubio, M., Fukaya, M., & Bergles, D. E. Vesicular release of glutamate from unmyelinated axons in white matter. *Nature Neuroscience*, 2007, *10*(3), 321–330

Zonouzi, M., Renzi, M., Farrant, M., & Cull-Candy, S. G. Bidirectional plasticity of calcium-permeable AMPA receptors in oligodendrocyte lineage cells. *Nature Neuroscience*, 2011, *14*(11), 1430–1438

8 Acknowledgement

I would like to express my gratitude to my supervisors Prof. Dirk Dietrich and Prof. Susanne Schoch for their support and guidance along my PhD. Thank you for teaching me science in the most detailed ways.

I extend my gratitude to Prof. Lena Dimou as my second supervisor for your support, and availability along my PhD. I share my gratitude to Prof. Stein as well for agreeing to be part of my PhD committee thesis.

I would like to thank deeply Wenjing Sun for her support at the beginning of my thesis, and her love for science.

I am grateful for the great support, Julia Kaspari and Pia Stausberg as technicians in the laboratory, brought to my experience. I appreciated their quality of work and their wish to constantly help us.

I would like to thank all the students that helped me in the cell counting process.
To all my colleagues in the lab and outside the lab, I owe a big thanks for the scientific talks and life talks that gave me the strength and helped me grow as a person. I am grateful for all the persons that crossed my way during this PhD adventure.

Finally, I would like to thank my family, friends and relatives which gave me the power and joy to continue this adventure.

Scientific presentations

Nicolas V, Sun W, Schoch S, Dietrich D. GABAergic input integration in NG2 glial cells, Neuroscience French society meeting, Bordeaux, May 2017.

Nicolas V, Sun W, Lamcaj A, Thanscheidt O, Schoch S, Dietrich D. Role of GluA2-containing AMPA-Receptors in regulating proliferation in NG2 cells, Bonn Brain^3 meeting, Bonn, 2018.

Nicolas V, Sun W, Lamcaj A, Thanscheidt O, Schoch S, Dietrich D. Role of GluA2-containing AMPA-Receptors in regulating the proliferation of NG2 cells, speaker at SPP 1757 meeting, Speyer, 2018.

Nicolas V, Sun W, Schoch S, Dietrich D, A proliferative-permissive role for GluA2 NG2 cells, European Glia meeting, Porto, 2019.

Publications

Sun, W., Matthews, E. A., Nicolas, V., Schoch, S., & Dietrich, D. (2016). NG2 glial cells integrate synaptic input in global and dendritic calcium signals. ELIFE, 1–25. DOI: 10.7554/eLife.16262.